SECTION 5. HETEROGENEOUS CHEMISTRY

Table of Contents

Tables

Figures

5.1   Introduction

We have evaluated and tabulated the currently available information on heterogeneous stratospheric processes. In addition, because of the increasing level of interest in tropospheric processes with a direct bearing on the fluxes of reactive species into the stratosphere, such as heterogeneous loss processes for partially oxidized degradation products of hydrohalocarbons and heterogeneous contrail and cloud processing of exhaust species from aircraft, we have included kinetic data for selected heterogeneous interactions relevant to modeling cloud droplet and aqueous aerosol chemistry in the free troposphere. However, both stratospheric and tropospheric heterogeneous chemistry are relatively new and rapidly developing fields, and further results can be expected to change our quantitative and even our qualitative understanding on a regular basis. The complexity is compounded by the difficulty of characterizing the chemical and physical properties of atmospheric heterogeneous surfaces and then reproducing suitable simulations in the laboratory [227]. New and/or updated evaluations in this document have focused on uptake measurements on binary liquid sulfuric acid/water, supplemented in a few cases by data on ternary liquid sulfuric acid/water solutions, on water ice, and on "soot" (see definitions below). No updates on solid acid/ice compositions are presented in this document, although evaluations for key nitrogen oxide sequestration and/or halogen activation reactions on nitric acid trihydrate (NAT) surfaces were recently re-evaluated and presented in JPL 00-3 [306]. Uptake data on alumina, salt and aqueous salt solutions have not been updated since JPL 97-4 [102]. Henry's law solubility data for reactive upper tropospheric/stratospheric species in binary liquid sulfuric acid/water and, where available, in ternary liquid sulfuric acid/nitric acid/water solutions have also been updated and a much more extensive compilation of Henry's law parameters for pure water has been added.

5.2 Surface Types—Acid/Water, Liquids, and Solids

To a first approximation there are three major types of surfaces believed to be present at significant levels in the stratosphere. They are: (1) Type I polar stratospheric clouds (PSCs), nominally composed of nitric acid trihydrate ($HNO_3 \bullet 3H_2O$); (2) crystals of relatively pure water ice, designated as Type II PSCs because they form at lower temperatures than Type I and are believed to be nucleated by Type I (similar surfaces may form as contrails behind high-altitude aircraft under some stratospheric conditions); and (3) sulfuric acid aerosol, which is nominally a liquid phase surface generally composed of 60–80 weight percent H_2SO_4 and, concomitantly, 40–20 weight percent H_2O. While PSCs, as their name suggests, are formed primarily in the cold winter stratosphere at high latitudes, sulfuric acid aerosol is present year round at all latitudes and may influence stratospheric chemistry on a global basis, particularly after large injections of volcanic sulfur episodically increase their abundance and surface area. There is also increasing evidence that ternary $H_2SO_4/HNO_3/H_2O$ liquid solutions may play a significant role in PSC formation.

In addition to the major stratospheric surface types noted above, several other types of heterogeneous surfaces are found in the stratosphere and may play a significant role in some stratospheric processes. For instance, laboratory work has indicated that nitric acid dihydrate (NAD) may play an important role in the nucleation of Type I PSCs (Worsnop et al. [358], Fox et al. [126]) and that mixtures of solid nitric acid hydrates and sulfuric acid tetrahydrate (SAT) (Molina et al. [261], Zhang et al. [370]) and/or a more complex sulfuric acid/nitric acid hydrate (Fox et al. [126]) may also be key to understanding Type I PSC nucleation and evolution. Analyses of the range of atmospheric conditions possible in the polar stratosphere have also led to interest in solid SAT surfaces and possibly other forms of frozen sulfuric acid aerosols (Toon et al. [334], Middlebrook et al. [256]), as well as liquid sulfuric acid aerosols significantly more dilute than the 60–80 weight percent normally present at lower latitudes (Wolff and Mulvaney [356], Hofmann and Oltmans [177], Toon et al. [334]). Some modeling studies also suggest that certain types of major volcanic eruptions transport significant levels of sodium chloride into the stratosphere (Michelangeli et al. [255]), so studies of stratospheric trace species interacting with solid NaCl or similar salts, as well as salt solutions, have also been included.

In the free troposphere the heterogeneous surfaces of interest include liquid or solid water (cloud droplets, contrails), and aqueous sulfate solutions. Uptake data are compiled for liquid water for several reasons. First this surface is one asymptote of the aqueous acid aerosol continuum; second, the interactions of some trace species with liquid water and water ice (Type II PSC) surfaces are often similar, and third, the uptake of some trace species by liquid water surfaces in the troposphere can play a key role in understanding their tropospheric chemical lifetimes and thus, the fraction that may be transported into the stratosphere.

5.3 Surface Types—Soot and Alumina

Aircraft at cruise altitudes and rocket exhausts contribute small but measurable amounts of carbonaceous "soot" (Pueschel et al. [280]) and aluminized solid propellant rocket exhausts and spacecraft debris produce increasing levels of alumina (Al_2O_3) and similar metal oxide particles (Zolensky et al. [373]) in the stratosphere and upper troposphere. Soot lofted above from surface combustion sources may also be present in the upper troposphere, and to a lesser extent in the lower stratosphere. Alumina from rocket exhausts is generally emitted as liquid droplets from the rocket nozzle and deposited in the alpha or metastable gamma phases as it quickly solidifies in the exhaust plume. "Soot" refers to a material that is a combination of elemental and organic carbon, with proportions varying depending on the source material and the combustion conditions. In studies of soot directed to understanding the interaction with atmospheric gases, two types of soot have been used: carbon blacks having relatively small hydrogen and oxygen contents (e.g. Degussa FW2, Cabot Monarch 1000, ground charcoal and spark-generated soot) and organic combustion soots having higher hydrogen, oxygen and nitrogen content (e.g. soots from the combustion of n-hexane, methane, propane, decane, ethylene, acetylene, toluene, stearic candles). In the case of organic combustion soots, even different fuels used to generate the soot have been reported to affect the chemistry; for example, the yields of HONO from the reaction of NO_2 with acetylene, toluene, ethylene and decane soots were observed to vary with the fuel used [14,134].

Polycyclic aromatic hydrocarbons (PAH) and oxygenated polycyclic aromatic compounds (O-PAC) are major constituents of soots formed from the combustion of liquid fuels [10-12,63,123,139,315]. The bulk composition of soot can have varying amounts of C, H, and O. For example, Chughtai et al. [77] report that the composition (in weight %) of *n*-hexane soot varies from 87 to 92 % C, 1.2 to 1.6 % H, and 11 to 6% oxygen. Stadler and Rossi [321] showed that the elemental composition of the soot as well as its surface area depended on whether the flame was rich or lean; in the case of the rich flame giving a grey-colored soot, the composition (weight %) was 97.3% C, 0.83% H, 1.65% O, and 0.20% N while the lean flame gave a black soot comprised of 96.4% C, 0.19% H, 3.2% O, and 0.27% N.

The functional groups on the soot surface are expected to be important in terms of the uptake and reaction of gases on the surface. XPS studies of *n*-hexane soot show surface carbon and oxygen, although the specific nature of the bonding could not be determined (Akhter et al. [12]). The surface functional groups on soot vary, depending on the fuel composition, method of generation and the post-treatment of the soot. For example, Degussa FW2 carbon black, which has been used in a number of studies of uptake and reactions of gases on soots, is post-treated with NO_2 by the manufacturer and Cabot Monarch 1000 is post-treated with aqueous HNO_3. There may be sufficient NO and NO_2 concentrations generated under some conditions during the formation of soots by spark generators that these may also have been reacted with these gases prior to collection and uptake studies. Studies of a number of gases interacting with soot surfaces suggest there are at least two and likely more, types of reactive surface sites; one type reacts very rapidly, e.g. with O_3, while others react more slowly. The first type may be most relevant to the reactions of soot particles in exhaust plumes from combustion sources, while the latter is most relevant to soot diluted in air.

Fourier transform infrared (FTIR) , Raman and electron paramagentic resonance (EPR) spectroscopic studies of n-hexane soot show C–O functionalities assigned to anhydrides and aryl ethers, alkyl ketones, as well as =C–H, highly substituted aromatics and conjugated carbonyl-aromatic groups [10,315]. Kirchner et al. [220] measured the FTIR spectra of soots from the combustion of diesel fuel and *n*-hexane (described as "flame deposited") and soots collected from a commercial spark generator in Ar, from the emissions of a diesel automobile and Degussa FW2 soot (described as "filter deposited"). In all cases, absorption peaks due to –C–C–, –C=C–, –C–O, aromatic –C=O, and carboxylic –C=O groups (both aromatic and aliphatic) were observed. However, the flame-deposited soot showed bands due to substituted aromatics while the filter-collected samples did not. The filter-deposited samples had bands due to aliphatic –C–H groups that were not observed for the flame-deposited soots. Only the spark-generated soot showed bands due to both –C=C–H and to –O–H.

For soot formed from the combustion of liquid fuels, the location in the flame at which the soot is collected also changes the surface enough to alter its reactions. For example, Akhter et al. [10] showed that the functional groups as well as particle size depend on the height of collection of soot from the base of the flame. Such changes appear to also alter the reactions of soot; for example, Gerecke et al. [134] measured HONO and NO yields from the reaction of NO_2 with ethylene soot and found that the HONO yield decreased with distance from the bottom of the flame that the soot was collected from, while the yield of NO increased. Kirchner et al. [220] reported much stronger infrared absorption bands due to substituted aromatics in soot samples collected from the combustion of *n*-hexane near the bottom of the flame compared to the top; in addition, absorption bands due to the –O–H group were only observed in samples collected at the bottom of the flame.

Not only can the surface groups directly affect its interaction with gases, but they determine the hygroscopic properties of the soot surface. Chughtai et al. [84,87] have shown that the hydration of soot surfaces depends on the fuel composition (particularly sulfur and trace metal content) and combustion conditions, as well as the extent of surface oxidation. A highly hygroscopic surface holding significant amounts of water may behave differently than a "dry" surface with respect to the interaction with gases; for example, black carbon suspended in aqueous solutions with ozone and irradiated to generate OH has been shown to help assist in the initiation of bulk solution phase OH chemistry [195]. There are also free radical sites on soot surfaces whose EPR signals are strongly affected by the adsorption of paramagnetic species such as NO_2 (e.g. see Chughtai et al. [77]). These unpaired electrons in soot may contribute to the surface reactivity.

The *International Steering Committee for Black Carbon Reference Materials* (http://www.du.edu/~dwismith/bcsteer.html) has issued preliminary recommendations for representative black carbon reference materials. They recommend that soot formed from the combustion of saturated hydrocarbons, preferably *n*-hexane, be used for soot black carbon. For aerosol black carbon, they recommend the use of Urban Dust Reference Material (SRM) 1649a, which is a sample collected in Washington, D.C. in a baghouse in 1976–1977. However, for studies of the uptake and reactions of gases in the atmosphere with combustion-generated soots, organic combustion generated soots, particularly *n*-hexane soot, appear to be the most reasonable surrogate.

5.4   Surface Composition and Morphology

The detailed composition and morphology of each surface type are uncertain and probably subject to a significant range of natural variability. Certain chemical and physical properties of these surfaces, such as their ability to absorb and/or solvate HCl and HNO_3, are known to be strongly dependent on their detailed chemical composition. Moreover, most heterogeneous processes studied under laboratory conditions (and in some cases proceeding under stratospheric conditions) can change the chemical composition of the surface in ways that significantly affect the kinetic or thermodynamic processes of interest. Thus, a careful analysis of the time-dependent nature of the active surface is required in the evaluation of measured uptake kinetics experiments.

Experimental techniques which allow the measurement of mass accommodation or surface reaction kinetics with high time resolution and/or with low trace gas fluxes are often more credible in establishing that measured kinetic parameters are not seriously compromised by surface saturation or changing surface chemical composition.

The measured kinetic uptake parameters, mass accommodation coefficients, and surface reaction probabilities are separately documented for relevant atmospheric trace gas species for the major and, where available, the minor stratospheric and upper tropospheric surfaces noted above. Since these parameters can vary significantly with surface composition (e.g., the H_2SO_4/H_2O ratio for sulfate aerosol or the HNO_3/H_2O ratio for Type I PSC) the dependence of these parameters on surface composition is reviewed where sufficient data are available. Due to its chemical and morphological complexity, uptake values for soot are documented in a separate table.

5.5 Surface Porosity

The experimental techniques utilized to measure mass accommodation, heterogeneous reaction, and other uptake coefficients generally require knowledge of the surface area under study. For solid surfaces, and most particularly for water and acid ice surfaces formed in situ, the determination of how the molecular scale ice surface differs from the geometrical surface of the supporting substrate is not easy. Keyser, Leu, and coworkers have investigated the structure of water and nitric acid ice films prepared under conditions similar to those used in their flow reactor for uptake studies [215,216,218]. They have demonstrated that ice films grown in situ from the vapor can have a considerably larger available surface than that represented by the geometry of the substrate; they have also developed a simple model to attempt to correct measured uptake rates for this effect [217,218]. This model predicts that correction factors are largest for small uptake coefficients and thick films. The application of the model to experimental uptake data remains controversial (Keyser et al. [217], Hanson and Ravishakara [162], Kolb et al. [227]). Some experimenters prefer to attempt growing ice surfaces as smooth as possible and to demonstrate that their measured uptake coefficients are only weakly dependent on surface thickness (Hanson and Ravishankara [160]). Similar issues arise for uptake experiments performed on powered, fused and single crystal salt or oxide surfaces (Fenter et al. [120]; Hanning-Lee et al. [147]).The issue of surface area available for uptake is also important for interpreting uptake measurements on soot and soot surrogate surfaces. The degree to which measured uptake parameters must be corrected for porosity effects will remain in some doubt until a method is devised for accurately determining the effective surface area for the surfaces actually used in uptake studies. Most studies evaluated in this review assume that the effective ice or salt surface area is the geometrical area.

5.6 Temperature Dependences of Parameters

A number of laboratory studies have shown that mass accommodation coefficients and, to some extent, surface reaction probabilities can be temperature dependent. While these dependencies have not been characterized for many systems of interest, temperature effects on kinetic data are noted where available. More work that fully separates heterogeneous kinetic temperature effects from temperature controlled surface composition is obviously needed.

5.7 Solubility Limitations

The uptake of certain trace gases by atmospherically relevant surfaces is usually governed by solubility limitations rather than kinetic processes. In these cases properly analyzed data can yield measurements of trace gas solubility parameters relevant to stratospheric conditions. In general, such parameters can be strongly dependent on both condensed phase composition and temperature. Such parameters may be very important in stratospheric models, since they can govern the availability of a reactant for a bimolecular heterogeneous process (e.g., the concentration of HCl available for the $HCl + ClONO_2$ reaction on sulfuric acid aerosols) or the gas/condensed phase partitioning of a heterogeneous reaction product (e.g., the HNO_3 formed by the reaction of N_2O_5 on sulfuric acid aerosols). Surface saturation limitations have also been observed in experimental uptake studies on solid surfaces, including water and water/acid ice surfaces.

5.8 Data Organization

Data for trace-gas heterogeneous interactions with relevant condensed-phase surfaces are tabulated in Tables 5-1 through 5-5. These are organized into

Table 5-1—Mass Accommodation Coefficients for Surfaces Other Than Soot.

Table 5-2—Surface Reaction Probabilities for Surfaces Other Than Soot.

Table 5-3—Soot-Surface Uptake Coefficients.

Table 5-4—Solubility Data for Pure Water.

Table 5-5—Solubility Data for Acids.

This compilation provides updated evaluations based on published literature available through 2001 for water ice, liquid sulfuric acid/nitric acid/water, and soot/soot surrogate surfaces. The evaluations for alumina, solid alkali salt, aqueous alkali salt, and liquid water (with the exception of Henry's law constants for liquid water) have not been re-evaluated since JPL Publication 97-4 [102]. Evaluations and recommendations for the latter surfaces should be used with caution since new studies have been published in some cases that would alter the recommended values or extend their range of applicability.

5.9 Parameter Definitions

Mass accommodation coefficients (α), represent the probability of reversible uptake of a gaseous species colliding with the condensed surface of interest. For liquid surfaces this process is associated with interfacial (gas-to-liquid) transport and is generally followed by bulk liquid phase solvation. Examples include: simple surface absorption, absorption followed by ionic dissociation and solvation (e.g., $HCl + nH_2O \leftrightarrow H^+(aq) + Cl^-(aq)$), and absorption followed by a reversible chemical reaction with a condensed phase substituent (e.g., $SO_2 + H_2O \leftrightarrow H^+ + HSO_3^-$ or $CH_2O + H_2O \leftrightarrow CH_2(OH)_2$).

The term "sticking coefficient" is often used for mass accommodation on solid surfaces where physisorption or chemisorption takes the place of true interfacial mass transport.

Processes involving liquid surfaces are subject to Henry's law, which limits the fractional uptake of a gas phase species into a liquid. If the gas phase species is simply solvated, a physical Henry's law constraint holds; if the gas phase species reacts with a condensed phase substituent, as in the sulfur dioxide or formaldehyde hydrolysis cases noted above, a "chemically modified" or "effective" Henry's law constraint holds (Clegg and Brimblecombe [88], Schwartz [308], Watson et al. [348]). Henry's law constants relate the equilibrium concentration of a species in the gas phase to the concentration of the same species in a liquid phase, and they have, in this report, units of
M atm^{-1}. These are tabulated for liquid surfaces in Table 5-4 and Table 5-5. Effective Henry's law constants are designated H*, while simple physical Henry's law constants are represented by H. Effective Henry's law constants are also employed to represent decreased trace gas solubilities in moderate ionic strength acid or salt solutions with the use of a Setchenow coefficient formulation which relates H* to the concentration of the acid or salt [185]. Available Henry's law constants for reactive upper tropospheric/stratospheric species in binary sulfuric acid/water solutions, and for a few cases of ternary sulfuric acid/nitric acid/water solutions, are tabulated as a function of acid weight percent and temperature. Temperature dependent Henry's law expressions for a larger set of gaseous species in pure water are presented in Table 5-4. It is presently unclear whether "surface solubility" effects govern the uptake on nominally solid water ice or HNO_3/H_2O ice surfaces in a manner analogous to bulk solubility effects for liquid substrates and no solubility parameters for these "ice" systems are presented.

For some trace species on some surfaces, experimental data suggest that mass accommodation coefficients untainted by experimental saturation limitations have been obtained. These are tabulated in Table 5-1. In other cases experimental data can be shown to be subject to Henry's law constraints, and Henry's law constants, or at least their upper limits, can be determined. Some experimental data sets are insufficient to determine if measured "uptake" coefficients are true mass accommodation coefficients or if the measurement values are lower limits compromised by saturation effects. These are currently tabulated, with suitable caveats, in Table 5-1.

Surface reaction probabilities (γ) are kinetic values for generally irreversible reactive uptake of trace gas species on condensed surfaces. The rates of such processes may not be limited by Henry's law constraints; however, the fate of the uptake reaction products may be subject to saturation limitations. For example, N_2O_5 has been shown to react with sulfuric acid aerosol surfaces. However, if the H_2SO_4/H_2O ratio is too high, the product HNO_3 will be insoluble, and a large fraction will be expelled back into the gas phase. Surface reaction probabilities for substantially irreversible processes are presented in Table 5-2. Reaction products are identified where known. .

The total experimental uptake coefficient measured in laboratory heterogeneous kinetic experiments are also often represented by the symbol γ. In those cases where surface and/or bulk reaction dominate the uptake, the total uptake coefficient (γ_{total}) and reactive uptake coefficient (γ_{rxn}) may well be identical. More formally, for cases where bulk liquid phase reaction is facile and there are no gas phase diffusion constraints, the total uptake coefficient for aerosol or cloud droplets can be approximated in terms of γ_{rxn} and γ_{sol} as [227]:

$$\frac{1}{\gamma_{total}} = \frac{1}{\alpha} + \frac{1}{\gamma_{sol} + \gamma_{rxn}}$$

where

$$\gamma_{sol} = \frac{8HRT}{\pi^{1/2}\overline{c}}\left(\frac{D}{t}\right)^{1/2}$$

and

$$\gamma_{rxn} = \frac{4HRT}{\overline{c}}\left(Dk_{rxn}\right)^{1/2}$$

where t is the time integrated exposure of the trace gas to the liquid surface, R is the gas constant, D is the liquid phase diffusion coefficient, and $\overline{c}$ is the mean trace gas molecular speed. In the limit of low solubility or long exposure time γ_{sol} becomes negligible and

$$\frac{1}{\gamma_{total}} = \frac{1}{\alpha} + \frac{1}{\gamma_{rxn}}$$

Discussion of how to use this approach to model chemical reactions in liquid stratospheric aerosols can be found in Hanson et al. [168] and Kolb et al. [227]. Note that these formulations are approximate. In cases where separate terms are competitive, more rigorous solution of the kinetic differential equations may be appropriate.

For solid surfaces, bulk diffusion is generally too slow to allow bulk solubility or bulk kinetic processes to dominate uptake. For solids, reactive uptake is driven by chemisorption/chemical reaction at the interface, a process that can also influence trace gas uptake on liquids. For liquids, surface reaction (γ_{surf}) occurs in parallel, rather than in series with mass accommodation, thus:

$$\gamma_{total} = \gamma_{surf} + \left[\frac{1}{\alpha} + \frac{1}{\gamma_{sol} + \gamma_{rxn}}\right]^{-1}$$

Examples where this more complex situation holds for liquid surfaces can be found in Hu et al. [181] and Jayne et al. [200]. In such cases γ may be significantly larger than α.

Uptake of gases on soot may occur due to three different processes: (1) physisorption (e.g. SO_2 or HNO_3 at room temperature and low nitric acid pressures); (2) reaction with the surface (e.g. NO_2), and (3) catalytic decomposition/reactions of the gas on the surface. All three processes may occur in parallel, and the relative contributions of each of these three may vary during the course of the reaction as the surface "ages." As discussed above, there are different types of reactive sites on soot, leading in some cases to a rapid initial uptake followed by a slower uptake; these are often characterized as reactions on "fresh" and "aged" surfaces respectively. Another complexity is that in some cases the geometric surface areas were used to calculate the uptake coefficients from the experimental data while in others, the available reactive surface area was estimated and used.

Because of these complexities with soot heterogeneous chemistry, uptake coefficients for soot interactions with gases have been broken out into a separate Table 5-3 rather than being included with the other surfacesin Table 5-1 and Table 5-2. When the uncertainty is more than an order of magnitude, a recommendation is not given in Table 5-3 and the range of reported values is given in the Notes. In most cases, the available reactive surface area rather than the geometric areas have been used in obtaining the uptake coefficients; in those cases where the geometric area was used but a higher available surface area was involved in the measured uptake, the uptake coefficient is given as an upper limit. Data are most commonly available for room temperature or there are very limited data at lower temperatures characteristic of the upper troposphere.

The data in Table 5-1 and Table 5-2 for uptake on non-soot surfaces are organized by trace gas species, since some systematic variation may be expected for surface accommodation or reaction as the surface composition and/or phase is varied. Data presented for one surface may be judged for "reasonableness" by comparing with data for a "similar" surface. In some cases it is not yet clear if surface uptake is truly reversible (accommodation) or irreversibly reactive in nature. In such cases the available uptake coefficients are generally tabulated in Table 5-1 as accommodation coefficients, a judgment that will be subject to change if more definitive data become available.

Where a specific evaluated value for an accommodation coefficient or reaction probability has been obtained, an estimated uncertainty factor is also tabulated. However, when the data evaluation yielded only a lower or upper limit, no uncertainty factor can be reliably estimated and none is presented.

Description of and reference citations to many of the laboratory techniques used to obtain the data in the following tables can be found in Kolb et al. [227].

Reactions of N_2O_5, $ClONO_2$, HOCl and $BrONO_2$ on/in sulfuric acid are generally dependent on the species' Henry's law solubility and liquid phase diffusion coefficient in the liquid acid as well as the surface and/or liquid phase reaction rate parameters. All of these processes are generally functions of the acid composition and temperature (Hanson et al. [168], Robinson et al. [293]Shi et al. [313]. Thus, these reactions' reactive uptake coefficients must be represented by a complex phenomenological or empirical models that defy simple entry into Table 5-2. The notes in Table 5-2 for these reactions discuss and present the models adopted.

To aid in visualizing the resulting reactive uptake parameters the results for several reactions have been plotted in **Figure 5-1** as a function of temperature for a background pressure of 50 mbar and background water vapor and HCl mixing ratios of 5 ppmv and 2 ppbv, respectively. These calculations are presented for monodisperse background sulfate aerosol particles with a radius of 1×10^{-5} cm (0.1 μm).
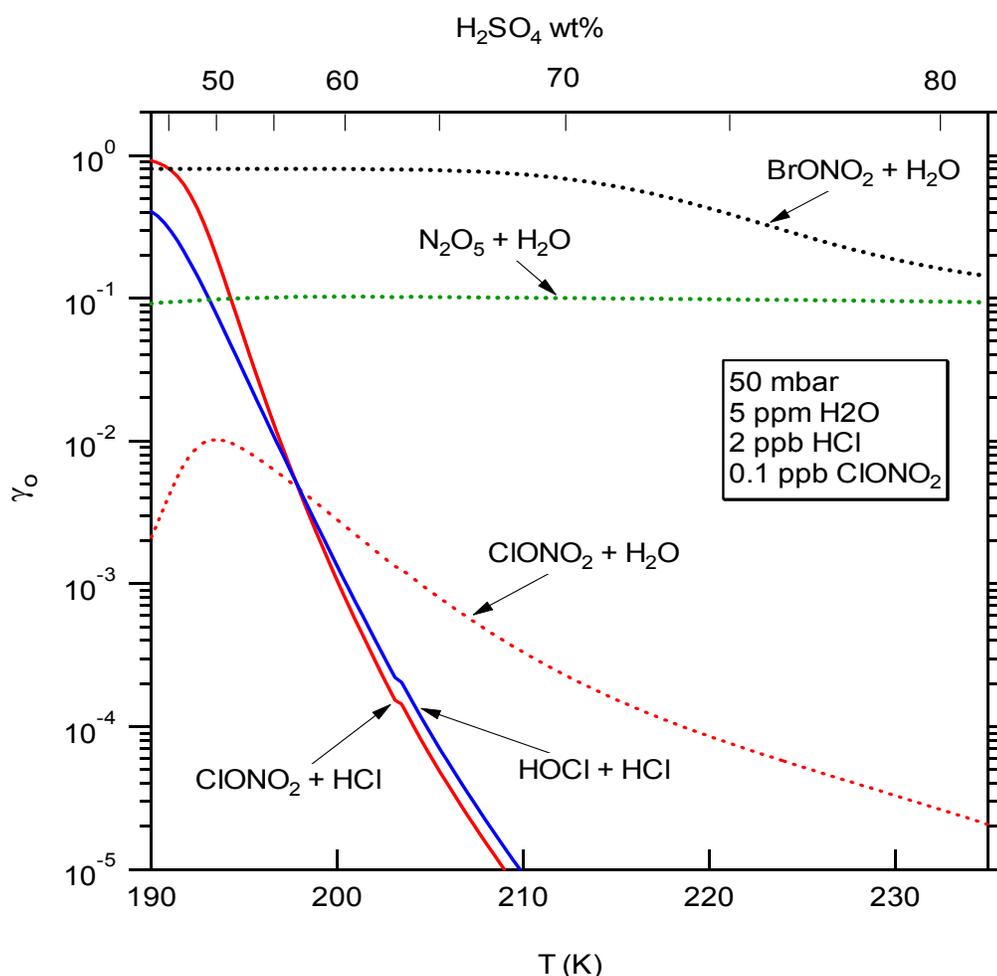

Figure 5-1. Recommended reactive uptake coefficients as a function of temperature for key stratospheric heterogeneous processes on sulfuric acid aerosols. For $ClONO_2$ and HOCl species, the aerosol radius used in the calculation is 10^{-5} cm, a typical value in the stratosphere. Because the current uptake models for N_2O_5 and $BrONO_2$ hydrolysis do not provide the information about the reacto-diffusive length (ℓ), the aerosol radius used in the calculation is assumed to be much larger than their reacto-diffusive length (i.e. ℓ for N_2O_5 and $BrONO_2$ are set to zero.)

5.10 Mass Accommodation Coefficients for Surfaces Other Than Soot

Table 5-1. Mass Accommodation Coefficients (α) for Surfaces Other Than Soot.

Gaseous Species	Surface Type	Surface Composition	T(K)	α	Uncertainty Factor	Notes
O	Sulfuric Acid	$H_2SO_4 \cdot nH_2O(l)$ (97 wt.% H_2SO_4)	298	See Note		1
O_3	Water Ice	$H_2O(s)$	195–262	>0.04		2
	Liquid Water	$H_2O(l)$	292	>2 × 10$^{-3\ddagger}$		3
	Nitric Acid Ice	$HNO_3 \cdot 3H_2O(s)$	195	2.5 × 10$^{-4\ddagger}$	3	2
	Sulfuric Acid	$H_2SO_4 \cdot nH_2O(l)$ (50–98 wt.% H_2SO_4)	193–295	See Note		4
OH	Water Ice	$H_2O(s)$	205–253	>0.1		5
	Liquid Water	$H_2O(l)$	275	>4 × 10^{-3}		6
	Sulfuric Acid	$H_2SO_4 \cdot nH_2O(l)$				
		(28 wt.% H_2SO_4)	275	>0.07		7
		(97 wt.% H_2SO_4)	298	>5 × 10$^{-4\ddagger}$		7
	Alumina	$Al_2O_3(s)$	253–348	0.04	5	8
HO_2	Liquid Water	$H_2O(l)$	275	> 0.02		9
	Aqueous Salts	$NH_4HSO_4(aq)$ and $LiNO_3(aq)$	293	> 0.2		9
	Sodium Chloride	$NaCl(s)$	295	2 × 10^{-2}	5	10
	Potassium Chloride	$KCl(s)$	295	2 × 10^{-2}	5	10
H_2O	Water Ice	$H_2O(s)$	200	0.5	2	11
	Liquid Nitric Acid	$HNO_3 \cdot nH_2O(l)$	278	>0.3		12
	Nitric Acid Ice	$HNO_3 \cdot 3H_2O(s)$	197	See Note		13
	Sulfuric Acid	$H_2SO_4 \cdot nH_2O$ (96 wt.% H_2SO_4)	298	> 2 × 10$^{-3\ddagger}$		14
	Sodium Chloride	$NaCl(s)$	~298	See Note		
		$NaCl(aq)$	~299	> 0.5		15
			~298	> 4 × 10^{-4}		16
H_2O_2	Liquid Water	$H_2O(l)$	273	0.18*	2	17
	Sulfuric Acid	$H_2SO_4 \cdot nH_2O(l)$ (96 wt.% H_2SO_4)	298	> 8 × 10$^{-4\ddagger}$		18
NO	Water Ice	$H_2O(s)$	195	See Note		19
	Sulfuric Acid	$H_2SO_4 \cdot nH_2O$		See Note		
		(70 wt.% H_2SO_4)	193–243	See Note		20
		(97 wt.% H_2SO_4)	298	See Note		20
NO_2	Water Ice	$H_2O(s)$	195	See Note		21
HONO	Water Ice	$H_2O(s)$	180–200	See Note		22
HNO_3	Water Ice	$H_2O(s)$	200	0.3	3	23
	Liquid Water	$H_2O(l)$	268	0.2*	2	24
	Nitric Acid Ice	$HNO_3 \cdot 3H_2O(s)$	191–200	0.4	2	25
	Liquid Nitric Acid	$HNO_3 \cdot nH_2O(l)$	278	0.6	2	26
	Sulfuric Acid	$H_2SO_4 \cdot nH_2O(l)$				
		(57.7 wt.% H_2SO_4)	191–200	>0.3		27
		(73 wt.% H_2SO_4)	283	0.1	2	27
		(75 wt.% H_2SO_4)	230	>2 × 10^{-3}		27
		(97 wt.% H_2SO_4)	295	>2.4 × 10^{-3}		27
	Sulfuric Acid Tetrahydrate	$H_2SO_4 \cdot 4 H_2O(s)$	~192	>0.02*		27
HO_2NO_2	Water Ice	$H_2O(s)$	[a]200	0.1$\ddagger$	3	28
	Sulfuric Acid	$H_2SO_4 \cdot nH_2O(l)$ (97 wt.% H_2SO_4)	298	See Note		29
NH_3	Liquid Water	$H_2O(l)$	~295	0.06*	3	30
CO_2	Liquid Water	$H_2O(l)$	293	See Note		31
CH_3OH	Liquid Water	$H_2O(l)$	260–291	0.12–0.02*	2	32
CH_3CH_2OH	Liquid Water	$H_2O(l)$	260–291	0.13–0.02*	2	33
$CH_3CH_2CH_2OH$	Liquid Water	$H_2O(l)$	260–291	0.08–0.02*	2	34
$CH_3CH(OH)CH_3$	Liquid Water	$H_2O(l)$	260–291	0.10–0.02*	2	34
$HOCH_2CH_2OH$	Liquid Water	$H_2O(l)$	260–291	0.13–0.04*	2	35
CH_2O	Liquid Water	$H_2O(l)$	260–270	0.04	3	36
	Sulfuric Acid	$H_2O \cdot mHNO_3 \cdot nH_2O(l)$	235–300	0.04	3	36
CH_3O_2	Sodium Chloride	$NaCl(s)$	296	>4 × 10^{-3}		37
CH_3CHO	Liquid Water	$H_2O(l)$	267	>0.03*		38
$CH_3C(O)CH_3$	Liquid Water	$H_2O(l)$	260–285	0.07–0.01*	2	39
$HC(O)OH$	Liquid Water	$H_2O(l)$	260–291	0.10–0.02*	2	40

Gaseous Species	Surface Type	Surface Composition	T(K)	α	Uncertainty Factor	Notes
CH$_3$C(O)OH	Liquid Water	H$_2$O(l)	260–291	0.15–0.03*	2	41
Cl$_2$	Water Ice	H$_2$O(s)	200	See Note		42
OClO	Water Ice	H$_2$O(s)	100,189, 200	See Note		43
HCl	Water Ice	H$_2$O(s)	191– 211	0.3	3	44
	Liquid Water	H$_2$O(l)	274	0.2*	2	45
	Nitric Acid Ice	HNO$_3$ • 3H$_2$O(s)	191– 211	0.3	3	46
	Sulfuric Acid	H$_2$SO$_4$ • nH$_2$O(l)	283	0.15*	2	47
		(n≥8, ≤40 wt.% H$_2$SO$_4$)	218	>0.005*		
		(n<8, >40 wt.% H$_2$SO$_4$)	†	†	†	
	Sulfuric Acid Tetrahydrate	H$_2$SO$_4$ • 4H$_2$O(s)	192–201	See Note		48
CCl$_2$O	Liquid Water	H$_2$O(l)	260–290	See Note		49
CCl$_3$CClO	Liquid Water	H$_2$O(l)	260–290	See Note		49
HBr	Water Ice	H$_2$O(s)	200	> 0.2		50
	Nitric Acid Ice	HNO$_3$ • 3H$_2$O(s)	200	> 0.3		50
HOBr	Sulfuric Acid	H$_2$O(s)	190–239	>10^{-3}		51
		H$_2$SO$_4$ in H$_2$O(l) (58 wt. % H$_2$SO$_4$)	228	>0.05‡		52
CHBr$_3$	Water Ice	H$_2$O(l)	220	See Note		53
	Sulfuric Acid	H$_2$SO$_4$ • nH$_2$O(l) (97 wt.% H$_2$SO$_4$)	220	>3 × 10^{-3}‡		53
HOI	Sulfuric Acid	H$_2$SO$_4$ • nH$_2$O(l)				54
		(40 wt % H$_2$SO$_4$)	195	0.07	3	
		(40 wt % H$_2$SO$_4$)	205	0.03	3	
		(40 wt % H$_2$SO$_4$)	212	0.04	3	
		(50 wt % H$_2$SO$_4$)	222–224	0.02	3	
		(70 wt % H$_2$SO$_4$)	230–232	0.02	3	
		(70 wt % H$_2$SO$_4$)	252	0.02	3	
HF	Water Ice	H$_2$O(s)	200	See Note		55
	Nitric Acid Ice	HNO$_3$ • 3H$_2$O(s)	200	See Note		55
CF$_2$O	Water Ice	H$_2$O(s)	192	See Note		56
	Liquid Water	H$_2$O(l)	260–290	See Note		49
	Nitric Acid Ice	HNO$_3$ • 3H$_2$O(s)	192	See Note		56
	Sulfuric Acid	H$_2$SO$_4$ • nH$_2$O(l)	215–230			
		(40 wt.% H$_2$SO$_4$)		>3 × 10^{-6}‡		56
		(60 wt.% H$_2$SO$_4$)		>6 × 10^{-5}‡		56
CF$_3$CFO	Liquid Water	H$_2$O(l)	260–290	See Note		49
CF$_3$COOH	Liquid Water	H$_2$O(l)	263–288	0.2–0.1*	2	57
CF$_3$CClO	Liquid Water	H$_2$O(l)	260–290	See Note		49
SO$_2$	Liquid Water	H$_2$O(l)	260–292	0.11	2	58
	Sulfuric Acid	H$_2$SO$_4$ • nH$_2$O(l) (97 wt.% H$_2$SO$_4$)	298	See Note		59
H$_2$SO$_4$	Sulfuric Acid	H$_2$SO$_4$ • nH$_2$O(l) (50–98 wt.% H$_2$SO$_4$)	200–300	0.7	1.4	60
CH$_3$S(O)CH$_3$	Liquid Water	H$_2$O(l)	262–281	0.16–0.08*	2	61
CH$_3$S(O$_2$)CH$_3$	Liquid Water	H$_2$O(l)	262–281	0.27–0.08*	2	61
CH$_3$S(O$_2$)OH	Liquid Water	H$_2$O(l)	264–278	0.17–0.11*	2	61

* Varies with T, see Notes
† No data—all measurements; limited by HCl solubility
‡ May be affected by surface saturation

5.11 Notes to Table 5-1

1. O on H$_2$SO$_4$ • nH$_2$O—Knudsen cell experiment of Baldwin and Golden [27] measured an uptake coefficient limit of <10^{-6}; this result probably cannot be equated with an accommodation coefficient due to surface saturation.

2. O$_3$ on H$_2$O(s) and HNO$_3$ • nH$_2$O—Undoped ice surfaces saturate too quickly for reliable measurements. When ice is doped with Na$_2$SO$_3$ to chemically remove absorbed O$_3$ the apparent α increases to 1×10^{-2} (0.1M) or up to 4×10^{-2} (1M) (Dlugokencky and Ravishankara [105]). Limit of $\gamma < 10^{-6}$ for undoped ice is consistent with

earlier measurement by Leu [233] of $\leq 1 \times 10^{-4}$ and with $< 6 \times 10^{-5}$ obtained by Kenner et al. [214]. Dlugokencky and Ravishankara also measured the tabulated value of an uptake coefficient for O_3 on a NAT "like" surface, but the data were difficult to reproduce and the surfaces were not well characterized. Kenner et al. also measured a lower limit for an uptake coefficient of 8×10^{-5} on NAT at 183 K, but this measurement is also certainly limited by surface saturation.

3. O_3 on $H_2O(l)$—Utter et al. [335] used a wetted wall flow tube technique with various chemical scavengers to measure a lower limit for α of 2×10^{-3}. The stopped flow measurement technique using an $SO_3^=$ scavenger (Tang and Lee [327]) is subject to saturation effects, so their quoted α of 5.3×10^{-4} is also taken as a lower limit.

4. O_3 on $H_2SO_4 \cdot nH_2O$—Flow tube measurements (Dlugokencky and Ravishankara [105]) of an uptake coefficient limit of $<10^{-6}$ on both 50 and 97 wt. % H_2SO_4 surfaces are consistent with earlier, but probably less quantitative, static systems measurements of Olszyna et al. [271] and aerosol chamber measurements of Harker and Ho [169], who report uptake coefficients of the order 10^{-8} or less for a variety of sulfuric acid concentrations and temperatures. In these earlier experiments, doping the H_2SO_4 with Ni^{2+}, Cr^{2+}, Al^{3+}, Fe^{3+}, and NH_4^+ (Olszyna et al. [271]) or Al_2O_3 or Fe_2O_3 (Harker and Ho [169]) did not significantly increase measured O_3 loss. An upper limit of 1×10^{-6} was also reported by Baldwin and Golden [26]for 97 wt % H_2SO_4 at 295 K. Il'in et al. [187] performed static tube reactor measurements on 98 wt. % sulfuric acid at 239, 258, 273 K measuring uptake coefficients between 1.2 and 1.75×10^{-6}. Although these measurements are slightly larger than the limits in the other studies, uptake values this small are extremely hard to quantify and these measurements are not seen to be in serious disagreement with other studies finding slightly lower upper limits. All measurements are subject to solubility limitations and probably do not reflect true limits on mass accommodation.

5. OH on $H_2O(s)$—Cooper and Abbatt[91] analyzed uptake rates in a wall-coated flow tube to determine an initial $\gamma \sim 0.1$ over the temperature range of 205 – 230 K. Uptake coefficients decreased at longer exposure times, indicating surface saturation. These data indicate that α is at least 0.1 and possibly much larger. This is confirmed by an earlier experiment using a coated insert/flow tube technique by Gershenzon et al. [136], which yielded $\alpha > 0.4$ at 253 K.

6. OH on $H_2O(l)$—see Note for HO_2 on $H_2O(l)$. The OH and HO_2 measurements of Hanson et al. [151] are subject to the same analysis issues.

7. OH on $H_2SO_4 \cdot nH_2O$—See Note for HO_2 on $H_2O(l)$ for measurement (28 wt.% H_2SO_4) by Hanson et al. [151] and Note for O on H_2SO_4 for measurement (97 wt. % H_2SO_4) by Baldwin and Golden [27].

8. OH on $Al_2O_3(s)$—Measured value is from flow tube experiment with native oxide on aluminum as the active surface. An uptake coefficient of 0.4 ± 0.2 independent of temperature over the range of 253–348 K was measured (Gershenzon et al. [136]).

9. HO_2 on $H_2O(l)$—Determination of α in liquid-wall flow tube (Hanson et al. [151]) is dependent on gas-phase diffusion corrections; measured limit ($\alpha >0.02$) is consistent with $\alpha = 1$. In the aqueous salt aerosol measurements of Mozurkewich et al. [264], HO_2 was chemically scavenged by Cu^{++} from added $CuSO_4$ to avoid Henry's law constraints; the measured limit of >0.2 is also consistent with $\alpha = 1$.

10. HO_2 on NaCl(s) and KCl(s)—Based on measured values of $\gamma = 1.8 \times 10^{-2}$ for KCl and 1.6×10^{-2} for NaCl, both at 295 K by Gershenzon et al. [135] supplementing an earlier value of $\gamma - 8 \times 10^{-3}$ measured by Gershenzon and Purmal [137]. Results have not been calibrated with a competitive technique.

11. H_2O on $H_2O(s)$—Measurements are available from Leu [232] giving 0.3 (+0.7, –0.1) at 200 K and Haynes et al. [172] (1.06 ± 0.1 to 0.65 ± 0.08) from 20 to 185 K. Brown et al.[59] used molecular beam reflection techniques to measure a value of $\alpha = 0.99 \pm 0.03$ between 85 and 150 K and optical interference methods to obtain $\alpha = 0.97 \pm 0.10$ between 97 and 145 K.

12. H_2O on $HNO_3/H_2O(l)$—Rudolf and Wagner[302] used aerosol expansion chamber techniques to illustrate that on liquid water/nitric acid aerosols α is greater than 0.3 and is consistent with 1.0 at 278 K.

13. H_2O on $HNO_3 \cdot nH_2O(s)$—Middlebrook et al. [257] measured an uptake coefficient of .002 for water vapor co-depositing with nitric acid over NAT at 197 K.

14. H_2O on $H_2SO_4 \cdot nH_2O$—Baldwin and Golden [26] measured $\gamma \sim 2 \times 10^{-3}$, which is almost certainly affected by surface saturation. See Note for H_2O_2 on $H_2SO_4 \cdot nH_2O$.

15. H_2O on NaCl(s)—Fenter et al. [118] used Knudsen cell/mass spectrometry methods to measure $\gamma < 2 \times 10^4$ for H_2O(g) uptake on NaCl powders, an observation confirmed by Beichert and Finlayson-Pitts [46], who found
$\gamma < 1 \times 10^{-5}$. However, Dai et al. [94] used FTIR spectroscopy on NaCl crystallite films at 240 and 296 K to determine that a water adlayer does adhere to dry salt and that a small fraction of surface sites (<1%) cause H_2O dissociation. It is likely that the measurements of Fenter et al. and Beichert and Finlayson-Pitts were affected by surface saturation.

16. H_2O on NaCl(aq)—Fung et al.[130] used Mie resonance scattering techniques to quantify aqueous NaCl droplet growth (5.8 to 7.8 μm), yielding fitted values of $\alpha > 0.5$ and consistent with 1.0.

17. H_2O_2 on H_2O(l)—Measured accommodation coefficient (Worsnop et al. [359]) has a strong negative temperature dependence over the measured range of 260–292 K, with $\alpha = 0.3$ at 260 K decreasing to 0.1 at 292 K.

18. H_2O_2 on $H_2SO_4 \cdot nH_2O$—Knudsen cell uptake measurements are subject to surface saturation, thus uptake coefficient value of 7.8×10^{-4} quoted by Baldwin and Golden [26] is almost certainly a lower limit for α. This effect is probably also responsible for the lack of measured uptake ($\gamma < 10^{-6}$) for NO, NO_2, SO_2, Cl_2, and other species reported in this reference and Baldwin and Golden [27].

19. NO on H_2O(s)—NO data (Leu [233], Saastad et al. [303]) subject to same concerns as NO_2. See Note for NO_2 on H_2O(s).

20. NO on $H_2SO_4 \cdot nH_2O$—See Notes for H_2O_2 on $H_2SO_4 \cdot nH_2SO_4$ and NO_2 on $H_2SO_4 \cdot nH_2O$. NO is subject to the same concerns as NO_2 for both reported measurements (Saastad et al. [303]; Baldwin and Golden [26]).

21. NO_2 on H_2O(s)—In the absence of a chemical sink, Leu [233] measured no sustained uptake of NO_2 on ice yielding an apparent $\alpha \leq 1 \times 10^{-4}$. Saastad et al. [303] measured a lower limit of 5×10^{-5} for temperatures between 193 and 243 K. However these values are probably influenced by surface saturation.

22. HONO on H_2O(s)—Fenter and Rossi [120] measured reversible uptake on water ice between 180 and 200 K using a Knudsen cell technique. An initial uptake coefficient of 1×10^{-3} suggests that α equals or exceeds this value. Chu et al. [73] used a cylindrical flow reactor to measure the uptake coefficient as a function of temperature, obtaining values ranging from 3.7×10^{-3} at 178 K to 6.4×10^{-4} at 200 K, in good agreement with the results of Fenter and Rossi. On the other hand, Chu et al. report significantly lower values after correction for the effects of surface porosity, i.e. 1.4×10^{-4} at 178 K and 1.3×10^{-5} at 200 K (see Keyser et al. [218]).

23. HNO_3 on H_2O(s)—Leu [232] reports 0.3 (+0.7, –0.1). Some additional uncertainty is introduced by effective ice surface area in fast-flow measurement (see Keyser et al. [218]). Hanson [148] measured an uptake coefficient of > 0.3 at 191.5 and 200 K. Aguzzi and Rossi [9] measured an uptake coefficient of 0.3 over the temperature range from 180 to 190 K, the value decreasing at T < 195 K with an exponential temperature dependence of $-(3400 \pm 500)/T$. They attributed this change to an increasing evaporation rate, concluding that the accommodation coefficient most likely remains large. Abbatt [4] measured equilibrium uptake values at 208–248 K on the order of 1 to 3×10^{14} molecule cm^{-2}. Zondlo et al. [374] report the formation of a supercooled H_2O/HNO_3 liquid layer at 185 K, forming NAT or NAD only after decreasing the relative humidity below the ice frost point.

24. HNO_3 on H_2O(l)—Measured α has a strong negative temperature dependence varying from 0.19 ± 0.02 at 268 K to 0.07 ± 0.02 at 293 K (Van Doren et al. [338]). Ponche et al. [276] measured an accommodation coefficient of 0.05 ± 0.01 at 297 K.

25. HNO_3 on $HNO_3 \cdot nH_2O$(s)—Hanson [148] measured uptake coefficients of >0.3 and >0.2 on NAT surfaces at 191 K and 200 K, respectively. Middlebrook et al. [257] measured an uptake coefficient of 0.7 on NAT at 197 K under conditions where both nitric acid and water vapor were co-depositing.

26. HNO_3 on $HNO_3 \cdot nH_2O$(l)—Rudolf and Wagner [302] used aerosol expansion chamber techniques to deduce that α for HNO_3 on 278 K H_2O/HNO_3 droplets is > 0.3 and probably close to 1. The consistency of this value with smaller (~0.2) values measured for uptake on pure water by Van Doren et al. [338] is unclear, since the mechanism of co-condensation is unknown and the composition of the surface in the aerosol expansion chamber experiments may be kinetically controlled and has not been well determined.

27. HNO$_3$ on H$_2$SO$_4$•nH$_2$O and H$_2$SO$_4$ • 4H$_2$O(s)—Initial uptake at 73 wt. % H$_2$SO$_4$ allows a measurement of $\alpha = 0.11 \pm 0.01$ at 283 K (Van Doren et al. [338]). This value is expected to increase at lower temperatures, in a manner similar to H$_2$O(1) uptake (Van Doren et al. [337]). Total HNO$_3$ uptake is subject to Henry's law solubility constraints, even at stratospheric temperatures (Reihs et al. [283]). Solubility limitations also affected the earlier "sticking coefficient" measurements of Tolbert et al. [332] for 75 wt % H$_2$SO$_4$ at 230 K. Hanson [148] measured an uptake coefficient of >0.3 for frozen 57.7 wt. % sulfuric acid at 191.5 and 200 K. Baldwin and Golden [26] reported a lower limit of 2.4×10^{-4} on 97 wt. % H$_2$SO$_4$ at 295 K, also reflecting solubility limits. Iraci et al. [191] monitored nitric acid trihydrate growth on sulfuric acid tetrahydrate with infrared techniques, measuring HNO$_3$ uptake coefficient limits of >0.03 at 192.5 K and >0.08 at 192 K. These measurements involved co-deposition of water vapor.

28. HO$_2$NO$_2$ on H$_2$O(s)—Li et al. [237] measured an uptake coefficient of 0.15 ±0.10; uptake may be limited by surface saturation.

29. HO$_2$NO$_2$ on H$_2$SO$_4$•nH$_2$O(l)—Baldwin and Golden [26] measured $\gamma = 2.7 \times 10^{-5,}$ which is probably solubility limited; see Note for H$_2$O$_2$ on H$_2$SO$_4$ • nH$_2$O.

30. NH$_3$ on H$_2$O(l)—Ponche et al. [276] used a droplet train technique to obtain $\alpha = (9.7 \pm 0.9) \times 10^{-2}$ at 290 K, and Bongartz et al.[57] used a liquid jet technique to obtain $\alpha = 4.0 (+3.0, -0.05) \times 10^{-2}$. Earlier levitated droplet evaporation experiments [328] on NH$_4$Cl obtained a larger evaporation coefficient of $\alpha = 0.29 \pm 0.03$, which is discounted because of the indirect nature of the experiment.

31. CO$_2$ on H$_2$O(l)—Noyes et al.[270] used a dynamic stirring technique to monitor pressure decreases in a closed cylinder. They inferred $\alpha = (5.5 \pm 0.5) \times 10^{-8}$ at 293 K. This technique is uncalibrated against more widely used procedures and probably suffers from surface saturation effects. Measured α is probably many orders of magnitude too small.

32. CH$_3$OH on H$_2$O(l)—Jayne et al. [197] measured uptake from 260–291 K and derived accommodation coefficients fitting $\alpha/(1-\alpha) = \exp(-\Delta G^{\ddagger}_{obs}/RT)$, where $\Delta G^{\ddagger}_{obs} = -8.0$ kcal/mol + 34.9 cal mol^{-1} K^{-1} T(K).

33. CH$_3$CH$_2$OH on H$_2$O(l)—Jayne et al. [197] measured uptake from 260–291 K and derived accommodation coefficients fitting $\alpha/(1-\alpha) = \exp(-\Delta G^{\ddagger}_{obs}/RT)$, where $\Delta G^{\ddagger}_{obs} = -11.0$ kcal/mol + 46.2 cal mol^{-1} K^{-1} T(K). Similar, but somewhat larger values were reported for chloro-, bromo-, and iodo-ethanols.

34. CH$_3$CH$_2$CH$_2$OH and CH$_3$CH(OH)CH$_3$ on H$_2$O(l)—Jayne et al. [197] measured uptake coefficients between 260 and 291 K and derived accommodation coefficients fitting $\alpha/(1-\alpha) = \exp(-\Delta G^{\ddagger}_{obs}/RT)$, where $\Delta G^{\ddagger}_{obs} = -9.2$ kcal mol^{-1} + 40.9 cal mol^{-1} K^{-1} T(K) for 1-propanol and -9.1 kcal mol^{-1} + 43.0 cal mol^{-1} K^{-1} T(K) for 2-propanol. Similar data for t-butanol were also reported.

35. HOCH$_2$CH$_2$OH on H$_2$O(l)—Jayne et al. [197] measured uptake coefficients for ethylene gycol between 260 and 291 K and derived accommodation coefficients fitting $\alpha/(1 - \alpha) = \exp(-\Delta G^{\ddagger}_{obs}/RT)$, where $\Delta G^{\ddagger}_{obs} = -5.3$ kcal mol^{-1} + 24.5 cal mol^{-1} K^{-1} T(K).

36. CH$_2$O + H$_2$O(l), H$_2$SO$_4$ • mHNO$_3$ • nH$_2$O(l)—Jayne et al.[200] report uptake measurements for 0 – 85 wt % H$_2$SO$_4$ and 0 – 54 wt% HNO$_3$ over a temperature range of 241–300 K. Measured uptake coefficients vary from 0.0027–0.027, increasing with H$^+$ activity (Jayne et al ([200]; Tolbert et al., [330]), and with increasing pH above 7 (Jayne et al., [198]). Reversible uptake is solubility limited through reactions to form H$_2$C(OH)$_2$ and CH$_3$O$^+$. A model of uptake kinetics (Jayne et al., [200]) is consistent with $\gamma = 0.04 \pm 0.01$ for all compositions. A chemisorbed surface complex dominates uptake at 10 – 20 wt % H$_2$SO$_4$, and CH$_3$O$^+$ formation dominates above 20 wt % (Tolbert et al., [330]; Jayne et al. [200], Iraci and Tolbert [192]). Low temperature (197–214 K) uptake studies by Iraci and Tolbert [192] confirm that uptake is solubility limited for uptake coefficients in the 10^{-3} to 10^{-2} range even at low temperatures. These chemical mechanisms allow γ to greatly exceed α for strong acidic and basic solutions. A full uptake model for acid solutions is presented in Jayne et al. [200], and for basic solutions in Jayne et al. [198]. XPS surface analysis by Fairbrother and Somorjai [114] failed to see CH$_3$O$^+$ surface species reported by Jayne et al.; however, their sensitivity of 1% of surface coverage is too poor to see the predicted amounts of the surface species.

37. CH$_3$O$_2$ + NaCl(s)—Gershenzon et al. [135] measured the uptake of CH$_3$O$_2$ on crystalline NaCl(s) in a central rod flow apparatus. They determined a value of $\gamma = (4 \pm 1) \times 10^{-3}$ at 296 K, suggesting that $\alpha \geq 4 \times 10^{-3}$.

38. CH$_3$CHO on H$_2$O(l)—Jayne et al. [198] measured a lower accommodation coefficient limit of > 0.03 at 267 K. Uptake can be limited by Henry's law and hydrolysis kinetics effects—see reference.

39. $CH_3C(O)CH_3$ on $H_2O(l)$—Duan et al. [108] measured uptake between 260 and 285 K, deriving $\alpha = 0.066$ at the lower temperature and 0.013 at the higher, with several values measured in between. Measured values fit $\alpha/(1-\alpha) = \exp(-\Delta G^{\ddagger}_{obs}/RT)$, where $\Delta G^{\ddagger}_{obs} = -12.7$ kcal/mol $+ 53.6$ cal mol^{-1} K^{-1} T(K).

40. $HC(O)OH$ on $H_2O(l)$—Jayne et al. [197] measured uptake coefficients for formic acid between 260 and 291 K and derived accommodation coefficients fitting $\alpha/(1-\alpha) = \exp(-\Delta G^{\ddagger}_{obs}/RT)$, where $\Delta G^{\ddagger}_{obs} = -7.9$ kcal mol^{-1} $+ 34.9$ cal mol^{-1} K^{-1} T(K).

41. $CH_3C(O)OH$ on $H_2O(l)$—Jayne et al. [197] measured uptake coefficients for acetic acid between 260 and 291 K and derived an accommodation coefficient fitting $\alpha/(1-\alpha) = \exp(-\Delta G^{\ddagger}_{obs}/RT)$, where $\Delta G^{\ddagger}_{obs} = -8.1$ kcal mol^{-1} $+ 34.9$ cal mol^{-1} K^{-1} T(K).

42. Cl_2 on $H_2O(s)$—Measurement of Leu [232] yielded a limit of $<1 \times 10^{-4}$ for Cl_2 and is subject to same concern as NO_2 (see Note) A similar limit of $<5 \times 10^{-5}$ has been measured by Kenner et al. [214], which is also probably limited by surface saturation.

43. $OClO + H_2O(s)$—Brown et al.[60] and Graham et al.[142] used complementary ultra high-vacuum (UHV) and coated-wall flow tube techniques to show sub-monolayer reversible absorption of OClO on water ice at 100 K (UHV) and 189 and 200 K (flow tube). No kinetic data are available at stratospheric temperatures but the mass accommodation coefficient for 100 K ice surfaces is near unity, with values of 0.8 ± 0.2 reported for amorphous ice and 0.6 ± 0.2 for crystalline ice [142].

44. HCl on $H_2O(s)$—Leu [232] (0.4; +0.6, −0.2) and Hanson and Ravishankara, [158] ($\alpha \geq 0.3$) are in reasonable agreement at stratospheric ice temperatures. More recently, a great deal of experimental effort (Abbatt et al. [5], Koehler et al. [225], Chu et al. [75], Graham and Roberts [140], Graham and Roberts[141]; Rieley et al.[286]) has gone into understanding the uptake of HCl by ice surfaces. Rieley et al. measured $\alpha = 0.95 \pm 0.05$ at 80–120 K. Water ice at stratospheric temperatures can take up a large fraction of a monolayer even at HCl partial pressures typical of the stratosphere. Both the thermodynamic and spectroscopic properties of this absorbed HCl indicate that it has dissociated to ions, forms ionic hydrates, and is highly reactive. These experimental results contrast with initial theoretical calculations that predicted undissociated HCl hydrogen bonded to the ice surface and a very small adsorption probability at stratospheric temperatures (Kroes and Clary [228]); more recent simulations result in higher adsorption energies and theoretical accommodation coefficients of one for 190-K surfaces (Wang and Clary [346]). Recent molecular dynamics calculations by Gertner and Hynes[138] also show that ionic absorption is thermodynamically favorable by about 5 kcal/mole. At HCl partial pressures significantly above those typical of the stratosphere, a liquid surface layer forms on the ice, greatly enhancing the total amount of HCl that the surface can absorb.

45. HCl on $H_2O(l)$—Recommendation is based on Van Doren et al. [337]. Measured α's decrease from 0.18 ± 0.02 at 274 K to 0.064 ± 0.01 at 294 K, demonstrating strong negative temperature dependence. Tang and Munkelwitz [328] have measured a larger (0.45 ± 0.4) HCl evaporation coefficient for an aqueous NH_4Cl droplet at 299 K.

46. HCl on $HNO_3 \cdot nH_2O$—There was previously severe disagreement between Hanson and Ravishankara [158] ($\alpha \geq 0.3$) for NAT (54 wt. % HNO_3), and Leu and coworkers (Moore et al. [262], Leu et al. [234]). However, subsequent experiments at lower HCl concentrations by Leu and coworkers (Chu et al. [75]) as well as Abbatt and Molina [6] are generally consistent with Hanson and Ravishankara. In particular, Abbatt and Molina [6] report a large uptake coefficient ($\alpha > 0.2$). The measurements of Hanson and Ravishankara are consistent with $\alpha = 1$. The experiments at stratospherically representative HCl concentrations show that HNO_3-rich NAT surfaces adsorb significantly less HCl than H_2O-rich surfaces.

47. HCl on $H_2SO_4 \cdot nH_2O$—Measurements by Watson et al. [348] at 284 K show $\alpha = 0.15 \pm 0.01$ independent of n for $n \geq 8$. Experimental uptake and, therefore, apparent α falls off for $n \leq 8$ (≥ 40 wt. % H_2SO_4). This behavior is also observed at stratospheric temperature (218 K) by Hanson and Ravishankara [158]. More recent measurements by Robinson et al. [294]extend mass accommodation measurements to lower temperatures, yielding significantly higher values. Solubility constraints also controlled earlier low temperature uptake measurements of Tolbert et al. [332]. A review of the most recent solubility data is presented in Table 5-5.

48. HCl on $H_2SO_4 \cdot 4H_2O(s)$—Uptake is a strong function of temperature and water vapor partial pressure (relative humidity) (Zhang et al. [370]), both of which affect adsorbed surface water.

49. Halocarbonyls on $H_2O(l)$—Uptake is limited by Henry's law solubility and hydrolysis rate constants (De Bruyn et al. [98,100] and Georg et al. [131,133]. See Table 5-4 and Table 5-5.

50. HBr on $H_2O(s)$ and $HNO_3 \cdot nH_2O$—Hanson and Ravishankara [159,163] have reported large uptake coefficients for HBr on 200-K ice and NAT. Lower limits of >0.3 and >0.2 for ice are reported in the two referenced publications, respectively, and a limit of >0.3 is reported for NAT. No surface saturation was observed, leading to the supposition that HBr, like HCl, dissociates to ions on ice surfaces at stratospheric temperatures. Abbatt [1] measured an uptake coefficient lower limit of >0.03 on water ice at 228 K consistent with Hanson and Ravishankara. Rieley et al. [286] measured an α of 1.0 ± 0.05 for water ice at 80–120 K. Flückiger et al. [124] report α values of ~0.2 at 210 K, increasing to ~0.3 at 190 K, while Percival et al. [274] measured an α of 0.03 ± 0.005 for water ice at T > 212 K, and α > 0.1 at T< 212 K, attributing the apparent increase in the uptake coefficient to an increase in the surface area of the ice. More definitive experiments will need to be carried out to resolve the discrepancy. Hudson et al. [183] report $\alpha = 0.61 \pm 0.06$ at 140 K, and
$\alpha = 0.24 \pm 0.05$ at 100 K, for HBr pressures ranging from 3×10^{-8} to 1.4×10^{-7} Torr. Equilibrium HBr coverages for ice are reported by Chu and Heron [74] at 188 and 195 K, and by Chu and Chu [71] at 180–220 K. The latter authors also report the formation of various solid HBr hydrates.

51. HOBr on $H_2O(s)$—Abbatt [1] measured an uptake coefficient for water ice of 2×10^{-3} at 228 K. Chu and Chu [71] report an uptake coefficient corrected for porosity effects in the range 0.11 to 0.007 at 190–218 K, with an exponential temperature dependence of $(3809 \pm 76)/T$, and in the range 2×10^{-3} to 6×10^{-4} at 223–239 K, with an exponential temperature dependence of $(4658 \pm 456)/T$. Chaix et al. [69] measured the uptake coefficient as a function of temperature on three different types of water-ice, obtaining values ranging from ~0.3 at 185 K to ~0.03 at 205 K, with an exponential temperature dependence of $(4900 \pm 500)/T$. The three sets of results are in reasonable agreement with each other, and the temperature dependence is attributed predominantly to changes in the evaporation rate.

52. HOBr on $H_2SO_4 \cdot nH_2O(l)$—Abbatt [1] measured an uptake coefficient of 0.06 ± 0.02 by measuring HOBr gas phase loss at 228 K. This result may well be a lower limit due to surface saturation effects.

53. $CHBr_3$ on $H_2O(s)$ and $H_2SO_4 \cdot nH_2O(l)$—Hanson and Ravishankara [163] investigated the uptake of bromoform on ice and 58 wt.% sulfuric acid at 220 K. No uptake on ice was observed, with a measured uptake coefficient of $<6 \times 10^{-5}$. Reversible uptake by the sulfuric acid surface was observed with an initial uptake coefficient of $>3 \times 10^{-3}$; both measurements are probably limited by surface saturation.

54. HOI on $H_2SO_4 \cdot nH_2O$—Knudsen cell studies by Allanic and Rossi [18] measured uptake at several temperatures for 40, 50, and 70 acid wt. %. Time dependent studies show no sign of saturation, so uptake coefficients should correspond to mass accommodation coefficients. Some acid concentration data in the table have been averaged for similar temperatures and rounded to one significant figure. An uncertainty factor of three has been assigned due to the relatively small number of temperature/concentration points studied and a lack of confirming studies from other laboratories. The authors note evidence of HOI disproportionation to form I_2, however, this second order reaction is unlikely to occur under atmospheric conditions.

55. HF on $H_2O(s)$ and $HNO_3 \cdot nH_2O(s)$—Hanson and Ravishankara [159] attempted to measure the uptake of HF by 200 K water ice and NAT surfaces but were unable to observe measurable adsorption. They surmise that, unlike HCl and HBr, HF does not dissociate to ions on ice or NAT surfaces at 200 K. Lack of measurable uptake is probably due to surface saturation.

56. CF_2O on $H_2O(s)$, $HNO_3 \cdot nH_2O$ and $H_2SO_4 \cdot nH_2O$—Uptake coefficient measurements by Hanson and Ravishankara [156] on stratospheric surfaces are probably subject to surface and/or bulk saturation effects and may not represent accommodation coefficient measurements, particularly the lower limits of $>3 \times 10^{-6}$ reported for water and nitric acid ices.

57. CF_3COOH on $H_2O(l)$—Hu et al. [182] measured mass accommodation coefficients for five haloacetic acids, including trifluoroacetic acid (TFA); the others were mono-, di-, trichloro-, and chlorodifluoro-acetic acids. All displayed negative temperature dependence and values for α of about 0.1 at 273 K.

58. SO_2 on $H_2O(1)$—Measured α of 0.11 ± 0.02 has no significant temperature variation over a temperature range of 260–292 K (Worsnop et al. [359]). Ponche et al. [276] measured 0.13 ± 0.01 at 298 K, in agreement with the earlier measurement. Shimono and Koda [314] estimated an α of 0.2 at 293.5 K from analysis of pH-dependent uptake coefficients in a novel liquid impingement technique that has not been calibrated with

other gases. Donaldson et al. [106] have used second harmonic generation spectroscopy to detect a chemisorbed SO_2 surface species which was predicted from earlier uptake measurements by Jayne et al.[196]; this surface complex may play a role in SO_2 heterogeneous reactions on aqueous surfaces.

59. SO_2 on $H_2SO_4 \cdot nH_2O$—See Note for H_2O_2 on $H_2SO_4 \cdot nH_2O$.

60. H_2SO_4 on $H_2SO_4 \cdot nH_2O$—Poschl et al. [277] measured $0.43 < \alpha < 1.0$ for 73–98 wt. % H_2SO_4 at 303 K in a wetted wall flow tube. Lower temperatures and acid concentrations would be expected to lead to larger values of α. As discussed in Poschl et al. [277] this contradicts an indirect measurement of $0.02 < \alpha < 0.09$ at 42.5 wt. % at 298 K by Van Dingenen and Raes [336] in a photochemical aerosol reactor. The Poschl et al. [277] result is consistent with room temperature α values very near that measured for $(NH_4)_2SO_4$ particles in an aerosol flow reactor by Jefferson et al. [201].

61. $CH_3S(O)CH_3$, $CH_3S(O_2)CH_3$ and $CH_3S(O_2)OH$ on $H_2O(l)$—De Bruyn et al. [99] measured uptake over the temperature range ~262–281 K and derived accommodation coefficients fitting $\alpha / (1 - \alpha) = \exp(-\Delta G^{\ddagger}_{obs}/RT)$, where $\Delta G^{\ddagger}_{obs} =$

-0.12 kcal molecule^{-1} + 23.1 cal molecule^{-1} K^{-1} T(K) for dimethylsulfoxide

-10.7 kcal molecule^{-1} + 43.0 cal molecule^{-1} K^{-1} T(K) for dimethylsulfone

-3.50 kcal molecule^{-1} + 16.7 cal molecule^{-1} K^{-1} T(K) for methanesulfonic acid.

5.12   Gas/Surface Reaction Probabilities for Surfaces Other Than Soot.

Table 5-2. Gas/Surface Reaction Probabilities (γ) for Surfaces Other Than Soot.

Gaseous Species	Surface Type	Surface Composition	T(K)	γ	Uncertainty Factor	Notes
O_3 + Surface → Products						
O_3	Alumina	$Al_2O_3(s)$	210–300	See Note		1
	Sodium Chloride	$NaCl(s)$	300	$>2 \times 15^{-10}$		1
OH + Surface →Products						
OH	Water Ice	$H_2O(s)$	205–230	>0.01		2
	Hydrochloric Acid	$HCl \cdot nH_2O(l)$	220	>0.2		3
	Nitric Acid Ice	$HNO_3 \cdot 3HzO(s)$	200–228	>0.2		4
	Sulfuric Acid	$H_2SO_4 \cdot nH_2O(l)$	200–298	>0.2		5
	Sodium Chloride	$NaCl(s)$	245–339	1.2×10^{-5} exp 1750/T	3	6
HO_2 + Surface →Products						
	Water Ice	$H_2O(s)$	223	0.025	3	7
	Sulfuric Acid	$H_2SO4 \cdot nH_2O(l)$				7
		(28 wt %)	275	>0.07		
		(55 wt %)	223	>0.05		
		(80–96 wt %)	243	>0.2		
$2NO_2 + H_2O(l)$ →HONO + HNO_3						
NO_2	Liquid Water	$H_2O(l)$		See Note		8
	Sulfuric Acid	$H_2SO_4 \cdot nH_2O$ (40–98 wt. %)	250–325	5×10^{-7}	3	9
$2NO_2 + NaCl(s)$ →ClNO + $NaNO_3$						
$2NO_2 + NaBr(s)$ →BrNO + $NaNO_3$						
NO_2	Sodium Chloride	$NaCl(s)$	298	See Note		10
	Sodium Bromide	$NaBr(s)$	298	See Note		10
$NO_3 + H_2O$ →HNO_3 + OH						
NO_3	Water Ice	$H_2O(s)$	170–200	$<10^{-3}$		11
	Liquid Water	$H_2O(l)$	273	2×10^{-4}	20	12
$N_2O_5 + H_2O$ →$2HNO_3$						
N_2O_5	Water Ice	$H_2O(s)$	188–195	0.02	2	13
	Liquid Water	$H_2O(l)$	260–295	See Note	See Note	14
	Nitric Acid Ice	$HNO_3 \cdot 3H_2O(s)$	200	4×10^{-4}	3	15
	Sulfuric Acid	$H_2SO_4 \cdot nH_2O(l)$	195–300	See Note*	See Note	16
	Sulfuric Acid Monohydrate	$H_2SO_4 \cdot H_2O(s)$	200–300	See Note	3	17
	Sulfuric Acid Tetrahydrate	$H_2SO_4 \cdot 4H_2O(s)$	195–207	0.006	2	18
	Ternary Acid	$H_2SO_4 \cdot nHNO_3 \cdot nH_2O(l)$	195–218	See Note		16
$N_2O_5 + HCl(s)$ → $ClNO_2 + HNO_3$						
N_2O_5	Water Ice	$H_2O(s) \cdot HCl(s)$	190–220	0.03	See Note	19
	Nitric Acid Ice	$HNO_3 \cdot 3H_2O(s) \cdot HCl(s)$	200	0.003	2	20
	Sulfuric Acid Monohydrate	$H_2SO_4 \cdot H_2O(s)$	195	$<1 \times 10^{-4}$		21
$N_2O_5 + NaCl(s)$ → $ClNO_2 + NaNO_3(s)$						
N_2O_5	Sodium Chloride	$NaCl(s)$	–300	5×10^{-4}	20	22
		$NaCl(aq)$		>0.02		22
$N_2O_5 + HBr(s)$ →$BrNO_2 + HNO_3$						
N_2O_5	Water Ice	H_2O	180–200	See Note		23
	Nitric Acid Ice	$HNO_3 \cdot 3H_2O(s)$	200	0.005	10	24
$N_2O_5 + MBr(s)$ →Products						
N_2O_5	Sodium Bromide	$NaBr(s)$	~300		See Note	25
	Potassium Bromide	$KBr(s)$	~300	4×10^{-3}	10	25
HONO + H_2O →Products						
HONO	Liquid Water	$H_2O(l)$	247–297	0.04	5	26
HONO + H_2SO_4 →Products						
HONO	Sulfuric Acid	$H_2SO_4 \cdot nH_2O(l)$	180–200	See Note		27
HONO + HCl →ClNO + H_2O						

Gaseous Species	Surface Type	Surface Composition	T(K)	γ	Uncertainty Factor	Notes
HONO	Water Ice	$H_2O(s)$	180–200	0.05	3	28
	Sulfuric Acid	$H_2SO_4 \cdot nH_2O(l)$		See Note	See Note	29
HONO + NaCl →Products						
HONO	Sodium Chloride	NaCl(s)	~300	$<1 \times 10^{-4}$		30
HNO_3 + Na×(s) →H× + $NaNO_3$						
HNO_3	Sodium Chloride	NaCl(s)	295–298	0.02	3	31
	Sodium Bromide	NaBr(s)	~290	0.02	10	31
	Potassium Chloride	KCl(s)	~290	0.02	10	31
	Potassium Bromide	KBr(s)	~290	0.02	10	31
HO_2NO_2 + HCl → Products						
HO_2NO_2	Sulfuric Acid	$H_2SO_4 \cdot nH_2O$ (50–75 wt. %)	200–225	$<1 \times 10^{-4}$		32
NH_3 + H_2SO_4 →NH_4HSO_4						
NH_3	Sulfuric Acid	$H_2SO_4 \cdot nH_2O$	288–300	0.4	2.5	33
$CH_3C(O)O_2$ + H_2O →$CH_3C(O)OH$ + HO_2						
$CH_3C(O)O_2$	Liquid Water	$H_2O(l)$	225	4×10^{-3}	3	34
	Sulfuric Acid	$H_2SO_4 \cdot nH_2O$				34
		(84 wt % H_2SO_4)	246	3×10^{-3}	3	
		(51 wt % H_2SO_4)	223	1×10^{-3}	3	
		(71 wt % H_2SO_4)	298	1×10^{-3}	3	
$CH_3C(O)O_2NO_2$ + HCl, Cl, ClO, and OClO → Products						
$CH_3C(O)O_2NO_2$	Sulfuric Acid	$H_2SO_4 \cdot nH_2O$ (40–70 wt. %)	200–225	$<1 \times 10^{-4}$		35
Cl + Surface →Products						
Cl	Sulfuric Acid	$H_2SO_4 \cdot nH_2O(l)$	221–296	2×10^{-4}	10	36
Cl_2 + HBr(s) →BrCl + HCl						
Cl_2	Water Ice • HBr(s)	$H_2O(s)$	200	>0.2		37
Cl_2 + KBr(s) →BrCl + KCl(s)						
Cl_2	Potassium Bromide	KBr(s)	~295	>0.1		38
Cl_2 + Na× (aq) →Cl× + NaCl (aq)						
Cl_2	Aqueous Sodium Bromide	NaBr(aq)	See Note			39
	Aqueous Sodium Iodide	NaI(aq)	See Note			39
ClO + Surface →Products						
ClO	Water Ice	$H_2O(s)$	190	See Note		40
	Nitric Acid Ice	$HNO_3 \cdot 3H_2O(s)$	183	See Note		40
	Sulfuric Acid	$H_2SO_4 \cdot nH_2O(l)$ (60 to 95 wt.% H_2SO_4)	221–296	See Note		41
HCl + HNO_3 → Products						
HCl + HNO_3	Sulfuric Acid	$H_2SO_4 \cdot mHNO_3 \cdot nH_2O(l)$		See Note	See Note	42
HOCl + HCl(s) →Cl_2 + H_2O						
HOCl	Water Ice	$H_2O(s) \cdot HCl(s)$	195–200	0.2	2	43
	Nitric Acid Ice	$HNO_3 \cdot 3H_2O(s) \cdot HCl(s)$	195–200	0.1	2	43
	Sulfuric Acid	$H_2SO_4 \cdot nH_2O(l)$	198–209	See Note	See Note	44
HOCl + HBr(s) → BrCl + H_2O						
HOCl	Water Ice	$I_2O(s)$	189–220	See Note		45
	Sulfuric Acid	$I_2SO_4 \cdot nH_2O(l)$	228	See Note	See Note	46
ClNO + NaCl(s) →Products						
ClNO	Sodium Chloride	NaCl(s)	298	$>1 \times 10^{-5}$		47
$ClNO_2$ + NaCl(s) →Products						
$ClNO_2$	Sodium Chloride	NaCl(s)	298	$<1 \times 10^{-5}$		47
$ClONO_2$ + H_2O(s) →HOCl + HNO_3						
$ClONO_2$	Water Ice	$H_2O(s)$	180–200	0.3	3	48
	Nitric Acid Ice	$HNO_3 \cdot 3H_2O(s)$	200–202	0.004	3	49
	Sulfuric Acid	$H_2SO_4 \cdot nH_2O(l)$	200–265	See Note*	See Note	50
	Sulfuric Acid Monohydrate	$H_2SO_4 \cdot H_2O(s)$	195	$<1 \times 10^{-3}$		51
	Sulfuric Acid Tetrahydrate	$H_2SO_4 \cdot 4H_2O(s)$	196–206	See Note		51
$ClONO_2$ + HCl(s) →Cl_2 + HNO_3						

Gaseous Species	Surface Type	Surface Composition	T(K)	γ	Uncertainty Factor	Notes
$ClONO_2$	Water Ice	$H_2O(s)$	180–200	0.3	3	52
	Nitric Acid Ice	$HNO_3 \cdot 3H_2O \cdot HCl$	185–210	0.2	2	53
	Sulfuric Acid	$H_2SO_4 \cdot nH_2O(l) \cdot HCl(l)$	195–235	See Note	See Note	54
	Sulfuric Acid Monohydrate	$H_2SO_4 \cdot H_2O(s)$	195	$<1 \times 10^{-4}$		55
	Sulfuric Acid Tetrahydrate	$H_2SO_4 \cdot 4H_2O(s)$	195–206	See Note		55
	Alumina	Al_2O_3	180–200	0.3	3	56
$ClONO_2 + Mx(s) \rightarrow xCl + MNO_3$						
$ClONO_2$	Sodium Chloride	$NaCl(s)$	200–300	5×10^{-2}	10	57
	Potassium Bromide	$KBr(s)$	~295	5×10^{-2}	10	57
	Sodium Bromide	$NaBr(s)$	~295	See Note		57
$ClONO_2 + HBr(s) \rightarrow BrCl + HNO_3$						
$ClONO_2$	Water Ice	$H_2O(s) \cdot HBr(s)$	200	>0.3		58
	Nitric Acid Ice	$HNO_3 \cdot 3H_2O(s) \cdot HBr(s)$	200	>0.3		58
$ClONO_2 + HF(s) \rightarrow Products$						
$ClONO_2$	Water Ice	$H_2O(s) \cdot HF(s)$	200	See Note		59
	Nitric Acid Ice	$H_2O(s) \cdot HNO_3(s) \cdot HF(s)$	200	See Note		59
$CF_xCl_y + Al_2O_3(s) \rightarrow Products$						
CCl_4	Alumina	$Al_2O_3(s)$	120–300	1×10^{-5}	10	60
$CFCl_3$	Alumina	$Al_2O_3(s)$	120–300	1×10^{-5}	10	60
CF_2Cl_2	Alumina	$Al_2O_3(s)$	120–300	1×10^{-5}	10	60
CF_3Cl	Alumina	$Al_2O_3(s)$	120–300	1×10^{-5}	10	60
$BrCl + KBr(s) \rightarrow Br_2 + KCl(s)$						
$BrCl$	Potassium Bromide	$KBr(s)$	~295	>0.1		38
$Br_2 + NaI(aq) \rightarrow BrI + NaBr(aq)$						
Br_2	Aqueous Sodium Iodide	$NaI(aq)$	See Note			39
$2BrO \rightarrow Br_2 + O_2$						
BrO	Water Ice	$H_2O(s)$	213	See Note		61
	Sulfuric Acid	$H_2SO_4 \cdot nH_2O$				
		(60 wt% H_2SO_4)	213	See Note		61
		(70 wt % H_2SO_4)	213	See Note		61
	Aqueous Sodium Chloride	$NaCl(aq)$ (23 wt% NaCl)	53	See Note		61
$HOBr + HCl(s) \rightarrow BrCl + H_2O$						
$HOBr$	Water Ice	$H_2O(s) \cdot HBr(s)$	180–228	0.3	3	62
	Sulfuric Acid	$H_2SO_4 \cdot nH_2O$ (60–69 wt% H_2SO_4)	198–218	See Note		62
$HOBr + HBr(s) \rightarrow Br_2 + H_2O$						
$HOBr$	Water Ice	$H_2O(s) \cdot HBr(s)$	228	0.1	3	63
	Sulfuric Acid	$H_2SO_4 \cdot nH_2O$	228	See Note		63
$BrONO_2 + H_2O \rightarrow HOBr + HNO_3$						
$BrONO_2$	Water Ice	$H_2O(s)$	190–200	>0.3	2	64
	Sulfuric Acid	$H_2SO_4 \cdot nH_2O$	210–300	See Note	See Note	65
$BrONO_2 + HCl \rightarrow BrCl + HNO_3$						
$BrONO_2/HCl$	Water Ice	$H_2O(s)$	200	See Note		64
	Sulfuric Acid	$H_2SO_4 \cdot nH_2O$	229	0.9	2	65
$CF_2Br_2 + Al_2O_3(s) \rightarrow Products$						
CF_2Br_2	Alumina	Al_2O_3	210, 315	2×10^{-5}	10	60
$CF_3OH + H_2O \rightarrow Products$						
CF_3OH	Water Ice	$H_2O(l)$	274	>0.01		66
	Sulfuric Acid	$H_2SO_4 \cdot nH_2O$				
		(40 wt% H_2SO_4)	210–250	0.07	3	66
		45 wt% H_2SO_4)	210–250	0.04	3	66
		(50 wt% H_2SO_4)	210–250	0.01	3	66
		(50 wt% H_2SO_4)	210–250	0.001	3	66
$SO_2 + H_2O_2, O_3, HONO, NO_2$ and $HNO_3 \rightarrow Products$						
SO_2	Sulfuric Acid	$H_2SO_4 \cdot nH_2O$ (20–60 wt. % H_2SO_4)	293	See Note		67
$SO_3 + H_2O \rightarrow Products$						
SO_3	Sulfuric Acid	$H_2SO_4 \cdot nH_2O$ (78–92 wt. % H_2SO_4)	300	1.0	+0.0, −0.3	68

*γ is temperature dependent

5.13   Notes to Table 5-2

1. $O_3 + Al_2O_3(s)$ and $NaCl(s)$. Very low ozone decomposition efficiencies for reaction on coarse (3 µm dia.) and fine (0.1 µm dia., partially hydroxylated) γ-alumina and coarse (3 µm dia.) α-alumina were measured in flowing and static systems by Hanning-Lee et al.[147] at temperatures ranging between 212 and 473 K. Based on measured BET surface areas, γs ranged from 2×10^{-11} to 4×10^{-10} over the 212 to 298 K temperature range. γs for γ-alumina at lower temperatures exceeded those for α-alumina. Results are roughly consistent with earlier, unpublished flow tube data from L.F. Keyser and from fluidized bed reactor studies of Alebić-Juretić et al. [15]. Note that γs based on geometric surface particle surface areas would be significantly $(10^4–10^7)$ larger. Alebić-Juretić et al. also studied ozone decomposition on small (<180 µm) NaCl crystals in their fluidized bed reactor and observed no effect, indicating γ for O_3 decomposition on NaCl(s) is much smaller than that for α-alumina.

2. $OH + H_2O(s)$. Cooper and Abbatt [91] measured initial irreversible OH uptake coefficients of ~ 0.1 for water ice between 205–230 K; these decayed to γ = 0.03 ±0.02 after repeated exposure to OH. Self-reaction to form H_2O or H_2O_2 was indicated by the lack of observable gas phase products despite observation of first-order OH loss.

3. $OH + HCl \cdot nH_2O(l)$. Cooper and Abbatt [91] demonstrated significant enhancement of OH uptake (to γ > 0.2) after HCl doping of 220 K ice surfaces sufficient to melt the surface layer. It is unclear whether OH is lost to self-reaction or reaction with hydrated Cl^- ions.

4. $OH + HNO_3 \cdot 3H_2O$. Cooper and Abbatt [91] measured γ > 0.2 for nitric acid-doped ice surfaces under conditions suitable for NAT formation at 200 and 228 K. Increase over pure ice uptake rates is probably due to $HNO_3 + OH \rightarrow H_2O + NO_3$ reaction.

5. $OH + H_2SO_4 \cdot nH_2O$. Lower limits of 0.2 for uptake coefficients on 45–65 wt % H_2SO_4 between 220 and 230 K and for 96 wt % H_2SO_4 at 230 and 298 K by Cooper and Abbatt [91] are consistent with a lower limit of 0.07 on 28 wt % H_2SO_4 at 275 K in similar experiments by Hanson et al. [151] and a probable surface saturated value of $(4.9 ±0.5) \times 10^{-4}$ from Knudsen cell measurements by Baldwin and Golden [27] and an estimate of γ = 1 on ~96 wt % H_2SO_4 at 298 K by Gerhenzon et al. [136] using a coated insert flow tube technique. Uptake is probably reactive with $OH + HSO_4^- \rightarrow H_2O + SO_4^-$ the hypothesized process.

6. $OH + NaCl(s)$. Ivanov et al. [193] used a fast flow reactor with a central salt coated rod to measure heterogeneous loss of OH between 245 and 339 K. Their fit for NaCl(s) yielded
γ = $(1.2 ±0.7) \times 10^{-5}$ exp[(1750 ±200)/T]. Similar data for NH_4NO_3 yielded
γ – $(1.4 ±0.5) \times 10^{-4}$ exp [(1000 ±100)]. Since uptake was irreversible, it is assumed that the loss was self-reaction.

7. HO_2 on $H_2O(s)$ and $H_2SO_4 \cdot nH_2O(l)$. Uptake of HO_2 on ice and super-cooled 55 wt % sulfuric acid at 223 K has been demonstrated to be limited by HO_2 surface saturation by Cooper and Abbatt [91]. They argue that self-reaction, presumably $2HO_2 \rightarrow H_2O_2 + O_2$ is limiting measured uptake coefficients of 0.025 ±0.005 for ice and 0.055 ±0.020 for 55 wt % H_2SO_4. However, Gershenzon et al. [135]measured γ > 0.2 for 80 and 96 wt % H_2SO_4 at 243 K and Hanson et al. [151] measured a lower limit for 28 wt % H_2SO_4 at 275 K of 0.07. However, large gas phase diffusion corrections mean this value is consistent with γ = 1.

8. $NO_2 + H_2O(1)$. Value for γ of $(6.3 ± 0.7) \times 10^{-4}$ at 273 K (Tang and Lee, [327]) was achieved by chemical consumption of NO_2 by $SO_3^=$; their stopped-flow measurement was probably still affected by surface saturation, leading to the measurement of a lower limit. Ponche et al. [276] measured an uptake coefficient of $(1.5 ± 0.6) \times 10^{-3}$ at 298 K, which was also probably subject to saturation limitations. Mertes and Wahner [254] used a liquid jet technique to measure a lower limit of $γ \geq 2 \times 10^{-4}$ at 278 K, and they observed partial conversion of the absorbed NO_2 to HONO. Msibi et al. [266] used a cylindrical/annular flow reactor to derive g = $(8.7 ±0.6) \times 10^{-5}$ on pH = 7 deionized water surfaces and $(4.2 ± 0.9) \times 10^{-4}$ on pH = 9.3 wet ascorbate surfaces; it seems likely that these results are also subject to surface saturation given the gas/surface interaction times involved in the experiment. Data are consistent with an $α \geq 1 \times 10^{-3}$ for 278–298 K and a liquid-phase second-order hydrolysis of NO_2 to HONO and HNO_3 which depends on temperature and pH. However, the interplay between accommodation, possible surface reaction, and bulk reaction may be complex.

9. $NO_2 + H_2SO_4 \cdot nH_2O$. Kleffman et al. [224] performed bubble tube reactor uptake measurements for 0–98 wt. % acid at 298 K and for 44.6 and 56.1 wt % from 250–325 K. At 298 K, measured uptake coefficients varied between 6 and 3×10^{-7} with a minimum near 70 wt. %. Most measurements at 44.6 and 56.1 wt. % overlapped within their error limits and showed little temperature dependence although there is evidence that uptake increases at the lowest temperatures. The data can all be captured with a recommended value of 5×10^{-7} with an uncertainty factor of three.

    This recommendation is consistent with earlier upper limits of 1×10^{-6} by Baldwin and Golden [26] for 96 wt. % at 295 K and 5×10^{-6} for 70 wt. % between 193 and 243 K by Saastad et al. [303]. Kleffman et al. [224] conclude that their uptake measurements are mass accommodation limited; however, it is not clear that their values are not influenced by bulk or surface reaction of two NO_2 with H_2O to form HONO and HNO_3 at lower acid wt. % values and the formation of nitrosyl sulfuric acid at higher acid concentrations. Kleffman et. al. [224] did perform separate static wetted wall reactor studies showing the formation of gas phase HONO at acid concentrations below 60 wt. %. It is more likely that reactive uptake is a controlling factor and the measured uptakes are solubility and/or reaction rate limited. Thus, the mass accommodation coefficient may be much larger than the recommended uptake values.

10. $NO_2 + NaCl(s), NaBr(s)$. Vogt and Finlayson-Pitts [342,344] used diffuse reflectance infrared spectroscopy to study the reaction of NO_2 with NaCl(s) at 298 K, and Vogt et al. [341] used the same technique to study $NO_2 + NaBr(s)$ at 298 K. Both reactions were shown to be approximately second order in NO_2. Assuming that adsorbed N_2O_4 is the reactant leads to $\gamma = (1.3 \pm 0.6) \times 10^{-4}$ for NaCl(s) and 2 (+4, −1.3) $\times 10^{-4}$ for NaBr(s). Peters and Ewing [275] measured reactive uptake for single-crystal NaCl(100) surfaces and observed both NO_3^-(c) and ClNO products. The value of $\gamma(N_2O_4)$ measured by Peters and Ewing at 298 K was only
    $(1.3 \pm 0.3) \times 10^{-6}$. They noted that small amounts of water vapor (9.5 mbar) cause γ to increase by two orders of magnitude.

11. NO_3 on $H_2O(s)$. Fenter and Rossi [121] measured an upper limit for γ of 10^{-3} over the range from 170 to 200 K.

12. $NO_3 + H_2O(l)$. Rudich et al. [300,301] used wetted-wall flow tube techniques to measure uptake coefficients for NO_3 on pure water and aqueous NaCl, NaBr, NaI, and $NaNO_2$ solutions. These studies were extended to other aqueous solutions by Imamura et al. [189]. Uptake on pure water was consistent with reaction of NO_3 to produce HNO_3 and OH. Uptake coefficients with solutions containing I^-, Cl^-, Br^-, NO_2^- and other anions were larger and scaled with anion concentration, indicating electon transfer reactions to produce NO_3^-. The γ of $(2.0 \pm 1.0 \times 10^{-4})$ at 273 K determined for pure water by Rudich et al. is significantly lower than the lower limit of 2.5×10^{-3} quoted by Mihelcic et al. [258]. A detailed analysis of uptake coefficients for KI aqueous solutions indicated that the NO_3 mass accommodation coefficient is >0.04 [301].

13. $N_2O_5 + H_2O(s)$. Leu [232] and Hanson and Ravishankara [157] measured nearly identical values of 0.028 ($\pm$0.011) and 0.024 ($\pm$30%) in the 195–202 K range on relatively thick ice films in coated wall flow tubes. Quinlan et al. [281] measured a maximum value for γ on ice surfaces at 188 K of 0.03 in a Knudsen cell reactor. The average of these three studies is 0.027 with a standard deviation of 0.003. Hanson and Ravishankara [158,160] presented new and re-analyzed data as a function of ice thickness, with a value of ~0.008 for the thinnest ice sample, rising to 0.024 for the thickest. From these data there would appear to be no strong dependence on temperature, at least over the 188–195 K range. It is unclear whether the measured dependence on ice film thickness is due to added porosity surface area in the thicker films or decreased ice film integrity in thinner films. The error estimate in the table is driven by the possible systematic error due to unresolved film thickness effects rather than the small statistical error among the "thick film" values from the three groups.

    Zondlo et al. [374] report the formation of a supercooled H_2O/HNO_3 liquid layer at 185 K as a reaction product, forming NAT or NAD only after decreasing the relative humidity below the ice frost point. This effect is similar to that resulting from the interaction of gaseous HNO_3 or $ClONO_2$ with the ice surface. These authors measured $\gamma = (7 \pm 3) \times 10^{-4}$ at 185 K for the reaction of N_2O_5 with this supercooled liquid layer.

14. $N_2O_5 + H_2O(l)$. Reaction on liquid water has a negative temperature dependence. Van Doren et al. [337] measured γs of 0.057 ± 0.003 at 271 K and 0.036 ± 0.004 at 282 K using a droplet train uptake technique. George et al. [132] also used a droplet train technique to measure γs of $(3.0 \pm 0.2) \times 10^{-2}$ (262 K), $(2.9 \pm 1.2) \times 10^{-2}$ (267 K), $(2.0 \pm 0.2) \times 10^{-2}$ (273 K), $(1.6 \pm 0.8) \times 10^{-2}$ (276 K), and $(1.3 \pm 0.8) \times 10^{-2}$ (277 K) on pure water, while Schweitzer et al. [310] used the same approach for pure water

and salt solutions between 262 and 278 K, obtaining similar results. Mozurkewich and Calvert [263] studied uptake on $NH_3/H_2SO_4/H_2O$ aerosols in a flow reactor. For their most water-rich aerosols (RH = 76%) they measured γs of 0.10 ±0.02 at 274 and 0.039 ±0.012 at 293 K. However, similar studies by Hu and Abbatt [180] on $(NH_3)_2SO_4$ aerosols at 297 K showed that uptake rises with decreasing relative humidity (RH); their 94% RH results agree very well with the temperature trend measured by Van Doren et al. Msibi et al.[265] measured a smaller γ of 2.5×10^{-3} for water adsorbed on a denuder flow tube well under 66–96% relative humidity conditions at room temperature. The higher γ values of Van Doren et al., Mozurkewhich and Calvert, and Hu and Abbatt are quite consistent when temperature and RH effects are factored in. The lower values from the Louis Pasteur (George et al.; Schweitzer et al.) and Birmingham (Msibi et al.) groups appear to have much less pronounced temperature dependence and are inconsistent with the other measurements. The same function used to fit the N_2O_5 uptake on sulfuric acid as a function of temperature and concentration, discussed in note 17 below, has been extended to the Van Doren et al. and Hu and Abbatt data for pure water and very high RH aerosols. See note 17 for the functional fit and its error discussion.

15. $N_2O_5 + HNO_3 \cdot 3H_2O(s)$. Hanson and Ravishankara [155] have measured γ = 0.0006 (± 30%) near 200 K. They presented re-analyzed and additional data as a function of ice thickness (Hanson and Ravishankara [158,160]), deriving a value of 3×10^{-4} for the thinnest NAT covered ice layer, with values up to three times higher for thicker NAT-covered ice layers. As in the case of uptake on water ice this may be due to increased surface area from porosity in the thicker films, or less integrity in the thinner films. The uncertainty listed in Table A-1 is driven by this observed effect. All of the Hanson et al. data are in very poor agreement with the γ = 0.015 (±0.006) reported by Quinlan et al. [281] from their Knudsen cell measurements; this measurement may have been biased by formation of a super-cooled aqueous nitric acid surface and is judged to be unreliable.

16. $N_2O_5 + H_2SO_4 \cdot nH_2O(l)$. This reaction has been intensively studied between 195 and 296 K for a wide range of H_2SO_4 wt. % values using four complementary experimental techniques. Data are available from aerosol flow tube studies (Fried et al. [129], Hanson and Lovejoy [152], Hu and Abbatt [180], and Hallquist et al. [145]), coated wall flow tube studies (Hanson and Ravishankara [155], Zhang et al. [365]), a stirred Knudsen cell (Manion et al. [249]) and droplet train studies (Van Doren et al. [337], Robinson et al. [293]). All studies have yielded γs between ~0.05 and 0.20 with modest dependence on surface H_2SO_4 wt. % and temperature. The Knudsen cell studies, aerosol flow tube studies at higher N_2O_5 exposure and the ternary $H_2SO_4/HNO_3/H_2O$ studies of Zhang et al. [365] all illustrate that significant levels of HNO_3 in the H_2SO_4/H_2O solutions will reduce γ measurably; this fact explains some of the scatter in aerosol flow tube studies and the surface saturation evident in the Knudsen cell studies. The effect of 5.0×10^{-7} Torr HNO_3 on γ as a function of temperature at two water vapor concentrations are plotted in Zhang et al. [365]; the decrease in γ is greatest at low temperatures, approaching a factor of 2–5 between 200 and 195 K.

Experimental data on sulfuric acid surfaces between 40 and 80 wt. % sulfuric acid deemed to be free of saturation effects, plus the pure water uptake data of Van Doren et al. [337] and high relative humidity ammonium sulfate aerosol uptake data of Hu and Abbatt [180] were all fit to a polynomial expression to yield a single model describing γ for N_2O_5 uptake valid between 0 and 80 wt. % H_2SO_4 and 180 to 300 K (Robinson et al. [293]). The form of this function is: $\gamma_o = \exp(k_o + k_1/T + k_2/T^2)$, where T is the temperature in K. The parameters k_o, k_1, and k_2 obtained from the best-fit are:

$$k_o = -25.5265 - 0.133188 wt + 0.00930846 wt^2 - 9.0194 \times 10^{-5} wt^3$$

$$k_1 = 9283.76 + 115.345 wt - 5.19258 wt^2 + 0.0483464 wt^3$$

$$k_2 = -851801 - 22191.2 wt + 766.916\ wt^2 - 6.85427 wt^3$$

where wt is the weight percentage of H_2SO_4.

The overall error of applying the uptake function provided here consists of two components. One is the standard deviation of the model-calculated value with respect to measured data, σ_m, which is given by

$$\sigma_m = \sqrt{\frac{\sum_{i=1}^{N}\left(1 - \frac{\gamma_i}{\gamma_{\text{model}}}\right)^2}{N-1}}\ .$$

The other is the standard deviation of relative experimental measurement error from the mean, σ_d, which is given by

$$\sigma_d = \sqrt{\frac{\sum\limits_{i=1}^{N}\left(\frac{\Delta\gamma_i}{\gamma_i}\right)^2}{N(N-1)}} \; .$$

The overall error is

$$\sigma = \sqrt{\sigma_m^2 + \sigma_d^2} \; .$$

(These formulations are also applied below in the error estimation for the $ClONO_2 + H_2O$ and HCl, $BrONO_2 + H_2O$, and HOCl + HCl reaction system. For N_2O_5, the error is estimated to be 15% (one sigma), with σ_m=14.7% and σ_d=2.9%).

17. $N_2O_5 + H_2SO_4 \cdot H_2O(s)$. Zhang et al. [366] used coated flow tube techniques to measure the uptake of N_2O_5 on solid sulfuric acid monohydrate over a temperature range of 200 to 225 K. The measurement values of γ were significantly higher at 200 K ($\gamma \sim 1 \times 10^{-3}$) than at 225 K ($\gamma \sim 10^{-4}$) and were well fit by $\log \gamma = [4.78 - 0.0386T(K)]$. Acid-rich $H_2SO_4 \cdot H_2O$ surfaces had a lower γ than water rich surfaces ($\log \gamma = [0.162 - 0.789 \times \log p_{H2O}]$ where p_{H2O} is their experimental water vapor partial pressure).

18. N_2O_5 on $H_2SO_4 \cdot 4H_2O(s)$. Hanson and Ravishankara [162] studied N_2O_5 uptake by frozen 57.5 and 60 wt % H_2SO_4 as a function of temperature and relative humidity. The 57.5 wt % surface was not sensitive to relative humidity and was slightly more reactive ($\gamma = 0.008$ vs 0.005) at 205 K than at 195 K. Reaction probabilities on the 60 wt % surface dropped off with temperature and relative humidity.

19. N_2O_5 + HCl on $H_2O(s)$. Leu [233] measured $\gamma = 0.028$ (± 0.011) at 195 K, while Tolbert et al. [331] measured a lower limit of 1×10^{-3} at 185 K. These experiments were done at high HCl levels probably leading to a liquid water/acid surface solution (Abbatt et al. [5]). Seisel et al. [311] measured $\gamma \sim 0.03$ at 200 K using a Knudsen flow reactor with a range of HCl flows. The uptake coefficient at low HCl flows is only slightly enhanced compared to the uptake on a pure ice surface.

20. N_2O_5 + HCl on $HNO_3 \cdot 3H_2O(s)$. Hanson and Ravishankara [155] measured $\gamma = 0.0032$ ($\pm 30\%$) near 200 K.

21. N_2O_5 + HCl on $H_2SO_4 \cdot H_2O(s)$. Zhang et al. [366] saw no increase in N_2O_5 uptake on sulfuric acid monohydrate at 195 K upon exposure to HCl, setting $\gamma < 10^{-4}$.

22. N_2O_5 + NaCl (s,aq). Using FTIR analysis, Livingston and Finlayson-Pitts [241] have demonstrated that N_2O_5 reacts with crystalline NaCl to form $NaNO_3(s)$, and they report $\gamma > 2.5 \times 10^{-3}$ at 298 K. However, Leu et al.[235] used flow tube/mass spectrometric techniques to obtain $\gamma < 1 \times 10^{-4}$ for dry salt at 223 and 296 K; they also noted that exposing salt surfaces to small amounts of H_2O vapor increased γ significantly. Fenter et al.[119] measured $\gamma = (5.0 \pm 0.2) \times 10^{-4}$ on fused salt surfaces at room temperature, assuming the geometrical surface area is the only surface accessed. Msibi et al. [265] measured NO_3^- deposition on an annular flow reactor to determine $\gamma = 1 \times 10^{-3}$ for salt surfaces between 45 and 96% relative humidity at room temperature, rising to $\gamma = 1.5 \times 10^{-2}$ at 96–97% relative humidity, but they argue that most of the uptake is due to reaction with H_2O. On aqeous NaCl solutions, Zetzsch, Behnke, and co-workers [43,44,362] have studied the reaction of N_2O_5 with aqueous NaCl aerosols in an aerosol chamber. The relative yields of $ClNO_2$ and HNO_3 rise with the NaCl concentration. A reaction probability of ~0.03 is measured with a 50% $ClNO_2$ yield at the deliquescence point (Zetsch and Behnke). This picture is confirmed by droplet uptake studies on 1 M NaCl solutions reported by George et al. [132] which confirm that uptake on salt solutions in the 263–278 K temperature range is larger than that on pure water droplets.

23. N_2O_5 + HBr on $H_2O(s)$. Seisel et al. [311] report γ values ranging from ~3×10^{-3} to 0.1, depending on the HBr concentrations employed; the measurements were conducted at 180 and 200 K. These authors report Br_2 and HONO in 80% yield as products with respect to N_2O_5 taken up, generated presumably by the secondary reaction of the primary product $BrNO_2$ with HBr.

24. N_2O_5 + HBr on $HNO_3 \cdot 3H_2O$(s). This reaction, yielding $\gamma \sim 0.005$, was investigated on NAT surfaces near 200 K by Hanson and Ravishankara [159]. Under some conditions a much higher reaction coefficient of ~ 0.04 was observed.

25. N_2O_5 + MBr. Finlayson-Pitts et al. [122] used FTIR techniques to demonstrate that $BrNO_2$(ads) is a major product of the N_2O_5(g) + NaBr(s) reaction. However, Fenter et al. [119] failed to measure gas-phase evolution of $BrNO_2$ using Knudsen cell/mass spectrometry techniques, detecting Br_2(g) instead. They propose that $BrNO_2$ reacts with KBr(s) to yield KNO_2(s) + Br_2(g). A γ of $(4.0 \pm 2.0) \times 10^{-3}$ at room temperature was determined for fused KBr surfaces with well-defined surface areas.

26. HONO + H_2O(l). Bongartz et al. [56] present uptake measurements by two independent techniques, the liquid jet technique of Schurath and co-workers and the droplet train/flow tube technique of Mirabel and co-workers (Ponche et al. [276]). With a surface temperature of ~ 245 K the droplet train techniques yielded $0.045 < \gamma < 0.09$, while the liquid jet operating with a surface temperature of 297 K obtained $0.03 < \gamma < 0.15$. Mertes and Wahner used a liquid jet technique to measure $4 \times 10^{-3} < \gamma < 4 \times 10^{-2}$ at 278 K. Since HONO uptake by liquid water probably involved hydrolysis, an increase in Henry's law solubility with decreasing temperature may be offset by a decreasing hydrolysis rate constant, leaving the uptake coefficient's temperature trend uncertain. Measured uptake coefficients will not correspond to the mass accommodation coefficient.

27. HONO + $H_2SO_4 \cdot nH_2O$(l). Zhang et al. [368] measured uptake coefficients for HONO on sulfuric acid that increased from $(1.6 \pm 0.1) \times 10^{-2}$ for 65.3 wt. % H_2SO_4 (214 K) to $(9.1 \pm 1.6) \times 10^{-2}$ for 73 wt. % H_2SO_4 (226 K). Fenter and Rossi [120] measured uptake coefficients rising from 1.8×10^{-4} for 55 wt. % H_2SO_4 (220 K) to 3.1×10^{-1} for 95 wt. % H_2SO_4 (220 K and 273 K). Baker et al. [24] measured much smaller uptake coefficients for 60 wt. % at 298 K. In general, the values measured by Zhang et al. [368] are a factor of 2 to 5 higher than those of Fenter et al. [120] for comparable acid concentrations. Since the reaction probably depends on both temperature and acid concentration and since the data scatter is high in both experiments, further independent data will be required to define γ as a function of acid concentration and temperature. These data are generally consistent with the effective Henry' law constant measurements of Becker et al. [42] who illustrate that HONO solubility decreases exponentially with H_2SO_4 concentration until ~ 53 wt %, at which point reaction to form nitrosyl sulfuric acid increases H* dramatically as H_2SO_4 concentration increases. Baker et al. [24] invoke surface decomposition of HONO to explain their room temperature data, since they separately determine that the bulk second-order disproportionation rate for HONO is too slow to account for even their small uptake coefficients. It is possible that surface formation of nitrosyl sulfuric acid and not HONO disproportionation is responsible for much of their measured uptake. The Zhang et al. [368] and Fenter and Rossi [120] data have been combined and fit with a four-term polynomial as a function of acid wt. % (these data did not show an obvious temperature dependence):

$$\ln \gamma = a + b \text{ wt} + c \text{ wt}^2 + d \text{ wt}^3$$

where wt is the H_2SO_4 wt. %, and

$$a = -155.7 \pm 29.7$$
$$b = 5.663 \pm 1.232$$
$$c = -0.07061 \pm 0.01679$$
$$d = 0.000297 \pm 0.000076$$

This parameterization should be used only within the 55–95-wt.-%-H_2SO_4 range and the 214-to-273-K temperature range.

28. HONO + HCl + H_2O(s). Knudsen cell uptake studies for HONO/HCl co-deposited on ice (180–200 K) and for HONO on 0.1 to 10 m HCl frozen solutions (~ 190 K) by Fenter and Rossi [120] showed HONO uptake coefficients in the 0.02 to 0.12 range as long as surface HCl concentrations significantly exceed HONO concentrations. ClNO was evolved quantitatively with HONO consumption.

29. HONO + HCl on $H_2SO_4 \cdot nH_2O$(l). Fenter and Rossi [120] saw no reaction for acid wt. % > 65. They measured $\gamma = 2.0 \pm 0.7 \times 10^{-3}$ for 60 wt. % acid saturated with HONO at 230 K. Zhang et al. [368] also measured the uptake of HCl after exposure to HONO, they observed HCl uptake with γs between 0.01–0.02 over an acid wt. % range of 60.8–71.3 (T = 207.9–222.6 K). The reaction was also studied by Longfellow et al. [242] using both HCl doped and HONO doped sulfuric acid aerosols. Their uptake measurements

confirmed reaction at higher acid wt. %, but by using lower HONO partial pressures they measured smaller γs. The reverse reaction, ClNO hydrolysis, was also studied in a wetted wall flow reactor and in the aerosol flow reactor by Longfellow et al. [242] and in a Knudsen cell reactor by Fenter and Rossi [120]. Data show clear evidence of both surface and bulk kinetics for the forward reaction. Longfellow et al. [242] report k^{II} values for the bulk reaction (in units of 10^4 $M^{-1}s^{-1}$) for 50 wt. %: 81 at 250 K and 15 at 205 K; for 60 wt. %: 9.4 at 250 K, 6.9 at 230 K and 5.0 at 219 K; for 67 wt. %: 3.9 at 250 K; and for 70 wt. %: 5.8 at 269 K and 0.35 at 215 K. The reaction is clearly complex and will require a comprehensive model of both the surface and bulk processes to arrive at an appropriate parameterization for γ.

30. HONO + NaCl(s). Diffuse reflectance experiments by Vogt and Finlayson-Pitt [343] on room temperature NaCl(s) and Knudsen cell uptake experiments by Fenter and Rossi on room temperature NaCl(s) and frozen 0.1 M NaCl aqueous solutions, all failed to show HONO uptake. The latter results yield $\gamma < 1 \times 10^{-4}$.

31. HNO_3 + NaX(s)/KX(s). Vogt and Finlayson-Pitts [342,344] used diffuse infrared reflectance spectroscopy to characterize the process. There was absorption of HNO_3, but no reaction was observed on completely dry NaCl(s); however, $NaNO_3$ forms in the presence of very low (well below the deliquescence point) levels of $H_2O(g)$. Using XPS spectroscopy to identify surface products and a dry HNO_3 source, Laux et al. [230] (also see Vogt et al.) measured $\gamma = (4 \pm 2) \times 10^{-4}$ at 298 K. Fenter et al. [118] measured the room temperature uptake of HNO_3 on solid powders of NaCl, NaBr, KCl, KBr, and $NaNO_3$, using Knudsen cell/mass spectrometry techniques. They saw similar uptake for all surfaces, including unreactive $NaNO_3$, and recommend $\gamma = (2.8 \pm 0.3) \times 10^{-2}$ for all salts. HCl or HBr was produced with ~100% yield from the halide surfaces. There is some concern about the effective surface area of the powders used by Fenter et al. (see Leu et al.[235]). Fenter et al. report new HNO_3 data to support their argument that "sticky" gases such as HNO_3 cannot penetrate below the top surface layer of the powders used in their experiments. Leu et al. [235] used flow tube/mass spectrometry techniques to measure $\gamma = (1.3 \pm 0.4) \times 10^{-2}$ at 296 K and $\gamma > 8 \times 10^{-3}$ at 223 K, both in the presence of low levels of $H_2O(g)$. They determined that uptake at 296 K was reactive, producing HCl but that at 223 K reaction was suppressed and uptake was largely absorptive. Beichert and Finlayson-Pitts [46] measured $\gamma = (1.4 \pm 0.6) \times 10^{-2}$ at 298 K with a Knudsen cell technique, and, using D_2O, demonstrated that chemisorbed water, presumably retained on defect sites, was crucial for $NaNO_3$ formation. This suggests that low levels of defect-retained water are responsible for the small uptake values measured by Laux et al.

32. HO_2NO_2 + HCl on $H_2SO_4 \cdot nH_2O(l)$. Zhang et al. [369] performed wetted-wall flow-reactor studies with HCl and HO_2NO_2 partial pressures in the 10^{-6} to 10^{-7} Torr range. Using chemical ionization mass spectrometry (CIMS) to detect expected reaction products, no Cl_2 (using SF_4^- as an analyte ion) or HOCl (using F^-) was detected over a temperature range of 200–225 K and an acid concentration range of 50–70 wt. % H_2SO_4. An upper limit for the reactive uptake coefficient for HO_2NO_2 reacting with HCl of $\gamma < 1 \times 10^{-4}$ was deduced.

33. NH_3 + $H_2SO_4 \cdot nH_2O$. Robbins and Cadle [289], Huntzicker et al. [184], McMurry et al. [253], and Daumer et al. [97] all studied NH_3 uptake by sulfuric acid aerosols in near room temperature flow reactors (T = 281–300 K). Uptake coefficients varied between 0.1 and 0.5. Rubel and Gentry [299] used levitated H_3PO_4 acid droplets to show that heterogeneous reaction does control the initial NH_3 uptake on strong acid solutions. Both Rubel and Gentry and Däumer et al. also explored the effect of organic surface coatings.

34. $CH_3C(O)O_2$ + $H_2O(l)$ and $H_2SO_4 \cdot nH_2O$. Villalta et al. [339] used wetted-wall flow tube techniques to measure $\gamma = 4.3 (+ 2.4 /-1.5) \times 10^{-3}$ for water at 274 ± 3K. They also measured uptake for 34 wt % H_2SO_4 at 246 K ($\gamma = (2.7 \pm 1.5) \times 10^{-3}$), 51 wt % at 273 K ($\gamma = (0.9 \pm 0.5) \times 10^{-3}$), and 71 wt % at 298 K ($\gamma = (1.4 \pm 0.7) \times 10^{-3}$). They suggest that products subsequent to hydrolysis are HO_2 and $CH_3C(O)OH$.

35. $CH_3C(O)O_2NO_2$ + HCl, Cl, ClO, and OClO on $H_2SO_4 \cdot nH_2O(l)$. Zhang and Leu [364] performed wetted wall flow reactor studies with Cl species partial pressures in the 10^{-6} to 10^{-7} Torr range and $CH_3C(O)O_2NO_2$ at 3×10^{-6} Torr after equilibrating the acid surfaces (42, 51, and 69 wt. % at 202 and 224 K) with $CH_3C(O)O_2NO_2$. Also uptake studies with 5×10^{-7} Torr $CH_3C(O)O_2NO_2$ were performed after exposing the acid surface to the Cl species. No Cl species or $CH_3C(O)O_2NO_2$ uptake enhancements were observed under either condition and an upper limit for the reactive uptake coefficient of $\gamma < 1 \times 10^{-4}$ of $CH_3C(O)O_2NO_2$ was deduced. No gas phase reaction products were observed using CIMS after 42 wt. % H_2SO_4 at 210 K was exposed to $CH_3C(O)O_2NO_2$ and each Cl species for 20 minutes.

36. Cl + $H_2SO_4 \cdot nH_2O(l)$. Measured reaction probability (Martin et al. [250]) varies between 3×10^{-5} and 7×10^{-4} as H_2O and T co-vary. Reaction product is claimed to be HCl.

37. Cl_2+HBr + H_2O(s). Hanson and Ravishankara [159] measured a reaction probability of > 0.2 on water ice near 200 K. BrCl was not detected, presumably due to rapid reaction with excess HBr.

38. Cl_2 and BrCl + KBr(s). Caloz et al. [64] measured $\gamma > 0.1$ for reactive uptake of Cl_2 and BrCl on KBr(s) in a room temperature Knudsen cell experiment.

39. Cl_2 and Br_2 + NaBr(aq) and NaI(aq). Hu et al. [181] measured large uptake coefficients for Cl_2 on dilute aqueous droplets of NaBr and NaI solutions and Br_2 on NaI solutions using a droplet train technique. Reaction was demonstrated to proceed through both a chemisorbed surface complex and normal bulk solution second-order kinetics. Second-order bulk reaction rate constants near the diffusion limit and consistent with bulk-phase kinetic measurements were obtained between 263 and 293 K.

40. ClO + H_2O(s) and $HNO_3 \cdot nH_2O$(s). Proposed reaction (Leu [233]) is 2 ClO $\rightarrow$ Cl_2 + O_2; reactive uptake may depend on ClO surface coverage, which in turn may depend on gas phase ClO concentrations. Kenner et al. [214] measured reaction probabilities of $(8 \pm 2) \times 10^{-5}$ for ice at 183 K which is far lower than the limit of $>1 \times 10^{-3}$ obtained by Leu [233]. Abbatt [3], using nearly the same low levels of ClO as Kenner et al., obtained $\gamma < 1 \times 10^{-5}$ at 213 K. The difference may lie in the level of ClO or other adsorbable reactive species present. The lower value of Abbatt is probably closer to the expected reactivity under stratospheric conditions. Kenner et al. also measured a reaction probability limit of $< (8 \pm 4) \times 10^{-5}$ for NAT at 183 K.

41. ClO + $H_2SO_4 \cdot nH_2O$. Measured reaction probability (Martin et al. [250]) varies between 2×10^{-5} and 2×10^{-4} as H_2O content is varied by changing wall temperature. Reaction product is claimed to be HCl, not Cl_2. Abbatt [3] measured $\gamma < 1 \times 10^{-5}$ for 60 and 70 wt % H_2SO_4 at 213 K.

42. HCl + HNO_3 on $H_2SO_4 \cdot$ m $HNO_3 \cdot nH_2O$(l). Two studies have noted HCl activation in concentrated ternary $H_2SO_4/HNO_3/H_2O$ solutions or ice slurries. Luick et al. [246] saw only gas phase HCl in 64.6 wt. % H_2SO_4/ 4.8 wt. % HNO_3 at 200 K, but saw a vapor phase Cl partitioning of 50% HCl and 50% ClNO/$ClNO_2$ for a 76.6/20.1 wt. % solution (an ice slurry) at 200 K. Cappa et al. [65] saw substantial yields of ClNO, $ClNO_2$, and Cl_2 at 273 K for a range of solution compositions; e.g. 32.6%, 9.8% and 44.4% respectively for a total HCl conversion of 86.9% in a 35% H_2SO_4 /45% HNO_3 solution and 20.2%, 6.9%, 27.9% for a 60/25 wt. % solution. While no kinetic coefficients or detailed mechanisms are available, these studies do show the potential for HCl activation in strong $H_2SO_4/HNO_3/H_2O$ solutions.

43. HOCl + HCl + H_2O(s) and $HNO_3 \cdot 3H_2O$(s). Hanson and Ravishankara [158] and Abbatt and Molina [6] have investigated the HOCl + HCl reaction on water ice and NAT-like surfaces, and Chu et al. [76][72] studied the reaction on water ice. Product yield measurements support the identification of Cl_2 and H_2O as the sole products. The measured yield of product Cl_2 is 0.87 ± 0.20 and was stated to be similar on both surfaces according to Abbatt and Molina. Within the accuracy of the experiments, the reaction probability does not depend on the gas phase HCl and HOCl densities. Only Abbatt and Molina investigated at more than one temperature, their data indicates that γ increases at lower temperatures. A plot of data from the three studies does show a weak temperature trend, with γ increasing about a factor of two as the temperature drops from 202 to 188 K. However, the data are too sparse to assign a definitive temperature dependence. The average of all three studies yields $\gamma = 0.26 \pm 0.08$ for data based on the geometrical area of the flow tube surfaces. Chu et al. [72] indicate that a porosity correction for their data would reduce their value by a factor of 3 to 4. The real uncertainty would appear to be dominated by systematic uncertainties in porosity corrections and a potential temperature dependence. Given the fact that any porosity correction must reduce the value, a central value of 0.2 is adopted with an uncertainty factor of 2. The high reaction probabilities measured for water ice indicate that this reaction may play a significant role in release of reactive chlorine from the HCl reservoir.

    Two studies (Hanson and Ravishankara [158]; Abbatt and Molina [6]) have measured the reaction probability of HOCl + HCl on NAT surfaces. These data show γ increases as the ambient water pressure increases and then reaches a plateau. At relatively high water pressure, the two studies averaged $\gamma = 0.135 \pm 0.049$, with no porosity correction. The reaction probability on water poor NAT-like surfaces falls off dramatically (a factor of 10). A recommendation of 0.1 with an uncertainty factor of 2 is shown in Table 5-2. Carslaw and Peter [67] have published a model of this reaction and its dependence on HCl uptake.

44. HOCl + HCl + $H_2SO_4 \cdot nH_2O$(l). This process has been studied in coated flow tubes over ~200–260 K by Zhang et al. [363], Hanson and Ravishankara [161], Donaldson et al. [107], and Hanson and Lovejoy [154]. Hanson and Lovejoy also made measurements in an aerosol flow tube from 251 to 276 K. A model of this and related sulfuric acid aerosol reactions tailored to stratospheric conditions has been published by Hanson et al. [168]. Zhang et al. held the water vapor partial pressure at 3.8×10^{-4} Torr and showed γ increased by a

factor of 50 as the temperature was lowered from 209 to 198 K, showing that the reaction rate is strongly dependent on water activity.

A detailed kinetic uptake model has been developed to fit the experimental data [313]. The formulation for γ is given as:

$$\frac{1}{\gamma} = \frac{1}{\alpha} + \frac{1}{\Gamma_{HOCl}^{rxn}}$$

where

$$\Gamma_{HOCl}^{rxn} = \frac{4H_{HOCl}RT}{\bar{c}}\left(D_{HOCl}k_{HOCl\_HCl}\right)^{1/2}$$

At the low temperatures of interest, α for HOCl was assumed to be unity consistent with the value for HCl measured at 240 K and below (Robinson et al. [294]). The individual formulations for H_{HOCl}, D_{HOCl} and $k_{HOCl-HCl}$ are given in Table A-4 in Shi et al. [313]. Reaction of HOCl with HCl is considered to be acid catalyzed. It is known that the reaction rate for HOCl + HCl in pure water is low (Donaldson et al. [107]). Experimental data noted above indicated that the reaction rate of HOCl + HCl increases with acidity of H_2SO_4 solution. The data from the experimental studies noted above were fit to the model without bias. Using the same error analysis discussed in the note for N_2O_5 uptake on sulfuric acid, a detailed kinetic model yields a 33.4% error (one sigma fit to the available data set, with σ_m=33.3% and σ_d=3.0%).

In the cold stratosphere where T<190 K, the reaction of $ClONO_2$ + HCl is so fast that HCl is depleted which slows down the reaction of HOCl + HCl. As shown in Table A-4 in Shi et al., the effect of HCl depletion on the HOCl reactive uptake coefficient (due to reaction with $ClONO_2$ inside/on the surface of particles) is taken into account via the factor F_{HCl} (also see the note on chlorine nitrate/hydrochloric acid reactive uptake on sulfuric acid surfaces).

45. HOCl + HBr on H_2O(s). Chu and Chu [72] measured γ at 189 K to be in the range from 0.06 to 0.38 for HBr partial pressures ranging from 1.1×10^{-7} to 6.6×10^{-5} Torr. At 220 K they measured γ in the range from 0.01 to 0.07 for HBr partial pressures in the range from 7.2×10^{-7} to 1.3×10^{-5} Torr. These γ values were estimated assuming the area of the ice surface to be equal to the geometric area of the cylindrical flow reactor; corrections for surface porosity effects range from a factor of 3 to 10 lower.

46. HOCl + HBr on H_2SO_4.nH_2O(l). Abbatt and Nowak [8] measured uptake of HOCl in the presence of excess HBr on a 69.3 wt. % sulfuric acid solution in a wetted wall flow reactor at 228 K. A second order bulk reaction rate constant, k^{II}, of 2×10^6 $M^{-1}s^{-1}$ was derived; this is a factor of ~10 faster than HOBr + HCl under the same conditions. Since HOCl and HBr have similar solubilities under stratospheric conditions, characterizing this reaction with a simple uptake coefficient is not appropriate. A full reaction/solubility/liquid phase diffusion model will require further data.

47. ClNO and $ClNO_2$ + NaCl(s). Using a Knudsen cell technique Beichart and Finlayson-Pitts set upper limits of $\gamma < \sim10^{-5}$ for reactive uptake of ClNO and $ClNO_2$ on NaCl(s) powders at 298 K.

48. $ClONO_2$ + H_2O(s). Measurement of $\gamma = 0.3$ (+0.7, –0.1) (Hanson and Ravishankara [155]) significantly exceeds previous measurements of Molina et al. [260], Tolbert et al. [333], Leu [232] and Moore et al. [262] but agrees reasonably well with subsequent measurements by Chu et al. [76] and Zhang et al. [365] when geometrical surface areas are assumed for analysis. Previous measurements were probably complicated by NAT formation on the surface (Hanson and Ravishankara [158]; Chu et al. [76]). Lower levels of $ClONO_2$ (g) used by Hanson and Ravishankara [155] minimized this surface saturation problem. Also, using lower $ClONO_2$ concentrations, Zhang et al. obtained a reaction probability of 0.08 ± 0.02 at 195 K, in fair agreement with the range of 0.03 to 0.13 measured by Chu et al. Subsequent Knudsen cell measurements at 180 and 200 K by Oppliger et al. [272] showed initial uptake γs in the 0.2 to 0.4 range. Measured reaction products were HNO_3 and HOCl. All of the HNO_3 and much of the HOCl is retained on the surface under polar stratospheric conditions (Hanson and Ravishankara [155,158]). Hanson [149] deposited $ClONO_2$ on $H_2^{18}O$ enriched ice and detected $H^{18}OCl$ showing the Cl–ONO2 bond is broken at 191 K.

Data plots confirm a trend showing that at a high density of $ClONO_2$, the product HNO_3 covers the ice surface preventing the further reaction of $ClONO_2$ with H_2O molecules on the surface. Therefore, data obtained at high $ClONO_2$ densities ($>10^{14}$ molecules/cm^3) are excluded from further evaluation. An experiment (Berland et al. [53]) using a laser-induced thermal desorption technique yielded a much lower value of $ClONO_2$ reaction probability at 190 K (about 3 orders of magnitude lower) after extrapolating the

results obtained at temperatures of 140 K and below. We also exclude this point in the averaging of data since the physical characteristics of ice surfaces at these very low temperatures may not be very representative of those found at stratospheric temperatures. Selected data show no temperature dependence between T=180 and 200 K and averaged γ_o= 0.28 ± 0.25. Again, within the experimental accuracy, the Hanson and Ravishankara [158,160] and Chu et al. [76] data show that uptake measurements are nearly independent of ice substrate thickness. See Henson et al. [173,174] for discussion of a model which accounts for the effect of HNO_3 on the reaction $ClONO_2$ on water and nitric acid ice surfaces.

Zondlo et al. [374] report the formation of a supercooled H_2O/HNO_3 liquid layer at 185 K as a reaction product, forming NAT or NAD only after decreasing the relative humidity below the ice frost point. This effect is similar to that resulting from the interaction of gaseous HNO_3 or N_2O_5 with the ice surface. These authors measured $\gamma = (3 \pm 2) \times 10^{-3}$ at 185 K for the reaction of $ClONO_2$ with this supercooled liquid layer.

49. $ClONO_2 + HNO_3 \cdot nH_2O(s)$. Hanson and Ravishankara [155] report a γ value of 0.006 at 201 K for the $ClONO_2$ reaction with the water on NAT ($HNO_3 \cdot nH_2O$). However, these authors present re-analyzed and additional data with $\gamma \approx 0.001$ at 191 K in Hanson and Ravishankara [158,160]. Similar experiments (Moore et al. [262], Leu et al. [234]) report a larger value of 0.02 ±0.01 which falls very rapidly as slight excesses of H_2O above the 3/1 H_2O/HNO_3 ratio for NAT are removed. They measure γ of less than 1×10^{-6} for slightly water poor NAT surfaces. The inconsistency between Hanson and Ravishankara and the JPL group (Moore et al. [262]; Leu et al., [234]) has not been resolved. Abbatt and Molina [7] report γ values reaching 0.002 at 202 K and high RH. Hanson and Ravishankara [158] reported that γ for this reaction increases by a factor of 4 as the surface temperature increases from 191 to 211 K. However, Knudsen cell measurements at 185 K by Barone et al. [30] reported $\gamma = 0.004$ at a relative humidity (RH) of 100%, rising to 0.007 near RH = 120%, indicating a possible mild negative temperature dependence when high RH values from this and other studies are compared. Excluding the JPL data, the other data obtained at high RH (~90%) were averaged, assuming no temperature dependence, to yield $\gamma = 0.0043$ ±0.0021. The strong dependence on RH and the possible temperature dependence suggest that systematic error probably exceeds the calculated statistical error. Within the experimental accuracy, the data of Hanson and Ravishankara [158,160] show that measured uptake coefficients are independent of ice substrate thickness. Barone et al. report very similar uptake coefficients for nitric acid dihydrate (NAD) as for NAT as a function of RH at 202 K. See Henson et al. [173,174] for discussion of a model which accounts for the effect of HNO_3 on the reaction of $ClONO_2$ on water and nitric acid ice surfaces.

50. $ClONO_2 + H_2SO_4 \cdot nH_2O(l)$. Results from wetted-wall flow tube (Hanson and Ravishankara [165]) Knudsen cell reactor (Manion et al. [249]), aerosol flow tube (Hanson and Lovejoy [153]), and droplet train uptake (Robinson et al. [293]) experiments supplement older wetted-wall flow tube (Hanson and Ravishankara, [157]) and Knudsen cell measurements (Rossi et al. [298]), (Tolbert et al [332]). Although earlier Knudsen cell measurements probably suffered from surface saturation, more recent results compare well with those from other techniques. Saturation free results, available over a temperature range of 200–265 K and a H_2SO_4 concentration range of 39 to 75 wt. %, were fit to a phenomenological model developed by Robinson et al. [293]. Measured γ values depend strongly on H_2SO_4 concentration and vary modestly with temperature, with a trend to somewhat higher values for the 210–220 K temperature range. The temperature-dependent uptake model takes into account the temperature and composition dependence of the effective Henry's Law constant, liquid phase diffusion coefficient, and the liquid phase hydrolysis rate constant. The hydrolysis reaction was treated by modeling two reaction channels, a direct hydrolysis process dominating reaction at low H_2SO_4 concentrations with a reaction rate proportional to water activity and a proton-catalyzed reaction with a rate proportional to H^+ activity, which dominates at higher acid concentrations.

The data fit to the original Robinson et al. model have been supplemented by additional wetted-wall flow tube and aerosol flow tube data from Hanson [150] and aerosol flow tube data from Ball et al. [28]. A revised kinetic model (Shi et al. [313]) incorporating these data has been developed that is based on the earlier work of Robinson et al. [293].In this model, γ is calculated using the expression

$$\frac{1}{\gamma} = \frac{1}{\alpha} + \frac{1}{\Gamma_b^{H_2O}}$$

where,

$$\Gamma_b^{H_2O} = \frac{4H_{ClONO_2}RT}{\overline{c}}\left(D_{ClONO_2}k_{hydr}\right)^{1/2}$$

The detailed parameterizations for H_{ClONO_2}, D_{ClONO_2}, and k_{hydr} are given in the Appendix in Shi et al. [313] As was the case for N_2O_5 hydrolysis k_{hydr} is seen to have a direct and an acid catalyzed channel. Using the same error analysis approach as in the note on N_2O_5 uptake, the model error is about 32.4% (one sigma), with σ_m=32.2% and σ_d=4.0%.

In the calculation of the chlorine activation (Cl_2 production) rate under stratospheric conditions, one needs to take into account the competition between the reactions of $ClONO_2 + H_2O$ and $ClONO_2 + HCl$. The presence of HCl will depress the reaction probability of $ClONO_2$ with H_2O (see note 49).

51. $ClONO_2 + H_2SO_4 \cdot H_2O(s)$ and $H_2SO_4 \cdot 4H_2O(s)$. Measurements by Hanson and Ravishankara [162] and Zhang et al. [363] demonstrate that the reaction probability on the tetrahydrate is a strong function of both temperature and relative humidity, both of which affect the level of adsorbed H_2O. Both groups covered the temperature range of 192–205 K. The reaction is slowest at higher temperatures and lower relative humidities. Zhang et al. [363] have parameterized their data in the form of $\log \gamma = a_1 + a_2 \log x + a_3 \log^2 x$; for 195 K and x = water partial pressure in Torr: $a_1 = 10.12$, $a_2 = 5.75$ and $a_3 = 0.62$; for a water partial pressure of
3.4×10^{-4} Torr and x = T(K) between 182 and 206: $a_1 = 318.67$, $a_2 =-3.13$ and $a_3 = 0.0076$. Zhang et al.[367] have also measured a low value of $\gamma \sim 2 \times 10^{-4}$ on sulfuric acid monohydrate at 195 K.

52. $ClONO_2 + HCl + H_2O(s)$. Reaction probabilities of 0.27 (+0.73, –0.13) (Leu [232]) and 0.05 to 0.1 (Molina et al. [260]) were reported at 195 and 185 K, respectively. Abbatt and Molina [7] and Hanson and Ravishankara [157] report that a portion of the reaction may be due to $HOCl + HCl \rightarrow Cl_2 + H_2O$, with HOCl formed from $ClONO_2 + H_2O(s) \rightarrow HOCl + HNO_3(s)$. Hanson and Ravishankara [155] saw no enhancement of the $ClONO_2$ reaction probability when $H_2O(s)$ is doped with HCl. Their preferred value at 192 K is $\gamma = 0.3$, but this is consistent with $\gamma = 1$. Chu et al. [76] also report a value of 0.27 (±0.19) at 188 K, assuming no correction for porosity, but suggest the true value is 0.10 (±0.08). Using a Knudsen cell technique and looking at initial uptake, Oppliger et al. [272] measured $\gamma = 0.7$ at 180 K and 0.2 at 200 K with HCl in excess. Eliminating the Molina et al. points, which were taken at much higher $ClONO_2$ concentrations than the others, plots of the remaining data show no obvious bias when plotted as a function of reactant concentration or temperature (180–200 K). Their average value $\gamma = 0.26 \pm 0.06$. The Oppliger et al. data were presented for two HCl concentrations, differing by a factor of three. All points from both HCl concentrations were included since all the data were generally consistent with previous measurements, although the higher HCl concentrations did tend to produce modestly higher uptake coefficients. Until a fuller model is available, a single temperature independent value with a moderate uncertainty due to surface porosity seems appropriate.

53. $ClONO_2 + HCl + HNO_3 \cdot 3H_2O$. Measurements by Hanson and Ravishankara [155,158], Leu and co-workers in Moore et al. [262] and Leu et al. [234], and Abbatt and Molina [7] all report high γ values (>0.1) on NAT for temperatures between 192 and 202 K. Hanson and Ravishankara indicate that reaction probabilities on NAD are similar to those on NAT. The most recent NAT studies (Abbatt and Molina [7]) show a strong fall-off with relative humidity from $\gamma > 0.2$ at 90% RH to 0.002 at 20% RH, indicating the necessity of sufficient water to solvate reactants. Within the limited measurements, data plots show no indication that the reaction probability of $ClONO_2 + HCl$ depends on HCl and $ClONO_2$ gas phase concentrations or temperature between 191 and 202 K. Averaged data yield is $\gamma = 0.23 \pm 0.10$. Carslaw and Peter [67] have published a model of this reaction and its dependence on HCl uptake.

54. $ClONO_2 + HCl + H_2SO_4 \cdot nH_2O(l)$. Early work by Tolbert et al. [332] and Hanson and Ravishankara [157] indicated that the presence of HCl had little effect on the reaction of $ClONO_2$ with concentrated sulfuric acid (>65 wt.% H_2SO_4). Subsequent realization that HCl would be more soluble, and therefore a more potent reactant, in the colder, more dilute sulfuric acid aerosols characteristic of the polar stratosphere led to additional investigations by Hanson and Ravishankara [165], Zhang et al. [363], Elrod et al. [113] and Hanson [150]. All these measurements show a strong dependence of reactivity on HCl solubility, which in turn depends on water activity. The solubility of HCl in a wide range of sulfuric acid solutions has been experimentally determined by a range of techniques that agree well with current thermodynamic models. See

Robinson et al. [294] for a review. Hanson and Lovejoy [153] measured a reacto-diffusive length, ℓ, of only 0.009±0.005 µm for 60 wt.% H_2SO_4 in an aerosol flow reactor. (See Hanson et al. [168] for a definition of

ℓ.) This is a factor of four lower than the value for the hydrolysis reaction of $ClONO_2$ showing the significant enhancement of $ClONO_2$ uptake due to HCl.

The $ClONO_2$ + HCl reaction on sulfuric acid has been modeled in Shi et al. [313] using the same phenomenological model for $ClONO_2$ hydrolysis driven uptake by sulfuric acid. Since the effect of HCl on the $ClONO_2$ uptake is to increase the $ClONO_2$ pseudo-first-order reaction rate, the model of $ClONO_2$ uptake (see note on $ClONO_2$ uptake on sulfuric acid) should include the pseudo first order reaction rate, k_{HCl}. The formulation of k_{HCl} is found in the Appendix in Shi et al. [313].. It is likely that the $ClONO_2$ reaction with HCl, like the $ClONO_2$ hydrolysis reaction, is acid catalyzed via protonated $HClONO_2^+$, where Cl^+ is activated as in the case of HOCl + HCl. For the $ClONO_2$ + HCl reaction, there is also a surface reaction (Hanson [150]). Hanson proposed that Γ_s is linearly proportional to water activity; however, the calculated value of γ_o at 250 K and 60 wt% H_2SO_4 using his formulation is 0.02 (here $\gamma_o \sim \Gamma_s$), which is contradictory to his aerosol flow reactor result, which yielded γ_o=0.0079 (here $\gamma_o \sim \Gamma_b$) (Hanson and Lovejoy [153]). In the model presented in the Shi et al. appendix, it is assumed that that Γ_s is linearly proportional to Henry's law constant of $ClONO_2$, rather than the water activity. The temperature dependence of Γ_s is determined, based on two measured values of Γ_s at 203 K (Hanson, [150]) and 250 K (Hanson and Lovejoy, [153]). The model yields a value of $\gamma_o \sim 0.011$ (here $\gamma_o \sim \Gamma_s$), which is close to the measured value.

In the stratosphere, when the reaction rate of $ClONO_2$ with HCl exceeds the flux of HCl to the particle surface, HCl is depleted. This, in turn, will depress the rate of both the $ClONO_2$ and HOCl + HCl reactions, and increase the $ClONO_2$ hydrolysis rate. Shi et al. [313] have proposed a model in which this effect is taken into account by including a factor F_{HCl} (see Table A–3 in Shi et al.). The formulation of F_{HCl} is based on scaling HCl reaction and accommodation fluxes. This flux correction is not exact (i.e. it does not rigorously calculate the HCl surface or bulk concentration) but provides a good approximation to the expected reduction in HCl + $ClONO_2$/HOCl reactivity and, just as importantly, the effective increase in $ClONO_2$ + H_2O reactivity when $p_{ClONO_2} > p_{HCl}$. This is particularly relevant during cold Cl activation events when HCl can be removed almost completely (i.e., see Jaegle et al. [194]).

Using the same error analysis approach as in the note on N_2O_5 uptake by sulfuric acid, the error of using the model in the Appendix is about 40.0% (one sigma), with σ_m=39.8% and σ_d=4.0%

55. $ClONO_2$+HCl + $H_2SO_4 \cdot H_2O(s)$ and $H_2SO_4 \cdot 4H_2O(s)$. This reaction has been studied by Hanson and Ravishankara [162] and Zhang et al. [363]. The reaction probability is strongly dependent on the thermodynamic state of the SAT surface, which is controlled by the temperature and the water vapor partial pressure. At a water vapor pressure of 5.6×10^{-4} Torr the measured γ drops by over two orders of magnitude as the SAT surface temperature rises from 195 to 206 K. The results from the two groups are in qualitative agreement, but sample different H_2O and HCl partial pressures. Zhang et al. have parameterized their data as a function of water partial pressure (at 195 K) and temperature (both at an HCl partial pressure of 4 to 8×10^{-7} Torr) in the form $\log \gamma = a_1 + a_2 \log x + a_3 (\log x)^2$. For H_2O partial pressure, $a_1 = 5.25$, $a_2 = 1.91$, and $a_3 = 0.0$; for T(K), $a_1 = 175.74$, $a_2 = -1.59$, and $a_3 = 0.0035$. Care must be taken in extrapolating either data set to lower HCl concentrations. Zhang et al. [367] measured no enhancement of $ClONO_2$ uptake on sulfuric acid monohydrate at 195 K with $(2–8) \times 10^{-7}$ Torr of HCl present, implying $\gamma < 1 \times 10^{-4}$.

56. $ClONO_2$ + HCl + $Al_2O_3(s)$. Molina et al. [259] used flow tube techniques to measure $\gamma = 0.020 \pm 0.005$ on α–alumina at 195–230 K with stratospheric (5 ppmV) water vapor levels. Measured γ was independent of T and was affected very little by 5 ppbv HNO_3 vapor. The same γ was measured for a Pyrex surface, indicating the absorbed water and not the inorganic substrate hosted the reaction.

57. $ClONO_2$ + MX(s). Finlayson-Pitts and co-workers have shown that $ClONO_2$ reacts with crystalline NaCl (Finlayson-Pitts et al. [122]) and NaBr (Berko et al. [52]) to produce Cl_2 and BrCl, respectively. Timonen et al. [329] have measured the reaction rate for $ClONO_2$ with dry and slightly wet (water vapor pressure 5×10^{-5} to 3×10^{-4} Torr) NaCl at temperatures of 225 and 296 K. Reaction probabilities were analyzed as $\gamma = 4$–7×10^{-3} and were independent of temperature and water vapor pressure within experimental error. The Cl_2 yield on dry NaCl was 1.0 ± 0.2. Caloz et al. [64] used a room temperature Knudsen cell technique to measure $\gamma = 0.23 \pm 0.06$ for NaCl(s) and $\gamma = 0.35 \pm 0.06$ for KBr(s). They argue that the surface corrections imposed by Timonen et al. were too large. Caloz et al. measured quantitative yields of Cl_2 and BrCl products.

58. $ClONO_2$+HBr + $H_2O(s)$ and $HNO_3 \cdot nH_2O(s)$. This reaction was studied by Hanson and Ravishankara [159] on water ice and NAT near 200 K. A diffusion-limited reaction probability of >0.3 was observed. Allanic et al. [17] measured $\gamma = 0.56 \pm 0.11$ at 200 K on water ice, observing Cl_2 and Br_2 to be formed in yields of 100% and 66 to 80%, respectively, in the range 180 to 200 K.

59. $ClONO_2$ + HF + $H_2O(s)$ and $HNO_3 \cdot nH_2O(s)$. Hanson and Ravishankara [159] were not able to observe this reaction on water ice and NAT surfaces near 200 K.

60. $CF_xCl_{(4-x)}$ (x=0–3) and $CF_2Br_2 + Al_2O_3$(s). Robinson et al. [291] reported dissociative uptake of CF_2Cl_2 and CF_2Br_2 on α-alumina surfaces at 210 and 315 K. Reaction probabilities of about 1×10^{-3} at 210 K were measured by monitoring the amounts of surface species bonded to the Al_2O_3 substrate. A re-analysis (Robinson et al. [292]) lowered this value by about a factor of 50. Moderate surface dosage with water vapor did not quench the reaction. In addition, Dai et al. [95] and Robinson et al. [290] studied dissociative chemisorption of CF_3Cl, CF_2Cl_2, $CFCl_3$, and CCl_4 on dehydroxylated γ-alumina powders. The obtained reactive uptake probabilities ranging from 0.4×10^{-5} for $CFCl_3$ to 1.0×10^{-5} for $CFCl_3$ over a temperature range of 120 to 300 K. HCl and halomethyl radicals were observed as desorption products. Loss of these products may point to somewhat higher γs, since they were measured by integrating halogen bound to Al_2O_3 substrates.

61. $BrO + H_2O$(s) and $H_2SO_4 \cdot nH_2O$(l) and NaCl(aq). Abbatt [3] used a coated flow tube technique to measure heterogeneous uptake on water ice, 60 and 70 wt % H_2SO_4 at 213 K, and 23 wt % aqueous NaCl at 253 K. He obtained γ(ice) = $(1.0 \pm 0.4) \times 10^{-3}$, γ (60 wt % H_2SO_4) = $(7 \pm 2) \times 10^{-4}$, γ (70 wt % H_2SO_4) = $(5 \pm 2) \times 10^{-4}$ and γ (23 wt % NaCl) $< 3 \times 10^{-3}$. He observed product Br_2, indicating BrO self-reaction on both water ice and sulfuric acid solutions. Since reaction rate will depend on BrO concentrations, no recommendation is made for an atmospheric rate.

62. HOBr + HCl(s). Abbatt [1] measured γ = 0.25 (+0.10/–0.05) for this reaction on ice at 228 K. The BrCl product was observed by mass spectrometry. No data on NAT surfaces are currently available.

For the sulfuric acid reaction, Abbatt [2] measured γs of ~ 0.1 to 0.2 for [HCl] $> 1 \times 10^{12}$ cm^{-3} over 68.8 wt. % H_2SO_4 at 228 K; yielding an estimated $k^{II}_{HCl+HOBr} = 1.4 \times 10^5$ M^{-1} s^{-1} with a factor of 2 uncertainty. Hanson and Ravishankara [166] also measured γ = 0.2 [+0.2, – 0.1] for 60 wt. % H_2SO_4 at 210 K. However, both of these measurements were based on significant underestimation of the solubility of HOBr in the relevant sulfuric acid solutions. More recent measurements by Waschewsky and Abbatt [347] indicate that H for HOBr varies slightly with acidity between 60 to 70 wt.% H_2SO_4 and more strongly with temperature between 208 and 238 K. (For 59.7 wt.% H_2SO_4, H (M atm^{-1}) = 1.2×10^6 at 208 K and and 2.2×10^5 at 228 K.) The HOBr + HCl second order liquid phase rate constant, $k^{II}_{HCl+HOBr}$, varies between 2×10^5 and 3×10^8 (M^{-1}s^{-1}) between 213 and 238 K over the same composition range (60–70 wt.% H_2SO_4). Such a strong dependence on acid composition for the reaction rate of HOBr + HCl and the very small acid composition dependence for HOBr solubility in H_2SO_4 solution might be partially due to the formation of H_2OBr^+ in the acidic solution as discussed in their paper. However, this acid catalyzed reaction, i.e. H_2OBr^+ + HCl, alone does not completely account for measured reaction rates over the acid composition range studied.

Using the Henry's Law data for HOBr reported by Waschewsky and Abbatt [347], the limiting reagent will vary depending on atmospheric temperature (H_2SO_4 wt.%) and the concentrations of HOBr and HCl. For stratospheric conditions where [HOBr] is 10 pptv and [HCl] 1ppbv, they predict dissolved HOBr will be in excess above 204 K and HCl in excess below 204 K for a H_2O vapor partial pressure of 3×10^{-7} atm. From their coated wall flow reactor uptake measurements, Waschewsky and Abbatt [347] derived expressions for $k^{II}_{HCl+HOBr}$ and predicted uptake coefficients. For temperature between 204 and 218 K where HOBr is likely to be in excess, they calculated HCl uptake coefficients, $γ_{HCl}$, which range between 7×10^{-5} and 9×10^{-5}. For temperatures in the 202–198 K range, where dissolved HCl is likely to be excess, the calculated uptake coefficients for HOBr, $γ_{HOBr}$, of ~1×10^{-2}. Clearly, the HOBr + HCl reaction will be difficult to parameterize in a simple manner. Potential inconsistencies in their $k^{II}_{HCl+HOBr}$ values, as discussed by Waschewsky and Abbatt, indicate that further measurements will be required before this reaction can be definitively modeled.

63. $HOBr + HBr + H_2O$(s) and $H_2SO_4 \cdot nH_2O$. Abbatt [1] measured γ = 0.12 ± (0.03) on ice at 228 K. The Br_2 product was observed by mass spectrometry. Abbatt [2] measured γ = 0.25 for [HBr] = 1×10^{12} cm^{-3} over 68.8 wt % H_2SO_4 at 228 K; yielding an estimated $k_{II} > 5 \times 10^4$ M^{-1} s^{-1}.

64. $BrONO_2 + H_2O$(s). Hanson and Ravishankara [160] investigated these reactions in an ice-coated flow reactor at 200 (± 10) K. The reaction of $BrONO_2$ with H_2O(s) proceeded at a rate indistinguishable from the gas phase diffusion limit, implying that the reaction probability may be as high as one; the product BrNO(g) was observed. Allanic et al [16] used a Knudsen cell reactor to measure $BrONO_2$ uptake between 190–200 K. Values of initial γs in the 0.2–0.3 range were observed. An average γ = 0.26 ± 0.05 was obtained from all of the appropriate data from both experiments.

65. $BrONO_2 + H_2SO_4 \cdot nH_2O$(l). Hanson and co-workers used both coated flow tube and aerosol flow tube techniques to show that the reaction of $BrONO_2$ with 45–70 wt. % H_2SO_4 is extremely facile at temperatures

from 210 to 298 K. Hanson and Ravishankara [166] measured γs of 0.5 (+0.5, –0.25) (45 wt. % H_2SO_4, 210 K, 0.4 (+0.6, –0.2) (60 wt. %, 210 K) , and 0.3 (+0.7, –0.1) (70 wt. %, 220 K) in a coated-wall flow tube experiment. Hanson et al. [167] measured γ ~ 0.8 (20 to 40% error) for submicron aerosols at temperatures between 249 and 298 K and H_2SO_4 concentrations of 45 to 70 wt. %; they did observe a sharp fall off in γ for H_2SO_4 concentrations between 73 and 83 wt. %. Hanson has analyzed these combined data sets, the data indicated that γ is a function of sulfuric acid concentration, but independent of temperature. He has fit an empirical expression for γ for $BrONO_2$ + H_2O of: γ = exp(a+b*wt.)+c [Hanson, priv. comm.]. The data have been fitted to the formulation $1/γ=1/α+1/γ_{rxn}$, yielding α=0.805, and a=29.24, b=–0.396, c=0.114. Additional unpublished measurements using both techniques at higher temperatures performed by Hanson [priv. comm.] also fit this functional form. Using the same approach as detailed in the note for N_2O_5 uptake on sulfuric acid, the error for $BrONO_2$+ H_2O is 27.3% (one sigma), with $σ_m$=26.6% and $σ_d$=6.3%.

66. CF_3OH + H_2O + H_2O(l) and H_2SO_4 • nH_2O(l). Lovejoy et al. [245] used both wetted-wall and aerosol flow tube techniques to measure reactive uptake of CF_3OH on water at 274 K and 39–60 wt % H_2SO_4 at various temperatures between 206 and 250 K. γ's showed a strong dependence on water activity. Aerosol uptake studies yielded reacto-diffusive lengths of > 0.4 μm for 40 wt % H_2SO_4 and 1.0 μm for 50 wt % H_2SO_4, both at 250 K. Recommended γ's were estimated by averaging bulk uptake measurements at similar H_2SO_4 concentrations and ignoring temperature effects on water activity.

67. SO_2 + H_2O_2, O_3, HONO, NO_2, HNO_3 on H_2SO_4·nH_2O(l). Rattigan et al. [282] used a bubble train reactor to measure the uptake of SO_2 in the presence of solvated oxidants at 293 K. For H_2O_2 the second order rate constant at 1 wt. % H_2SO_4 agreed well with previous bulk kinetics measurements and with previous droplet train/flow reactor measurements. Measurements at 20, 40, and 60 wt. % H_2SO_4 are the first reported for concentrated acid. Reaction rate data were fit to a two term (acid catalyzed and water catalyzed) bulk second order rate expression, which, in the limit of high acid activity (a_H^+ = $α_{H+}$[H^+], where $α_{H+}$ is the H^+ activity coefficient) reduces to: $k^{II}_{H_2O_2}$= 8.3 × 10^4 ($α_{H_2O}$/ a_H^+), where $α_{H_2O}$ is the water activity coefficient. Both $α_{H+}$ and $α_{H_2O}$ can be obtained from the sulfuric acid thermodynamic model of Carslaw et al. [66]. The high a_H^+ approximation for $k^{II}_{H_2O_2}$ should be accurate to a factor of two between 40 and 70 wt %.

Uptake of SO_2 in the presence of solvated O_3 was measured for 1–70 wt. % acid; the Henry's law expression for O_3 was determined in separate experiments. Measured second order rates agree reasonably well with previous results measured below 18 wt. %. A three term fit for reaction with SO_2(aq), HSO_3^-, and $SO_4^=$ was fit to the data: $k^{ii}_{O_3}$ = 6.6 × 10^3 [SO_2(aq)] + 3.2 × 10^5 [HSO_3^-] + 1 × 10^9 [$SO_4^=$]. This expression should be accurate to a factor of two between 20 and 70 wt. %.

The HONO reaction was studied by adding nitrosyl sulfuric acid to 20, 40, 60, and 70 wt. % acid. Measured second order rate constants were moderately consistent with previous measurements below 10 wt. %. A k^{ii}_{HONO} = 142[H^+] was fit to the full data set; it should be accurate to a factor of two for acid concentrations between 10 and 70 wt. %.

No enhanced SO_2 uptake was observed with added gas phase NO, NO_2, or with 20 wt. % HNO_3 added to 50–60 wt. % sulfuric acid.

68. SO_3 on H_2SO_4·nH_2O(l). Jayne et al. [199] measured the uptake coefficient in a wetted wall-flow reactor at 300 K over a composition range of 78–92 H_2SO_4 wt. %. The measured γ was indistinguishable from 1.0. Higher water concentrations and lower temperatures probably tend to increase γ, so a value near 1.0 probably holds for all atmospheric conditions.

5.14   Soot Surface Uptake Coefficients

Table 5-3. Soot Surface Uptake Coefficients.

Gaseous Species	Uptake Coefficient (γ)	Notes
SO_2	See Note	1, 2
NH_3	0, See Note	1, 3
O_3	See Note	1, 4
HNO_3	See Note	1, 5
N_2O_5	See Note	1, 6
NO_2	See Note	1, 7
NO_3	See Note	1, 8
HO_2	See Note	1, 9
HO_2NO_2	See Note	1, 10
H_2O	See Note	1, 11

5.15   Notes to Table 5-3

1.   See also the sections on soot under "Surface Types" and "Parameter Definitions" for a description of some of the factors affecting the uptake and reaction of gases on soot surfaces. In most cases, the available reactive surface area rather than the geometric areas have been used in obtaining the uptake coefficients; in those cases where the geometric area was used but a higher available surface area was involved in the measured uptake, the uptake coefficient is given as an upper limit. Most data are available at room temperature or there are very limited data at lower temperatures characteristic of the upper troposphere.

2. SO_2 + soot. $\gamma \leq 3 \times 10^{-3}$ measured using Degussa FW2 carbon black by Rogaski et al. [295]. This is an upper limit since it is based on the geometric surface area. Koehler et al. [226] measured an average value of $(2 \pm 1) \times 10^{-3}$ over the first 10–30 s on n-hexane soot at –100° C (the initial uptake may be larger), but indicate that taking into account surface roughness would reduce this value. A number of studies [25,77,78,90,226,238,295] suggest that uptake is primarily due to physisorption on the surface; oxidation occurs in the presence of water, oxidants and metals.

3. NH_3 + soot. Chughtai et al. [77] and Muenter and Koehler [267] measured the uptake of NH_3 on soot. Based on Muenter and Koehler [267] where conditions are closest to atmospheric, NH_3 is not taken up by soot particles at temperatures above 173 K.

4. O_3 + soot. Many studies report a rapid, initial loss of O_3 followed by a slower loss that also occurs on aged soot or soot pre-exposed to ozone [81,87,104,115,117,187,210,244,295,316,319,323]. Initial, rapid O_3 loss may be most applicable for soot as it comes out of aircraft exhaust, with $\gamma^{init} \sim 10^{-3}$ from most studies using both carbon black and organic combustion soots [115,117,187,295,323]. The second stage of the reaction is probably more applicable to soot dispersed in air; $\gamma^{aged} \sim 10^{-4}$–$10^{-6}$ using both carbon black and organic combustion soots [115,117,187,210,244,278,323], but in the range of 10^{-4} to 10^{-5} based on organic combustion soot data alone [187,244]. A few studies have been carried out at temperatures below room temperature [81,187,210,244]; given the wide ranges measured even at room temperature, these values generally fall in the same range. Il'in et al. [187] report a temperature dependence for the initial uptake on fresh soot of $\gamma^{fresh} = 1.9 \times 10^{-3}(\exp–780/T)$ and for aged soots, $\gamma^{aged} = 1.8 \times 10^{-4}(\exp–1000/T)$. Both physisorption and reaction of ozone with the surface appear to take place. The studies of Fendel et al. [115] suggest that lower particle growth in size below 40 ppb O_3 is due to less than a monolayer of O_3 on the surface. Stephens et al. [323] proposed a Langmuir-type reversible adsorption of O_3, followed by a slower reaction with the surface. Pöschl et al. [278] proposed a similar scheme for uptake of ozone on spark-generated graphite soot coated with benzo[a]pyrene. Initial reversible physisorption occurred with $\gamma \sim 10^{-3}$, and "apparent reaction probabilities" for O_3 with BaP on soot of $\gamma \sim 10^{-5}$–10^{-6} were reported. The presence of water inhibited the reaction, which was postulated to be due to competitive adsorption between water and ozone on the surface; this is in contrast to the report of Chughtai et al. [82] in which the rate of ozone loss increased with RH. Pöschl et al. [278] report Langmuir adsorption equilibrium constants for O_3 and H_2O, and a second order surface reaction rate constant for the O_3-BaP reaction of $(2.6 \pm 0.8) \times 10^{-17} \, cm^{-2} \, s^{-1}$. Three possible paths have been proposed: (1) chemisorption of O_3; (2) catalytic decomposition of O_3: $2O_3 \rightarrow 3O_2$; (3) surface oxidation and formation of gas-phase carbon oxides. The studies of Fendel et al. [116] suggest that lower particle growth in size below 40 ppb O_3 is due to less than a monolayer of O_3. Studies of Smith et

al. [319] and Smith and Chughtai [316] suggest that catalytic decomposition occurs to some extent over the entire reaction sequence. CO_2 and H_2O are the major gas phase and surface oxidized functional groups on the surface such as carboxylic acids are observed [82-84,104,115,210,252,316-318,323].

5. HNO_3 + soot. Studies of the uptake of HNO_3 on soot have been carried out over a range of nitric acid pressures [70,92,103,220,244,295,297,304,305]. Measured values of γ at room temperature are typically in the range 10^{-1}–10^{-5}, with smaller uptake coefficients measured at longer reaction times. Saatthoff et al. [304] report an upper limit of 3×10^{-7} as a time-averaged value over two days. At lower concentrations characteristic of the atmosphere, uptake appears to be primarily due to physisorption while at higher concentrations, $> 2 \times 10^{12}$ molecule cm^{-3}, a surface reaction occurs. At 220 K, $\gamma \sim 0.1$ with irreversible uptake attributed to reaction with surface groups [70]. Reaction of HNO_3 at concentrations from $(1–9) \times 10^{12}$ molecule cm^{-3} with "grey" soot from a rich flame using hexane has been reported [305] to generate HONO as the major gaseous product with initial and steady-state reaction probabilities of $\gamma_o = 4.6 \times 10^{-3}$ and $\gamma_{ss} = 5.2 \times 10^{-4}$ respectively; reaction with "black" soot from a lean flame gave NO as the major gaseous product, with initial and steady-state reaction probabilities of $\gamma_o = 2.0 \times 10^{-2}$ and $\gamma_{ss} = 4.6 \times 10^{-3}$ respectively (based on geometric surface area of sample holder). The NO was hypothesized to result from secondary reactions of an initial HONO product.

6. N_2O_5 + soot. Brouwer et al. [58], Longfellow et al. [244] and Saathoff et al. [304]studied the uptake of N_2O_5 at room temperature on a ground charcoal (carbon black) sample, on propane soot and on spark-generated graphite soot, respectively. Brouwer et al. and Longfellow et al. report uptake coefficients based on the geometric sample surface area, and therefore give upper limits. An upper limit of $\gamma \leq 0.02$ can be derived based on the larger value of 0.016 reported by Longfellow et al. As discussed below, much smaller values are reported by Saathoff et al.: 4×10^{-5} under dry conditions and 2×10^{-4} at 50% RH. Three possible reactions may occur: (1) Decomposition of N_2O_5 on the surface to generate $NO_2 + NO_3$; (2) reaction of N_2O_5 with the soot; (3) hydrolysis of N_2O_5 with water on the surface to generate HNO_3. The studies of Longfellow et al. support the decomposition reaction, with yields of NO_2 within experimental error of 100%; the generation of NO_3 on the surface followed by its decomposition to NO_2, may contribute to the observed production of NO_2. The studies of Brouwer et al. suggest that a redox reaction with the soot surface to generate NO occurs in parallel with hydrolysis of N_2O_5 to generate HNO_3. Saathoff et al. propose two independent, parallel reactions: (1) hydrolysis generating HNO_3, N_2O_5 + soot $\rightarrow$ 2 HNO_3 with $\gamma = (4 \pm 2) \times 10^{-5}$ under dry conditions (< 10 ppm H_2O) which increases to $(2 \pm 1) \times 10^{-4}$ at 50% RH. (2) decomposition to NO and NO_2: N_2O_5 + soot $\rightarrow$ NO + NO_2 + products, with $\gamma = (4 \pm 2) \times 10^{-6}$ under dry conditions.

7. NO_2 + soot. A fast initial uptake of NO_2 is observed on fresh soots [13,14,21,77,80,85,86,134,205,220,243,295,321,325,326] with the initial uptake coefficient in studies involving both carbon blacks and organic combustion soots in the range of $\gamma^{init} \cong 10^{-1}$ to 10^{-4}. For longer reaction times on carbon black soots, $\gamma^{aged} \sim 10^{-4}$ based on studies by Kalberer et al. [206] and Ammann et al. [21,22]. However, Kleffmann et al. [223] report a lower uptake coefficient of $\sim 10^{-7}$ on carbon black over the first 5 minutes of reaction and and Saathoff et al. [304] report an upper limit of $< 4 \times 10^{-8}$ averaged over 5 days under dry conditions (< 10 ppm H_2O) on spark-generated graphite. On organic combustion soots, γ^{aged} has been reported to be in the range of $\sim 10^{-4}$–10^{-6} [13,22,23,243,321][305]. All studies were done at room temperature except those of Longfellow et al. [243] which were carried out at 262 K. The surface deactivates on continued exposure to NO_2, suggesting a maximum amount of HONO that can be formed per cm^2 of soot area or mg of soot; this has been reported to be in the range of 10^{16} to 10^{18} HONO per mg of soot [23,134,204,205,223,321]. However, reactivation on heating of the surface, exposure to water vapor and/or with time after the exposure is stopped has been observed [134,243,321,325,326]. A small portion (~10-20%) of the NO_2 taken up appears to be chemisorbed to the surface [13,23,80,204,205,220,223,321,325,326]. Infrared studies [13,220,318] show that surface C–ONO, C–N–NO_2, and C–NO_2 groups are formed. The remainder of NO_2 reacted appears as gaseous HONO and NO; Salgado and Rossi [305] report HONO as the major product for hexane soot from a flame at near stoichiometric ratio but NO as the major product for soot from an extremely lean flame. In addition, N_2O, CO, and CO_2 have been observed as products at higher temperatures [34,35]. At lower NO_2 concentrations, the HONO yield can approach 100%; production of NO may be due to the bimolecular reaction of HONO on the surface at higher concentrations to give NO + NO_2 + H_2O. The HONO yield at 262 K appears to be smaller than at room temperature [243]. Formation of HONO is due to reaction with a reduced surface site and not to NO_2 surface-catalyzed hydrolysis. The formation of HONO from the reaction of NO_2 with unspecified semi-volatile organics in

diesel exhaust has been reported [143] and proposed to be a much larger source of HONO than the reaction with the soot itself.

8. NO_3 + soot. Saathoff et al. [304] report an upper limit of $\gamma < 3 \times 10^{-4}$ on dry soot (< 10 ppm H_2O) and $\leq 10^{-3}$ at 50% RH based on measurements of NO_3 and N_2O_5.

9. HO_2 + soot. Saathoff et al. [304] report an upper limit of $\gamma < 10^{-2}$ on dry soot (<10 ppm H_2O) based on the decay of HO_2NO_2 (in equilibrium with HO_2 and NO_2) in the presence and absence of soot.

10. HO_2NO_2 + soot. Saathoff et al. [304] report an upper limit of $\gamma < 10^{-5}$ on dry soot (<10 ppm H_2O) based on the decay of HO_2NO_2 in the presence and absence of soot.

11. H_2O + soot. Alcala–Jornod et al. [14] report an upper limit to the initial uptake coefficient of $\gamma < 2 \times 10^{-3}$, consistent with the earlier measurements of Rogaski et al. [295]. The uptake is most likely a reversible physisorption [14,277] although based on water uptake isotherms, Chughtai et al. [77,79,84,87] propose that at low relative humidities (< 25%) chemisorption occurs. While prior exposure of Degussa FW-2 to NO_2 and SO_2 was not found to increase the uptake coefficient for water, treatment with HNO_3 increased the measured uptake coefficient by a factor of 28 and with H_2SO_4 by a factor of 68 [295]. Water adsorption isotherms on soot have been measured in a number of studies, e.g. [77,79,82,84,87] and the amount of water taken up found to increase with the air/fuel ratio used to generate the soot, with the sulfur content, with aging and oxidation of the surface (e.g. by O_3) and with the presence of metals [77,79,82,84,87,350].

5.16 Henry's Law Constants for Pure Water

Table 5-4. Henry's Law Constants for Pure Water.

Substance	Temperature Range, K	H (298 K)[a]	*A*	*B*	*C*	Uncertainty Range[b]	Note
O_2	273–348	1.27×10^{-3}	−161.6	8160	22.39	A	1
O_3	273–333	1.03×10^{-2}	−14.08	2830		C	2
HO_2	298	1000				D	3
H_2O_2	278–303	7.73×10^4	−13.27	7310		C	4
N_2	273–348	6.52×10^{-4}	−177.1	8640	24.71	A	5
NH_3	273–348	60.2	−9.84	4160		C	6
NO	273–358	1.92×10^{-3}	−157.1	7950	21.298	B	7
NO_2	298	1×10^{-2}				E	8
N_2O	273–313	2.42×10^{-2}	−148.1	8610	20.266	A	9
CO	278–323	9.81×10^{-4}	−178.0	8750	24.875	A	10
CO_2	273–353	3.38×10^{-2}	−145.1	8350	19.960	A	11
CH_4	273–328	1.41×10^{-3}	−194.7	9750	27.274	A	12
C_2H_6	273–323	1.88×10^{-3}	−240.2	12420	33.744	A	13
C_3H_8	273–348	1.51×10^{-3}	−281.1	14510	39.652	A	14
$n–C_4H_{10}$	273–348	1.24×10^{-3}	−269.9	14330	37.734	A	15
$CH_3CH(CH_3)CH_3$	278–318	9.18×10^{-4}	−360.6	18020	51.444	B	16
C_2H_4	288–348	5.96×10^{-3}	−154.6	8540	21.202	B	17
C_2H_2	273–343	4.14×10^{-2}	−145.8	7880	20.384	B	18
CH_3OH	273–298	220	−12.08	5210		C	19
CH_3CH_2OH	273–298	200	−16.98	6630		C	20
$n–C_3H_5OH$	273–298	130	−20.16	7470		D	21
$iso–C_3H_5OH$	273–298	130	−20.15	7450		D	21
$n–C_4H_9OH$	273–298	127	−19.34	7210		D	21
$iso–C_4H_9OH$	298	102				D	21
$sec–C_4H_9OH$	273–298	110	−19.65	7260		D	21
$tert–C_4H_9OH$	273–298	70	−23.63	8310		D	21
CH_3OOH	277–293	300	−11.99	5280		D	22
$HOCH_2OOH$	278–293	1.7×10^6	−18.79	9870		E	23
$HCHO$	288–318	3.23×10^3	−15.73	7100		D	H* 24
CH_3CHO	273–313	12.9	−17.19	5890		D	H* 25
C_2H_5CHO	273–313	10.0	−12.20	4330		E	26
C_3H_7CHO	283–318	9.6	−18.59	6220		E	27
CH_3COCH_3	273–311	28.1	−13.62	5050		D	28
$C_2H_5COCH_3$	273–298	18	−16.40	5740		D	29
$HC(O)OH$	275–308	8.9×10^3	−11.40	6100		D	30
$CH_3C(O)OH$	275–308	4.1×10^3	−12.50	6200		D	31
CH_3CN	273–303	52.8	−9.35	3970		C	32
CH_3NO_2	293–323	34.6	−9.92	4010		D	33
$C_2H_5NO_2$	293–323	21.7	−11.80	4430		D	33
$C_3H_7NO_2$	293–323	13.1	−13.22	4710		D	33
$CH_3CH(NO_2)CH_3$	293–323	8.42	−13.02	4520		D	33
CH_3ONO_2	273–298	2.0	−15.20	4740		D	34
$C_2H_5ONO_2$	273–298	1.59	−17.50	5360		D	34
$1–C_3H_7ONO_2$	273–298	1.10	−18.31	5490		D	34
$2–C_3H_7ONO_2$	273–298	0.791	−18.20	5360		D	34
$1–C_4H_9ONO_2$	273–298	1.01	−19.40	5790		D	34
$2–C_4H_9ONO_2$	273–298	0.648	−18.59	5410		D	34
$CH_3C(O)O_2NO_2$	274–297	2.8	−18.15	5730		D	35
$O_2NOC_2H_4ONO_2$	293	640				D	36
$HOC_2H_4ONO_2$	293	3.99×10^4				D	36
$HOCH_2CH(ONO_2)CH_3$	293	7.3×10^3				D	36
$CH_3CH(OH)CH_2ONO_2$	293	6.7×10^3				D	36
$CH_3CH(ONO_2)CH_2ONO_2$	293	175				D	36
$CH_3C(O)CH_2ONO_2$	293	1.01×10^3				D	36
Cl_2	283–383	9.29×10^{-2}	−134.4	7590	18.702	B	37
Cl_2O	273–293	17	−3.23	1810		D	38

Substance	Temperature Range, K	H (298 K)[a]	A	B	C	Uncertainty Range[b]	Note
ClO_2	383–333	1.01	−11.65	3470		B	39
HOCl		660	−13.2	5880		D	40
Br_2	273–308	0.725	−15.05	4390		B	41
BrCl	279–299	0.98	−18.9	5630		C	42
SO_2	278–383	1.36	−39.72	4250	4.525	B	43
	278–298		−9.53	2930			
H_2S	273–323	0.102	−145.2	8120	20.296	C	44
CS_2	274–305	0.062	−17.05	4250		D	45
COS	273–288	2.02×10^{-2}	−15.68	3510		D	46
CH_3SH	298–368	0.39	−12.42	3420		E	47
C_2H_5SH	298–368	0.28	−13.82	3740		E	48
CH_3SCH_3	272–305	0.54	−12.19	3460		E	49
$CH_3S(O)CH_3$	298	9.9×10^4				E	50

a. $\ln H = A + B/T + C \ln(T)$ [M atm^{-1}]

b. Uncertainty Classes:
   A—Better than 10%
   B—10% to 50%
   C—50% to 100%
   D—Factor of 2 to factor of 10
   E—Factor of 10 to factor of 100
   F—Greater than a factor of 100

5.17   Notes to Table 5-4

Many of the data sets required various transformations to convert them to the units (mol L^{-1} atm^{-1}) and form (solubility instead of volatility) used in this Table. The transformations often involve either the mass or molar density of water, which in all cases was taken from [231].

1. O_2. The recommendation was taken from the studies of Benson [51] and Rettich [285]. The data show clear curvature in a plot of ln (K_h) v. 1/T. A two parameter fit gives A = −13.26 and B = 1950 K for the temperature range 273–285 K.

2. O_3. The recommendation of Rischbieter [288] was accepted and refitted.

3. HO_2. The recommendation was based on a calculation by Schwartz [307]. Thermodynamic values were updated to those in our Thermodynamic tables.

4. H_2O_2. The data of Lind and Kok [239,240], Hwang and Dasgupta [186], Yoshizumi et al. [361], and O'Sullivan et al. [273] are all in good agreement. The recommendation is from a two-parameter fit to all the results.

5. N_2. The recommendation of Battino [34] was accepted and refitted to three-parameter equations. A two parameter fit gives A = 12.81 and B = 1625 K for the temperature range 273–293 K.

6. NH_3. Based on the recommendation by Edwards et al. [111], refit to a two-parameter equation. Over the temperature range 273–348 K, there appears to be little curvature in the data. The more recent work of Dasgupta and Dong [96] are in quite good agreement with this recommendation, whereas the results of Hales and Drewes [144] are somewhat higher and those of Shi and Davidovits [312] (an uptake study) are significantly lower. The Hales and Drewes paper also included studies of the effect of dissolved CO_2 on the solubility of NH_3. The solubility of NH_3 in solutions containing a wide variety of ions is discussed by Clegg and Brimblecombe [89].

7.   NO. Three-parameter refit from the recommendation of Battino [32]. Two-parameter fit gives A = −12.27 and B = 1790 K for the temperature range 273–293 K.

8. NO_2. From analysis of studies of reactive dissolution of NO_2 by Schwartz and White [309].

9. N_2O. Three-parameter refit to the recommendation of Battino [31]. Two parameter fit gives A = 13.40 and B = 2880 K for the temperature range 273–293 K.

10. CO. The recommendation is based on smoothed data from Rettich et al. [284] and refit to three-parameter equation. A two parameter fit gives A = –12.72 and B = 1720 K for the temperature range 273–293 K.

11. CO_2. Refit to three- parameter equation from the recommendation of Wilhelm et al. [352]. Two parameter fit gives A = 12.49 and B = 2710 K for the temperature range 273–293 K.

12. CH_4. The recommendation is a three-parameter fit to the smoothed recommendation of Battino [41]. There is very good agreement with the more recent data of Ben-Naim and Battino [50]. A two parameter fit gives A = –13.45 and B = 2040 K for the temperature range 273–293 K.

13. C_2H_6. The recommendation is a three-parameter fit to the smoothed recommendation of Battino [33]. There is very good agreement with the more recent data of Ben-Naim and Battino [50]. Two parameter fit gives A = –15.95 and B = 2875 K for the temperature range 273–293 K.

14. C_3H_8. The recommendation is from a three-parameter fit to the smoothed recommendation of [40]. There is very good agreement with the more recent data of Ben-Naim and Battino [50]. A two parameter fit gives A = 17.52 and B = 3275 K for the temperature range 273–293 K.

15. n-C_4H_{10}. The recommendation is from a three-parameter fit to the smoothed recommendation of Battino [39]. There is very good agreement with the more recent data of Ben-Naim and Battino [50]. A two parameter fit gives A = –19.28 and B = 3740 K for the temperature range 273–288 K.

16. $CH_3CH(CH_3)CH_3$. The recommendation is from a three-parameter fit to the smoothed recommendation of Battino [38]. A two parameter fit gives A = 18.22 and B = 3340 K for the temperature range 278–293 K.

17. C_2H_4. The recommendation is from a three-parameter fit to the smoothed recommendation of Wilhelm [352]. A two parameter fit gives A = –12.40 and B = 2170 K for the temperature range 288–313 K.

18. C_2H_2. The recommendation is from a three-parameter fit to the smoothed recommendation of Wilhelm [352]. The recommendation of Yaws et al. [360] generates identical results. A two parameter fit gives A = –10.12 and B = 2065 K for the temperature range 273–298 K.

19. CH_3OH. The recommendation is based on the two data points of Snider and Dawson [320]. The 298 K result of Butler et al. [62] and a calculation based on the NBS Thermodynamic tables, [345], are in very good agreement. The 298 K result of Altschuh et al. [20] is about 40% lower.

20. C_2H_5OH. The recommendation is based on the two data points of Snider and Dawson [320]. The 298 K results of [62] and [296], and a calculation based on the NBS Thermodynamic tables, [345], are in very good agreement. The 298 K result of Altschuh [20] is about 50% lower.

21. All of the recommendations for the C3–C4 alcohols are based on two data points each from Snider and Dawson [320]. Room temperature data from other studies ([61],[62], and [20]) typically support these results.

22. CH_3OOH. The data of Lind and Kok [239,240] and O'Sullivan et al. [273] are in excellent agreement and were fit to a two-parameter expression.

23. $HOCH_2OOH$. The results of O'Sullivan [273] and Staffelback and Kok [322] are very close and were fit to obtain the recommended values. The results of Zhou and Lee [371] are much lower and were not included.

24. HCHO. The recommended value is the apparent Henry's law constant and includes a contribution due to hydrolysis $H^* = H(1 + K_{hyd})$. Data from Betterton and Hoffmann [54] and Zhou and Mopper [372] are in substantial agreement and were fit to a two-parameter expression. Betterton and Hoffmann have calculated $K_H = 2.5$ M atm^{-1} at 298 K for the physical solubility.

25. CH_3CHO. The recommended value is the apparent Henry's law constant and includes a contribution due to hydrolysis $H^* = H(1 + K_{hyd})$. The results of Snider and Dawson [320], Benkelberg et al. [49], and Betterton and Hoffmann [54] are in excellent agreement and have been fit to a two-parameter expression for the recommendation. The results of Zhou and Mopper [372] curve off at higher temperatures and were not included in the fit. (Note the similar situation for acetone.) Betterton and Hoffmann have calculated $K_H = 4.8$ M atm^{-1} at 298 K for the physical solubility.

26. C_2H_5CHO. Results of Zhou and Mopper [372] and Snider and Dawson [320] agree only to within about a factor of two. The two points from the former were weighted by 3 and combined with the five points of the latter to generate the recommendation.

27. C_3H_7CHO. The only results are from Zhou and Mopper [372], which have been fit to a two-parameter expression.

28. CH$_3$COCH$_3$. The recommendation is from a fit to the data of Snider and Dawson [320] and Benkelberg et al. [49]. Room temperature data points of Hoff et al. [176], Burnett [61] and Vitenberg et al. [340] are in very good agreement. Results of Zhou and Mopper [372] are somewhat higher, particularly at room temperature and above. The situation is similar for acetaldehyde.

29. C$_2$H$_5$COCH$_3$. The recommendation is from the two points of Snider and Dawson [320]. The room temperature points of Vitenberg et al. [340] and Rohrschneider [296] are in good agreement. The higher temperature data of Zhou and Mopper [372] are somewhat higher and the those of Friant and Suffet [128] are lower than the recommendation.

30. HC(O)OH. The results of Johnson et al. [203] are accepted. The 298 K result of Khan et al. [219] are about 75% lower. Bob, did you consider the results of Servant et al. (quoted in 97-4)?

31. CH$_3$C(O)OH. The results of Johnson et al. [203] are accepted. A value calculated from the NBS Thermodynamic tables [345] is about a factor of two higher. Bob, did you consider the results of Servant et al. (quoted in 97-4)?

32. CH$_3$CN. The values reported by Benkelberg [49], Snider and Dawson [320], Hamm et al. [146] are all in good agreement and have been fit to a two-parameter expression for the recommendation. The Hamm et al. paper includes a measurement with artificial seawater at 293 K.

33. Nitroalkanes (CH$_3$NO$_2$, C$_2$H$_5$NO$_2$, C$_3$H$_7$NO$_2$, and CH$_3$CH(NO$_2$)CH$_3$). The recommended values are all taken from the work of Benes and Dohnal [47]. For nitromethane, the 298 K value from Rohrschneider [296] is about 30% higher.

34. Alkyl nitrates (CH$_3$ONO$_2$, C$_2$H$_5$ONO$_2$, 1-C$_3$H$_7$ONO$_2$, 2-C$_3$H$_7$ONO$_2$, 1-C$_4$H$_9$ONO$_2$, 2-C$_4$H$_9$ONO$_2$). The recommended values are all taken from the work of Kames and Schurath [208]. The results of Luke et al. [247] are in very good agreement for 1-butyl and 2- butyl nitrates, but the values reported by Hauff [170] for 1- and 2-propyl and butyl nitrates by head-space chromatography are significantly (~50%) lower.

35. CH$_3$C(O)O$_2$NO$_2$. The results of Kames and Schurath [208] and Frenzel et al. [127] are close, but somewhat higher (~60%) than the single temperature point of Holdren et al. [178]. The recommendation is a fit to the data of Kames and Schurath, and Frenzel et al. Frenzel et al., Kames and Schurath, and Holdren et al. also measured hydrolysis rate constants and Kames and Schurath measured solubility in artificial sea water.

36. Bifunctional alkyl nitrates. The recommended values (at 293 K) are taken from the work of Kames and Schurath [207].

37. Cl$_2$. Three-parameter refit to the recommendation of Battino [36]. Two parameter fit gives A = 9.38 and B = 2090 K for the temperature range 283–313 K.

38. Cl$_2$O. Fit to recommendation of Wilhelm et al. [351]. Data appear somewhat uncertain.

39. ClO$_2$. Two-parameter fit to the recommendation of Battino [35].

40. HOCl. Huthwelker et al. [185] analyzed the limited data for pure water from Blatchley et al. [55] and Holzwarth et al. [179] along with the more extensive data for uptake by sulfuric acid from Hanson and Ravishankara [164], along with thermodynamic information, and obtained a consistent expression for the solubility of HOCl.

41. Br$_2$. The results of Kelley and Tartar [213] and Jenkins and King [202] agree well below about 313 K, and with the 298 K point of Hill et al. [175]. Recommendation based on a two-parameter fit to all data at and below 308 K.

42. BrCl. The recommendation is from the work of Barlett and Margerum [29].

43. SO$_2$. Two- and three-parameter fits to the recommendation of Battino [37]. The earlier recommendation of Edwards et al. [111] is slightly lower.

44. H$_2$S. In the recommendation of Fogg [125], two expressions were given, representing the results above and below 283 K. The predicted values from these expressions were calculated, with the points at 283 K averaged, converted to the desired units, and then fit with the two- and three-parameter expressions. These are the recommended values. More recent results of Rinker and Sandall [287] and Munder et al. [268] are slightly lower; in these studies, the physical solubility of H$_2$S was determined through measurements involving aqueous solutions of glycols or amines, neutralized with HCl. The reported values of De Bruyn et al. [101] are significantly (~30%) lower. The earlier recommendation of Edwards et al. [111] is very close to

the recommendation of Fogg [125] as is the recommendation of Yaws et al. [360]. The room temperature point calculated from the NBS Thermodynamic tables Wagman et al. [345] is also slightly lower. The work of De Bruyn et al. [101] covered also a wide range of NaCl and $(NH_4)_2SO_4$ concentration and of pH.

45. CS_2. The recommendation is from a fit to data of Elliott [112], who also present data in 0.5 mol L^{-1} NaCl. The results of De Bruyn et al. [101] are significantly (50%) lower. The work of DeBruyn et al. covered also a wide range of NaCl and $(NH_4)_2SO_4$ concentration and of pH.

46. COS. The reviews by Wilhelm et al. [352] and Yaws et al. [360] result in identical results over the low temperature range (<303 K) and are combined to generate the recommendation. The results of De Bruyn et al. [101] are somewhat (~25%) lower at the lower temperature range. The work of De Bruyn et al. covered also a wide range of NaCl and $(NH_4)_2SO_4$ concentration and of pH.

47. CH_3SH. The recommendation is based on the data of Przyjazny et al. [279]. Results of De Bruyn et al. [101] are about half the recommended value at 298 K. Similar low values were observed for other compounds in the work of De Bruyn et al. The work of De Bruyn et al. covered a wide range of pH and NaCl and $(NH_4)_2SO_4$ concentrations.

48. C_2H_5SH. The recommendation is based on the data of Przyjazny et al. [279]. The results of Vitenberg [340] are slightly lower than the extrapolated value at 293 K.

49. CH_3SCH_3. The recommendation is based on the values of Dacey et al. [93]. The single temperature point of Wong and Wang [357] and the higher temperature results of Przyjazny et al. [279] are in good agreement. The results of De Bruyn et al. [101] are about 30% lower. The studies of Dacey et al. [93] and Wong and Wang [357] were also carried out with seawater. The work of De Bruyn et al. [101] covered also a wide range of NaCl and $(NH_4)_2SO_4$ concentration and of pH.

50. $CH_3S(O)CH_3$. The recommendation is from Watts and Brimblecombe [349], cited by Allen et al. [19].

5.18   Henry's Law Constants for Acids

Table 5-5. Henry's Law Constants for Acids

	T(K)	Wt. % H_2SO_4	H or H* (M/atm)	Notes
O_3 in $H_2SO_4 \cdot nH_2O(l)$	293	1–70	$\ln(H_o/H) = (4.08 \pm 0.2) \times 10^{-3} \times wt$ $H_o = 0.012$ M atm^{-1} wt is the H_2SO_4 wt. %	1
NO_2 in $H_2SO_4 \cdot nH_2O(l)$	203–343	39–68	See Note	2
HONO in $H_2SO_4 \cdot nH_2O(l)$	248–298	>60	$\ln H^* = a_1 + a_2\,wt + a_3\,wt^2 + (b_1 + b_2\,wt)/T$ $a_1 = 26.1 \pm 9.4$, $a_2 = -1.095 \pm 0.21$, $a_3 = 0.00732 \pm 0.00121$ $b_1 = -5792 \pm 1610$, $b_2 = 181.3 \pm 24$	3
HNO_3 in $H_2SO_4 \cdot nH_2O(l)$	~195–300	0–80	See Note	4
HNO_3 and HCl in $H_2SO_4 \cdot nHNO_3 \cdot mH_2O(l)$	~195–300	0–80	See Note	4
HO_2NO_2 in $H_2SO_4 \cdot nH_2O(l)$	201–230	50–75	$\ln H = 3.69 - mH_2SO_4 \times (-0.25 + 65/T) - 8400 \times (1/T_o - 1/T)$ mH_2SO_4 is the molality of the H_2SO_4 solution, $T_o = 298.15$ K	5
CH_2O in $H_2SO_4 \cdot mHNO_3 \cdot nH_2O(l)$	240–300	10–85 also 8–40 wt. % HNO_3	See Note	6
CH_3OH in $H_2SO_4 \cdot nH_2O(l)$	197–223		See Note	7
$CH_3C(O)CH_3$ in $H_2SO_4 \cdot nH_2O(l)$	198–298	10–80	$\ln H^* = a_1 + a_2\,wt + a_3\,wt^2 + (b_1 + b_2\,wt + b_3\,wt^2)/T$ wt is the H_2SO_4 wt. %, $a_1 = -21.438 \pm 4.31$, $a_2 = -0.32163 \pm 0.207$, $a_3 = 0.0072935 \pm 0.00235$ $b_1 = 7292 \pm 1220$, $b_2 = 33.524 \pm 53.42$, $b_3 = -0.975 \pm 0.571$	8
$CH_3C(O)O_2NO_2$ in $H_2O(l)$, $H_2SO_4 \cdot nH_2O(l)$	199–295	0–75	$\ln H^* = 1.07 - mH_2SO_4 \times (0.69 - 152/T) - 5810 \times (1/T_o - 1/T)$, $mH_2SO_4 =$ molality of the H_2SO_4 solution $T_o = 298.15$ K	9
CF_2O in $H_2SO_4 \cdot nH_2O(l)$	215–230	60	< 5	10
CF_3OH in $H_2SO_4 \cdot nH_2O(l)$	250	40 50	> 240 210	11
HOCl in $H_2SO_4 \cdot nH_2O(l)$	200–300	46–80	$H_{HOCl} = 1.91 \times 10^{-6} \times \exp(5862.4/T) \times \exp(-S_{HOCl}\,M_{H2SO4})$ M atm^{-1} where: $S_{HOCl} = 0.0776 + 59.18/T$ M^{-1}, $M_{H2SO4} = H_2SO_4$ molar conc	12
$ClONO_2$ in $H_2SO_4 \cdot nH_2O(l)$	200–265	40–75	$H_{ClONO2} = 1.6 \times 10^{-6} \times \exp(4710/T) \times \exp(-S_{HOCl}\,M_{H2SO4})$ M atm^{-1} where: $S_{ClONO2} = 0.306 + 24.0/T$ M^{-1}, $M_{H2SO4} = H_2SO_4$ molar conc.	13
HBr in $H_2SO_4 \cdot nH_2O \cdot H_2O(l)$ and $H_2SO_4 \cdot nHNO_3 \cdot mH_2O(l)$	200–240	40–72	$\ln H^* = a_1 + (b_1 + b_2\,wt)/T$ $a_1 = -11.695 \pm 0.537$, $b_1 = 11{,}101 \pm 163$, $b_2 = -90.7 \pm 1.2$	14
SO_2 in $H_2O(l)$, $H_2SO_4 \cdot nH_2O(l)$	193–242	0–97	$\ln H^* = a_1 + a_2\,wt + a_3\,wt^2 + (b_1 + b_2\,wt + b_3\,wt^2)/T$, where: wt is the H_2SO_4 wt. %, $a_1 = -10.778 \pm 2.07$, $a_2 = -0.11541 \pm 0.0827$, $a_3 = 0.0012506 \pm 0.000811$ $b_1 = 3310 \pm 578$, $b_2 = 30.581 \pm 22.2$, $b_3 = -0.35469 \pm 0.209$	15

5.19   Notes to Table 5-5

1. O_3 in $H_2SO_4 \cdot nH_2O(l)$—Bubble train uptake measurements where performed by Rattigan et al. [282] at 293 K for 1–70 wt. % H_2SO_4. Recommended expression is a Setchenow coefficient formulation where $H_o = 0.012$ M atm^{-1} is the 293 K value of H for pure water fom Wilhelm et al. [351]. In the measurement, account was taken of the loss of O_3 due to reaction with H^+.

2. NO_2 in $H_2SO_4 \cdot nH_2O(l)$—Langenberg et al. [229] present novel capillary gas chromatography measurements for 39, 59, and 68 wt. % H_2SO_4 over the temperature range of 203 to 243 K. However, NO_2 solubility must be derived from chromatographic waveforms which are contorted by much higher N_2O_4 solubility. The resulting values for H_{NO2} are in the 1 to 10^2 range, but show inconsistent trends with temperature and concentration, indicating possibly large systematic error.

3.   HONO in $H_2SO_4 \cdot nH_2O(l)$—Becker et al. [42] measured HONO partial pressue, P_{HONO}, over bulk solutions in a temperature range of 248–298 K and a H_2SO_4 concentration range of 0–67 wt. %. Longfellow et al. [242] measured P_{HONO} in a wetted wall flow reactor over a temperature range of 218–295 K and an acid concentration range of 60–83 wt. %. Agreement between these two data sets is excellent. H* decreases from

0 wt. % to 53 wt. % due to physical solubility, then increases above 53 wt. % due to protonation and/or association with H_2SO_4 to make nitrosyl sulfuric acid. Becker et al. parameterize their data as a function of sulfuric acid wt. % and temperature. However, the Becker et al. parameterization is not able to fit the combined sets of Becker et al. [42] and Longfellow et al. [242] data, particularly at the lower temperatures and higher wt. % most relevant to the stratosphere. Therefore, the recommended functional form was used to fit the data for >60 wt. %. This function fits both sets of data very well It is important to note that this function is only valid for H_2SO_4 concentrations near 60 wt% and above. The parameterization in Becker et al. [42] should be used to calculate H for H_2SO_4 concentrations <60 wt %. (Note that the units for H are mol/kg-bar in Becker et al. [42]. The density parameterization of Myhre et al. [269] was used to convert to M/atm units.)

4. HNO_3 and HCl in $H_2SO_4 \bullet nH_2O(l)$ and $H_2SO_4 \bullet nHNO_3 \bullet mH_2O(l)$—Effective Henry''s law coefficients, H^*, for HNO_3, and HCl in binary H_2SO_4/H_2O and ternary $H_2SO_4/HNO_3/H_2O$ solutions over the temperature range 195 to 300 K are required to model the composition and heterogeneous chemistry of stratospheric and upper tropospheric aerosols. Solubility data can be obtained from analysis of heterogeneous uptake experiments with the liquid phase diffusion coefficient estimated from acid solution viscosity (Williams and Long [355]) Solubilities can also be obtained from equilibrium or from vapor pressure data.

Experimental solubility data for HNO_3 is provided by Van Doren et al. [338], Reihs et al. [283] and Zhang et al. [370]. Data for HCl solubility is provided by Watson et al. [348], Hanson and Ravishankara [158,161], Zhang et al. [370], Williams and Golden [353], Abbatt [2], Elrod et al.[113] and Robinson et al. [294].

These studies all show that trace species solubility in H_2SO_4/H_2O and $H_2SO_4/HNO_3/H_2O$ solutions is a strong function of water activity, which, in turn, depends on both temperature and acid concentrations. Prediction of HNO_3 and HCl H^* values for atmospheric compositions requires a sophisticated model. Comprehensive thermodynamic models of acid solutions for a range of atmospheric conditions have been published by Carslaw et al. [66], Tabazadeh et al. [324] and Luo et al. [248] and reviewed by Carslaw and Peter [68]. These models do an excellent job of reproducing the available experimental data, even for ternary $H_2SO_4/HNO_3/H_2O$ solutions (Elrod et al. [113]). These models and the Carslaw review should be consulted for plots/predictions of H^* for HNO_3 and HCl in strong acid solutions over the atmospheric temperature range. The most widely used model of Carslaw et al. [66] was revised in Massucci et al. [251].

5. HO_2NO_2 in $H_2SO_4 \bullet nH_2O(l)$—Zhang et al. [369] performed wetted wall flow reactor studies using CIMS to detect HO_2NO_2 uptake over a temperature range of 201–230 K and an acid concentration range of 52.9–74 wt. % H_2SO_4. $HD_l^{1/2}$ values where determined for 52.9, 58.3/59.1, 66.4 and 73.8/74 wt. %, with 5 to 15 data points per temperature or temperature pair. All uptake appeared to be reversible with the variation in H strongly temperature dependent, but only moderately dependent on H_2SO_4 wt. %. D_l values were calculated from a cubic cell model to derive H. Uncertainties in measured H values were estimated by authors to be 25% for H $<1 \times 10^6$ M atm^{-1} and 50% for H $>1 \times 10^6$ M atm^{-1}. These data were parameterized by Leu and Zhang [236] in the Setchenow coefficient form adopted by Huthwelker for HOCl [185], and their formulation is recommended.

6. CH_2O in $H_2SO_4 \bullet mHNO_3 \bullet nH_2O(l)$—The recommended Henry's Law relationship is:

$$H^* = H\left(1 + K_2 a_{H_2O} + K_3 a_{H^+}\right)$$

where: $H = 3.4 \times 10^{-5}$ exp $-[(-0.0456 + 55.5/T)(0.46\ m_{H_2SO_4} + 0.13\ m_{HNO_3})]$ M atm^{-1}, T is the temperature in K, and $m_{H_2SO_4}$ and m_{HNO_3} are the respective acid molalities; $K_2 = $ exp $(4020/T–5.83)$ M^{-1}, $K_3 = 0.56$ exp $[8.84–(T–260/T)]$ M^{-1}, and a_{H_2O} and a_{H+} are the water and H^+ activities which are obtained from a thermodynamic model of the solution, e.g. Carslaw et al. [66] Valid for 10–85 wt. % H_2SO_4, 8–40 wt % HNO_3, T = 240–300 K.

Knudsen cell studies by Tolbert et al. [330] and Iraci and Tolbert [192] and droplet train/flow reactor studies by Jayne et al. [200] all yield data showing that CH_2O is strongly absorbed by sulfuric acid solutions, and Jayne et al. also provide data for ternary acid solutions. The Jayne et al. [200] studies included H_2SO_4 concentrations from 10 to 85 wt. % and HNO_3 concentration between 8 and 40 wt. % with temperature variations from 241 to 300 K. These data were parameterized with three terms, representing physical CH_2O solubility, reversible hydrolysis to $CH_2(OH)_2$, important in more dilute solutions, and reversible formation of CH_3O^+, dominant at high acidities. The Jayne et al. [200] parameterization is recommended above. The H* data from Iraci and Tolbert [192] cover 49 to 95 wt. % H_2SO_4 and a temperature range of 197 to 214.5 K and are in fair agreement with extrapolation of H* expression from Jayne et al. [200] for concentrations below

~75 wt. %. However, the Iraci and Tolbert data are taken on such thin acid films that initial uptake slopes are difficult to determine accurately and the data scatter is large. While the Iraci and Tolbert data do indicate significantly larger H* values for H_2SO_4 concentrations above 75 wt. %, the data do not compel a reformulation of the Jayne et al. parameterization.

7. CH_3OH in $H_2SO_4 \cdot nH_2O(l)$—H* data from Kane and Leu [211], taken over 40–85 wt. % H_2SO_4 and from 210–235 K, indicate soluble uptake below 65 wt. % and predominately reactive uptake to form methanesulfonic acid and dimethysulfate above 65 wt. %. Uptake decreased slightly with temperature below 65 wt. % and increases slightly with temperature above. Data yield $H*k^{1/2}$ at high acid concentrations. Weakly temperature dependent γs of ~0.15 were measured for 65, 75, and 80 wt. %. However, Knudsen cell studies by Iraci et al. [190] at 45, 61 and 72 wt. % over a 197–223 K temperature range show only well behaved reversible uptake. They argue that low vapor pressures explain the lack of CH_3OH recovery for the short observation times used by Kane and Leu. They also cite three older literature studies on the reaction of methanol and ethanol at room temperature in sulfuric acid which report reaction rate constants much lower than those deduced by Kane and Leu [190]. Iraci et al. present the following parameterization of their data plus data for water:

$$\log H^* = A + 1000B/T$$

where $A = 7.00 + \log M_{H2O}$, $B = 0.000619 \, m^2 + 0.00544 \, m + 2.267$, M_{H2O} is the molarity of water in the solution (mol L^{-1}) and m is the molality of the H_2SO_4 (moles H_2SO_4 per kg H_2O).

Note that this parameterization is based only on the Iraci et al. data. A reanalysis of the Kane and Leu [211] results to provide additional data in the 40–72 wt. % range, and H* values for higher wt. % should be undertaken to validate and extend the Iraci et al. data.

8. $CH_3C(O)CH_3$ in $H_2SO_4 \cdot nH_2O(l)$—Duncan et al. [109,110] used IR spectra of thin sulfuric acid films to establish that acetone is absorbed as the protonated species. Above 70 wt. % protonated acetone undergoes a self-condensation/dehydration reaction to form protonated mesityl oxide, which, in turn, reacts with an additional protonated acetone to form trimethyl benzene. Duncan et al. [110] measured reversible uptake and derived Henry's law constants for 70 wt. % H_2SO_4 at 180, 187 and 195 K and a value at 201 K for 76 wt. %. Kane et al. [212] measured uptake in a wetted wall flow reactor and derived H* parameters for 40, 50, 65, and 75 wt. % over a much wider temperature range than Duncan et al. [110]. Their data diverge above 80 wt. % which they attribute to reactive uptake a la Duncan et al. [109,110]. Klassen et al. [221] provide Knudsen cell uptake derived data for 48.7 to 78.3 H_2SO_4 wt. % between 210 and 240 K that are generally consistent with that of Kane et al. [212]. Imamura and Akiyoshi [188] report wetted wall flow reactor H* measurements at 230 K for 50 and 60 wt. %, 250 K for 60, 69 and 76 wt. %, and 270 K for 76 and 79 wt. %; their data diverges a factor of 2 to 4 from that of Kane et al. [212] and Klassen et al. [221].

Equally weighted data sets from Kane et al. [212] and Klassen et al. [221] were combined and fit to generate the recommended parameterization. Two points for the solubility of acetone in water at 298 K and 273 K (Benkelberg et al. [48]) were included to improve the extrapolation to low wt. % solutions.

The data points from Imamura and Akiyoshi [188] were not included because they were inconsistent with the other data and have a very different temperature dependence. The few data points from Duncan et al. [109,110] are also inconsistent with the other data and were not included in the parameterization.

9. $CH_3C(O)O_2NO_2$ in H_2O and $H_2SO_4 \cdot nH_2O(l)$—Zhang and Leu [364] performed wetted wall flow reactor studies using CIMS to detect $CH_3C(O)O_2NO_2$ uptake over a temperature range of 199 to 226 K. Uptake studies were performed at 46, 54, 59, and 72 wt. % H_2SO_4 to yield $H^*D_l^{1/2}$ values. D_l values were calculated from a cubic cell model to derive H*. Leu and Zhang [236] fit their data from Zhang and Leu [364], including water data from Kames and Schurath [208] and Kames et al. [209], using the Setchenow coefficient form adopted by Huthwelker for HOCl [185]. This formulation is recommended for both water and sulfuric acid solutions.

10. CF_2O in $H_2SO_4 \cdot nH_2O(l)$—Hanson and Ravishankara [156] calculate an upper limit for H of CF_2O based on assumed solubility limit resulting in lack of measurable uptake into 60 wt% H_2SO_4.

11. CF_3OH in $H_2SO_4 \cdot nH_2O(l)$—Lovejoy et al. [245] determined reacto-diffusive lengths of > 0.4 μm and 1.0 μm for CF_3OH uptake at 250 K on 40 and 50 wt % H_2SO_4 aerosols, respectively. This leads to H* estimates of >240 and 210 M atm^{-1}, respectively.

12. HOCl in $H_2SO_4 \cdot nH_2O(l)$—Recommendation is from the model of Shi et al. [313] which is based on wetted wall flow tube data from Hanson and Ravishankara [162] and Hanson and Lovejoy [154], and uptake by stirred and static solutions by Donaldson et al. [107]. This model incorporates newer, higher temperature data and replaces earlier recommended formulation by Huthwelker et al. [185].

13. $ClONO_2$ in $H_2SO_4 \cdot nH_2O(l)$—Recommendation is from the model of Shi et al. [313] who used a measurement of the hydrolysis reaction's reacto-diffusive length by Hanson and Lovejoy [153] on 60 wt. % H_2SO_4 at 250 K to derive the hydrolysis rate constant, k_{hyd}, and constrain H_{ClONO2} at 250 K. Shi et al. fit the $Hk^{1/2}$ dependence of the $ClONO_2$ uptake coefficients for a variety of $ClONO_2$ hydrolysis and $ClONO_2 + HCl$ data to derive a parameterization for H as a function of wt. % and T.

14. HBr in $H_2SO_4 \cdot mHNO_3 \cdot nH_2O(l)$—Experimental data for HBr solubility is provided by Williams et al. [354], Abbatt [2], Abbatt and Nowak [8], Kleffman et al. [222], and Behr et al. [45]. Data from time-dependent uptake measurements and from vapor pressure measurements is in good agreement after correcting for the fact that for some of the vapor pressure measurements the HBr concentration in solution was high enough to increase the acidity and thereby decrease the HBr solubility. By comparing pairs of data points with different HBr concentrations (from the same experiment), an average correction factor was obtained. The correction factor was used to correct the vapor pressure data of Williams et al. [354], Abbatt and Nowak [8] and Kleffmann et al. to zero effective HBr concentration. (This is different than the approach taken in Kleffmann et al. of using a "corrected" H_2SO_4 wt. %. However, the resulting parameterization is very similar to the one in Kleffmann et al. [222].) The time-dependent uptake data of Williams et al. [354] and Abbatt [2], and the molecular beam uptake data of Behr et al. [45] did not require correction. All of the experimental data have been fit to obtain the recommended parameterization as a function of H_2SO_4 wt. % and temperature.

Agreement between this parameterization and the updated activity coefficient model of Massucci et al. [251] (and http://www.hpc1.uea.ac.uk/~e770/aim.html) is good for > 60 wt. %, but not very good at lower H_2SO_4 wt. %, particularly at low temperatures. Therefore, this parameterization is recommended for calculating HBr Henry's law solubilities.

The only data for HBr solubilities in ternary solutions is from Kleffmann et al. [222]. The data do not agree well with the updated activity coefficient in Massucci et al. [222] or with the older activity coefficient model in Luo et al. [248]. Until further information becomes available, the recommendation is to use the parameterization for ternary solutions given in Kleffmann et al. [222].

15. SO_2 in $H_2SO_4 \cdot nH_2O(l)$—Room temperature vapor pressure measurements reviewed by Hayduk et al. [171] and bubble train reactor uptake measurements by Rattigan et al. [282] for 0–70 wt. % H_2SO_4 agree very well. Langenberg et al. [229]] used a novel capillary gas chromatography technique to deduce H* values for 41–83 wt. % H_2SO_4 over a temperature range of 193–242 K. The recommended parameterization is a fair fit to the Rattigan et al. and Langenberg et al. data sets and allows reasonable extrapolation over the full range of atmospheric temperatures. Note that the Langenberg et al. [229] data is in mol/kg-bar units and was converted to mole/l units using the density parameterization of Myhre et al. [269].

5.20   References

1. Abbatt, J. P. D., 1994, Geophys. Res. Lett., **21**, 665-668.
2. Abbatt, J. P. D., 1995, J. Geophys. Res., **100**, 14009-14017.
3. Abbatt, J. P. D., 1996, Geophys. Res. Lett., **23**, 1681-1684.
4. Abbatt, J. P. D., 1997, Geophys. Res. Lett., **24**, 1479-1482.
5. Abbatt, J. P. D., K. D. Beyer, A. F. Fucaloro, J. R. McMahon, P. J. Wooldridge, R. Zhong and M. J. Molina, 1992, J. Geophys. Res., **97**, 15819-15826.
6. Abbatt, J. P. D. and M. J. Molina, 1992, Geophys. Res. Lett., **19**, 461-464.
7. Abbatt, J. P. D. and M. J. Molina, 1992, J. Phys. Chem., **96**, 7674-7679.
8. Abbatt, J. P. D. and J. B. Nowak, 1997, J. Phys. Chem. A, **101**, 2131-2137.
9. Aguzzi, A. and M. J. Rossi, 2001, Phys. Chem. Chem. Phys., **3**, 3707-3716.
10. Akhter, M. S., A. R. Chughtai and D. M. Smith, 1985, Appl. Spectrosc., **39**, 143-153.
11. Akhter, M. S., A. R. Chughtai and D. M. Smith, 1985, Appl. Spectrosc., **39**, 154-167.
12. Akhter, M. S., A. R. Chughtai and D. M. Smith, 1991, Appl. Spectrosc., **45**, 653-665.
13. Al-Abadleh, H. A. and V. H. Grassian, 2000, J. Phys. Chem. A, **104**, 11926-11933.
14. Alcala-Jornod, C., H. Van den Bergh and M. J. Rossi, 2000, Phys. Chem. Chem. Phys., **2**, 5584-5593.
15. Alebic'-Juretic', A., T. Cuitas and L. Klasine, 1992, Ber. Bunsenges Phys. Chem., **96**, 493-495.
16. Allanic, A., R. Oppliger and M. Rossi, 1997, J. Geophys. Res., **102**, 23529-23541.
17. Allanic, A., R. Oppliger, H. Van den Bergh and M. J. Rossi, 2000, Zeitschrift fur Physikalische Chemie, **214**, 11, 1479-1500.
18. Allanic, A. and M. J. Rossi, 1999, J. Geophys. Res., **104**, 18,689-18,696.
19. Allen, H. C., D. E. Gragson and G. L. Richmond, 1999, J. Phys. Chem. B, **103**, 660-666.
20. Altschuh, J., R. Bruggemann, H. Santl, G. Eichinger and O. G. Piringer, 1999, Chemosphere, **39**, 1871-1887.
21. Ammann, M., M. Kalberer, D. T. Jost, L. Tobler, E. Rossler, D. Piguet, H. W. Gaggeler and U. Baltensperger, 1998, Nature, **395**, 157-160.
22. Ammann, M., M. Kalberer, K. Tabor, K. Tobler, C. Zellweger, E. Weingartner, S. Nyeki, Y. Parrat, F. Li, D. Piguet, E. Rossler, D. T. Jost, H. W. Gaggeler and U. Baltensperger. "Proc. 7th Euro. Symp. on Physico-Chem. Behav. of Atmos. Poll.", 1996.
23. Arens, F., L. Gutzwiller, U. Baltensperger, H. Gaggeler and M. Ammann, 2001, Environ. Sci. Technol., **35**, 2191-2199.
24. Baker, J., S. F. M. Ashbourn and R. A. Cox, 1999, Phys. Chem. Chem. Phys., **1**, 683-690.
25. Baldwin, A. C., 1982, Int. J. Chem. Kin., **14**, 269-277.
26. Baldwin, A. C. and D. M. Golden, 1979, Science, **206**, 562.
27. Baldwin, A. C. and D. M. Golden, 1980, J. Geophys. Res., **85**, 2888-2889.
28. Ball, S. M., A. Fried, B. E. Henry and M. Mozurkewich, 1998, Geophys. Res. Lett., **25**, 3339-3342.
29. Barlett, W. P. and D. W. Margerum, 1999, Environ. Sce. Technol., **33**, 3410-3414.
30. Barone, S. B., M. A. Zondlo and M. A. Tolbert, 1997, J. Phys. Chem. A, **101**, 8643-8652.
31. Battino, R. Nitrous oxide in water. In *Oxides of Nitrogen*; Young, C. L., Ed.; Pergamon: Oxford, 1981; Vol. 8; pp 1-22.
32. Battino, R. Oxygen in water. In *Oxygen and Ozone*; Battino, R., Ed.; Pergamon: Oxford, 1981; Vol. 7; pp 1-5.
33. Battino, R. Ethane in water. In *Ethane*; Hayduk, W., Ed.; Pergamon: Oxford, 1982; Vol. 9; pp 1-26.
34. Battino, R. Nitrogen in water. In *Nitrogen and Air*; Battino, R., Ed.; Pergamon: Oxford, 1982; Vol. 10; pp 1-29.
35. Battino, R. Chlorine dioxide in water. In *Sulfur Dioxide, Chlorine, Fluorine and Chlorine Oxides*; Young, C. L., Ed.; Pergamon: Oxford, 1983; Vol. 12; pp 454-456.
36. Battino, R. Chlorine in water. In *Sulfur Dioxide, Chlorine, Fluorine and Chlorine Oxides*; Young, C. L., Ed.; Pergamon: Oxford, 1983; Vol. 12; pp 333-347.
37. Battino, R. Sulfur dioxide in water. In *Sulfur Dioxide, Chlorine, Fluorine and Chlorine Oxides*; Young, C. L., Ed.; Pergamon: Oxford, 1983; Vol. 12; pp 3-33.
38. Battino, R. 2-Methylpropane in water. In *Propane, Butane and 2-Methylpropane*; Hayduk, W., Ed.; Pergamon: Oxford, 1986; Vol. 24; pp 34-37.
39. Battino, R. Butane in water. In *Propane, Butane and 2-Methylpropane*; Hayduk, W., Ed.; Pergamon: Oxford, 1986; Vol. 24; pp 16-32.
40. Battino, R. Propane in water. In *Propane, Butane and 2-Methylpropane*; Hayduk, W., Ed.; Pergamon: Oxford, 1986; Vol. 24; pp 1-15.

41. Battino, R. Methane in water. In *Methane*; Clever, H. L., Young, C. L., Eds.; Pergamon: Oxford, 1987; Vol. 27/28; pp 1-44.
42. Becker, K. H., J. Kleffman, R. Kurtenbach and P. Wiesen, 1996, J. Phys. Chem., **100**, 14,984-14,990.
43. Behnke, W., H.-U. Kruger, V. Scheer and C. Zetzsch, 1992, J. Aerosol Sci., **23**, S923-S936.
44. Behnke, W., V. Scheer and C. Zetzsch, 1993, J. Aerosol Sci., **24**, S115-S116.
45. Behr, P., J. R. Morris, M. D. Antman, B. R. Ringeisen, J. Splan and G. M. Nathanson, 2001, Geophys. Res. Lett., **28**, 1961-1964.
46. Beichert, P. and B. J. Finlayson-Pitts, 1996, J. Phys. Chem., **100**, 15,218-15,228.
47. Benes, M. and V. Dohnal, 1999, J. Chem. Eng. Data, **44**, 1097-1102.
48. Benkelberg, H. J., S. Hamm and P. Warneck, 1995, J. Atmos. Chem., **20**, 17-34.
49. Benkelberg, H. J., S. Hamm and P. Warneck, 1995, J. Atmos. Chem., **20**, 17-34.
50. Ben-Naim, A. and R. Battino, 1985, J. Sol. Chem., **14**, 245-253.
51. Benson, B. B., D. Krause and M. A. Peterson, 1979, J. Sol. Chem., **8**, 655-690.
52. Berko, H. N., P. C. McCaslin and B. J. Finlayson-Pitts, 1991, J. Phys. Chem., **95**, 6951-6958.
53. Berland, B. S., M. A. Tolbert and S. M. George, 1997, J. Phys. Chem. A, **101**, 9954-9963.
54. Betterton, E. A. and M. R. Hoffmann, 1988, Environ. Sci. Technol., **22**, 1415-1418.
55. Blatchley, E. R., R. W. Johnson, , J. E. Alleman and W. F. McCoy, 1991, Wat. Res., **26**, 99-106.
56. Bongartz, A., J. Kames, U. Schurath, C. George, P. Mirabel and J. L. Ponche, 1994, J. Atm. Chem., **18**, 149-160.
57. Bongartz, A., S. Schweighoefer, C. Roose and U. Schurath, 1995, J. Atmos. Chem., **20**, 35-58.
58. Brouwer, L., M. J. Rossi and D. M. Golden, 1986, J. Phys. Chem., **90**, 4599-4603.
59. Brown, D. E., S. M. George, C. Huang, E. K. L. Wong, K. B. Rider, R. S. Smith and B. D. Kay, 1996, J. Phys. Chem., **100**, 4988-4995.
60. Brown, L. A., V. Vaida, D. R. Hanson, J. D. Graham and J. T. Roberts, 1996, J. Phys. Chem., **100**, 3121-3125.
61. Burnett, M. G., 1963, Anal. Chem., **35**, 1567-1570.
62. Butler, J. V. A., C. N. Ramchandani and D. W. Thomson, 1935, J. Chem. Soc., 280285.
63. Cachier, H. Carbonaceous Combustion Aerosols. In *Atmospheric Particles*; Harrison, R. M., VanGrieken, R., Eds.; Wiley: New York, 1998.
64. Caloz, F., F. F. Fentner and M. J. Rossi, 1996, J. Phys. Chem., **100**, 7494-7501.
65. Cappa, C. D., S. E. Kuipers, J. M. Roberts, A. S. Gilbert and M. J. Elrod, 2000, J. Phys. Chem. A, **104**, 4449-4457.
66. Carslaw, K. S., S. L. Clegg and P. Brimblecombe, 1995, J. Phys. Chem., **99**, 11,557-11,574.
67. Carslaw, K. S. and T. Peter, 1997, Geophys. Res. Lett., **24**, 1743-1746.
68. Carslaw, K. S., T. Peter and S. L. Clegg, 1997, Rev. Geophys., **35**, 125-154.
69. Chaix, L., A. Allanic and M. J. Rossi, 2000, J. Phys. Chem. A, **104**, 7268-7277.
70. Choi, W. and M. T. Leu, 1998, J. Phys. Chem A, **102**, 7618-7630.
71. Chu, L. and L. T. Chu, 1999, J. Phys. Chem. A, **103**, 8640-8649.
72. Chu, L. and L. T. Chu, 1999, J. Phys. Chem. A, **103**, 691-699.
73. Chu, L., G. Diao and L. T. Chu, 2000, J. Phys. Chem. A, **104**, 3150-3158.
74. Chu, L. T. and J. W. Heron, 1995, Geophys. Res. Lett., **22**, 3211-3214.
75. Chu, L. T., M.-T. Leu and L. F. Keyser, 1993, J. Phys. Chem., **97**, 7779-7785.
76. Chu, L. T., M.-T. Leu and L. F. Keyser, 1993, J. Phys. Chem., **97**, 12798-12804.
77. Chughtai, A. R., M. M. O. Atteya, J. Kim, B. K. Konowalchuck and D. M. Smith, 1998, Carbon, **36**, 1573-1589.
78. Chughtai, A. R., M. E. Brooks and D. M. Smith, 1993, Aer. Sci. Tech., **19**, 121-132.
79. Chughtai, A. R., M. E. Brooks and D. M. Smith, 1996, J. Geophys. Res., **101**, 19505-19514.
80. Chughtai, A. R., S. A. Gordon and D. M. Smith, 1994, Carbon, **32**, 405-416.
81. Chughtai, A. R., J. Kim and D. M. Smith, 2001, Croatica Chem. Acta, **in press**.
82. Chughtai, A. R., J. M. Kim and D. M. Smith, 2002, J. Atmos. Chem., **43**, 21-43.
83. Chughtai, A. R., J. M. Kim and D. M. Smith, 2002, J. Atmos. Chem., **in press.**
84. Chughtai, A. R., N. J. Miller, D. M. Smith and J. R. Pitts, 1999, J. Atmos. Chem., **34**, 259-279.
85. Chughtai, A. R., W. F. Welch, M. S. Akhter and D. M. Smith, 1990, Appl. Spectrosc., **44**, 294-298.
86. Chughtai, A. R., W. F. Welch and D. M. Smith, 1990, Carbon, **28**, 411-421.
87. Chughtai, A. R., G. R. Williams, M. M. O. Atteya, N. J. Miller and D. M. Smith, 1999, Atmos. Environ., **33**, 2679-2687.
88. Clegg, S. L. and P. Brimblecombe, 1986, Atmos. Environ., **20**, 2483.
89. Clegg, S. L. and P. Brimblecombe, 1989, J. Phys. Chem., **93**, 7237-7248.

90. Cofer, W. R., D. R. Schryer and R. S. Rogowski, 1981, Atm. Environ., **15**, 1281-1286.
91. Cooper, P. L. and J. P. D. Abbatt, 1996, J. Phys. Chem., **100**, 2249-2254.
92. Cowin, J. P., personal comm.
93. Dacey, J. W. H., S. G. Wakeham and B. L. Howes, 1984, Geophys. Res. Lett., **11**, 991-994.
94. Dai, D. J., S. J. Peters and G. E. Ewing, 1995, J. Phys. Chem., **99**, 10,299-10,304.
95. Dai, Q., G. N. Robinson and A. Freedman, 1996, J. Phys. Chem., submitted.
96. Dasgupta, P. K. and S. Dong, 1986, Atmos. Environ., **20**, 565-570.
97. Daumer, R. Nissner and D. Klockow, J. Aerosol Sci., **23**, 315-325.
98. De Bruyn, W. J., S. X. Duan, X. Q. Shi, P. Davidovits, D. R. Worsnop, M. S. Zahniser and C. E. Kolb, 1992, Geophys. Res. Lett., **19**, 1939-1942.
99. De Bruyn, W. J., J. A. Shorter, P. Davidovits, D. R. Worsnop, M. S. Zahniser and C. E. Kolb, 1994, J. Geophys. Res., **99**, 16927-16932.
100. De Bruyn, W. J., J. A. Shorter, P. Davidovits, D. R. Worsnop, M. S. Zahniser and C. E. Kolb, 1995, Environ. Sci Technol., **29**, 1179-1185.
101. De Bruyn, W. J., E. Swartz, J. H. Hu, J. A. Shorter, P. Davidovits, D. R. Worsnop and M. S. Zahniser, 1995, J. Geophys. Res., **100**, 7245-7251.
102. DeMore, W. B., S. P. Sander, D. M. Golden, R. F. Hampson, M. J. Kurylo, C. J. Howard, A. R. Ravishankara, C. E. Kolb and M. J. Molina "Chemical Kinetics and Photochemical Data for Use in Stratospheric Modeling, Evaluation Number 12," JPL Publication 97-4, Jet Propulsion Laboratory, California Institute of Technology, Pasadena, CA, 1997.
103. Disselkamp, R. S., M. A. Carpenter and J. P. Cowin, 2000, J. Atmos. Chem., **37**, 113-123.
104. Disselkamp, R. S., M. A. Carpenter, J. P. Cowin, C. M. Berkowitz, E. G. Chapman, R. A. Zaveri and N. S. Laulainen, 2000, J. Geophys. Res., **105**, 9767-9771.
105. Dlugokencky, E. J. and A. R. Ravishankara, 1992, Geophys. Res. Lett., **19**, 41-44.
106. Donaldson, D. J., J. A. Guest and M. C. Goh, 1995, J. Phys. Chem., **99**, 9313-9315.
107. Donaldson, D. J., A. R. Ravishankara and D. R. Hanson, 1997, J. Phys. Chem. A, **101**, 4717-4725.
108. Duan, S. X., J. T. Jayne, P. Davidovits, D. R. Worsnop, M. S. Zahniser and C. E. Kolb, 1993, J. Phys. Chem., **97**, 2284-2288.
109. Duncan, J. L., L. R. Schindler and J. T. Roberts, 1998, Geophys. Res. Lett., **25**, 631-634.
110. Duncan, J. L., L. R. Schindler and J. T. Roberts, 1999, J. Phys. Chem. B, **103**, 7247-7259.
111. Edwards, T. J., G. Maurer, J. Newman and J. M. Prausnitz, 1978, AIChE Journal, **24**, -.
112. Elliott, S., 1989, Atmos. Environ., **23**, 1977-1980.
113. Elrod, M. J., R. E. Koch, J. E. Kim and M. S. Molina, 1995, Faraday Discuss, **100**, 269-278.
114. Fairbrother, D. H. and G. Somorjai, 2000, J. Phys. Chem. B, **104**, 4649-4652.
115. Fendel, W., D. Matter, H. Burtscher and A. Schimdt - Ott, 1995, Atmos. Environ, **29**, 967-973.
116. Fendel, W., D. Matter, H. Burtscher and A. Schmidt-Ott, 1995, Atmos. Environ., **29**, 967-973.
117. Fendel, W. and A. S. Ott, 1993, J. Aerosol Sci., **24**, S317-S318.
118. Fenter, F. F., F. Caloz and M. J. Rossi, 1994, J. Phys. Chem., **98**, 9801-9810.
119. Fenter, F. F., F. Caloz and M. J. Rossi, 1996, J. Phys. Chem., **100**, 1008-1019.
120. Fenter, F. F. and M. J. Rossi, 1996, J. Phys. Chem., **100**, 13765-13775.
121. Fenter, F. F. and M. J. Rossi, 1997, J. Phys. Chem. A, **101**, 4110-4113.
122. Finlayson-Pitts, B. J., M. J. Ezell and J. N. Pitts, Jr., 1989, Nature, **337**, 241-244.
123. Finlayson-Pitts, B. J. and J. N. Pitts *Chemistry of the Upper and Lower Atmosphere: Theory, Experiments and Applications*; Academic: San Diego, 2000.
124. Fluckiger, B., A. Thielmann, L. Gutzwiller and M. J. Rossi, 1998, Ber. Bunsenges. Phys. Chem., **102**, 915-928.
125. Fogg, P. G. T. Hydrogen sulfide in water. In *Hydrogen Sulfide, Deuterium Sulfide and Hydrogen Selenide*; Fogg, P. G. T., Young, C. L., Eds.; Pergamon: Oxford, 1988; Vol. 32; pp 1-19.
126. Fox, L. E., D. R. Worsnop, M. S. Zahniser and S. C. Wofsy, 1994, Science, **267**, 351-355.
127. Frenzel, A., S. Kutsuna, K. Takeuchi and T. Ibusuki, 2000, Atmos. Environ., **34**, 3641-3544.
128. Friant, S. L. and I. H. Suffet, 1979, Anal. Chem., **51**, 21672176.
129. Fried, A., B. E. Henry, J. G. Calvert and M. Mozukewich, 1994, J. Geophys. Res., **99**, 3517-3532.
130. Fung, K. N., I. N. Tang and H. R. Munkelwitz, 1987, Appl. Optics, **26**, 1282-1287.
131. George, C., J. Lagrange, P. Lagrange, P. Mirabel, C. Pallares and J. L. Ponche, 1994, J. Geophys. Res., **99**, 1255-1262.
132. George, C., J. L. Ponche, P. Mirabel, W. Behnke, V. Sheer and C. Zetzsch, 1994, J. Phys. Chem., **98**, 8780-8784.
133. George, C., J. Y. Saison, J. L. Ponche and P. Mirabel, 1994, J. Phys. Chem., **98**, 10857-10862.

134. Gerecke, A., A. Thielmann, L. Gutzwiller and M. J. Rossi, 1998, Geophys. Res. Lett., **25**, 2453-2456.
135. Gershenzon, V. M., V. M. Grigorieva, A. V. Ivanov and R. G. Remorov, 1995, Faraday Discuss, **100**, 83-100.
136. Gershenzon, Y. M., A. V. Ivanov, S. I. Kucheryavyi and V. B. Rozenshtein, 1986, Kinet. Katal., **27**, 1069-1074.
137. Gershenzon, Y. M. and A. P. Purmal, 1990, Russ. Chem. Rev., **59**, 1007-1023.
138. Gertner, B. J. and J. T. Hynes, 1996, Science, **271**, 1563-1566.
139. Goldberg, E. D. *Black Carbon in the Environment*; Wiley: New York, 1985.
140. Graham, J. D. and J. T. Roberts, 1994, J. Phys. Chem., **98**, 5974-5983.
141. Graham, J. D. and J. T. Roberts, 1995, Geophys. Res. Lett., **22**, 251-254.
142. Graham, J. D., J. T. Roberts, L. A. Brown and V. Vaida, 1996, J. Phys. Chem., **100**, 3115-3120.
143. Gutzwiller, L., F. Arens, U. Baltensperger, H. W. Gäggeler and M. Ammann, 2002, Environ. Sci. Technol., **36**, 677-682.
144. Hales, J. M. and D. R. Drewes, 1979, Atmos. Environ., **13**, 1133-1147.
145. Hallquist, M., D. J. Stewart, J. Baker and R. A. Cox, 2000, J. Phys. Chem. A, **104**, 3984.
146. Hamm, S., J. Hahn, G. Helas and P. Warneck, 1984, Geophys. Res. Let., **11**, 1207-1210.
147. Hanning-Lee, M. A., B. B. Brady, L. R. Martin and J. A. Syage, 1996, Geophys. Res. Lett., **23**, 1961-1964.
148. Hanson, D. R., 1992, Geophys. Res. Lett., **19**, 2063-2066.
149. Hanson, D. R., 1995, J. Phys. Chem., **99**, 13,059-13,061.
150. Hanson, D. R., 1998, J. Phys. Chem. A, **102**, 4794-4807.
151. Hanson, D. R., J. B. Burkholder, C. J. Howard and A. R. Ravishankara, 1992, J. Phys. Chem., **96**, 4979-4985.
152. Hanson, D. R. and E. R. Lovejoy, 1994, Geophys. Res. Lett., **21**, 2401-2404.
153. Hanson, D. R. and E. R. Lovejoy, 1995, Science, **267**, 1326-1329.
154. Hanson, D. R. and E. R. Lovejoy, 1996, J. Phys. Chem., **100**, 6397-6405.
155. Hanson, D. R. and A. R. Ravishankara, 1991, J. Geophys. Res., **96**, 5081-5090.
156. Hanson, D. R. and A. R. Ravishankara, 1991, Geophys. Res. Lett., **18**, 1699-1701.
157. Hanson, D. R. and A. R. Ravishankara, 1991, J. Geophys. Res., **96**, 17307-17314.
158. Hanson, D. R. and A. R. Ravishankara, 1992, J. Phys. Chem., **96**, 2682-2691.
159. Hanson, D. R. and A. R. Ravishankara, 1992, J. Phys. Chem., **96**, 9441-9446.
160. Hanson, D. R. and A. R. Ravishankara, 1993, J. Phys. Chem., **97**, 2802-2803.
161. Hanson, D. R. and A. R. Ravishankara, 1993, J. Phys. Chem., **97**, 12309-12319.
162. Hanson, D. R. and A. R. Ravishankara, 1993, J. Geophys. Res., **98**, 22931-22936.
163. Hanson, D. R. and A. R. Ravishankara. In *The Tropospheric Chemistry of Ozone in the Polar Regions*; Niki, H., Becker, K. H., Eds.; NATO, 1993; pp 17281-17290.
164. Hanson, D. R. and A. R. Ravishankara, 1993, J. Phys. Chem., **97**, 12309-12319.
165. Hanson, D. R. and A. R. Ravishankara, 1994, J. Phys. Chem., **98**, 5728-5735.
166. Hanson, D. R. and A. R. Ravishankara, 1995, Geophys. Res. Lett., **22**, 385-388.
167. Hanson, D. R., A. R. Ravishankara and E. R. Lovejoy, 1996, J. Geophys. Res., **101**, 9063-9069.
168. Hanson, D. R., A. R. Ravishankara and S. Solomon, 1994, J. Geophys. Res., **99**, 3615-3629.
169. Harker, A. B. and W. W. Ho, 1979, Atmos. Environ., **13**, 1005-1010.
170. Hauff, K., R. G. Fischer and K. Ballschmiter, 1998, Chemosphere, **37**, 2599-2615.
171. Hayduk, W., H. Asatani and B. C. Y. Lu, 1988, J. Chem. Eng. Data, **33**, 506-509.
172. Haynes, D. R., N. J. Tro and S. M. George, 1992, J. Phys. Chem., **96**, 8502-8509.
173. Henson, B. F., K. R. Wilson and J. M. Robinson, 1996, Geophys. Res. Lett., **23**, 1021-1024.
174. Henson, B. F., K. R. Wilson and J. M. Robinson, 1999, submitted to J. Phys. Chem. A.
175. Hill, J. O., I. G. Worsley and L. G. Helper, 1968, J. Phys. Chem., **72**, 3695-3697.
176. Hoff, J. T., D. Mackay, R. Gillham and W. Y. Shiu, 1993, Environ. Sci. Tehcnol., **27**, 2174-2180.
177. Hofmann, D. J. and S. J. Oltmans, 1992, Geophys. Res. Lett., **22**, 2211-2214.
178. Holdren, M. W., C. W. Spicer and J. M. Hales, 1984, Atmos. Environ., **18**, 1171-1173.
179. Holzwarth, G., R. G. Balmer and L. Soni, 1984, Water Res., **18**, 1421-1427.
180. Hu, J. H. and J. P. D. Abbatt, 1997, J. Phys. Chem. A, **101**, 871-878.
181. Hu, J. H., Q. Shi, P. Davidovits, D. R. Worsnop, M. S. Zahniser and C. E. Kolb, 1995, J. Phys. Chem., **99**, 8768-8776.
182. Hu, J. H., J. A. Shorter, P. Davidovits, D. R. Worsnop, M. S. Zahniser and C. E. Kolb, 1993, J. Phys. Chem., **97**, 11037-11042.
183. Hudson, P. K., K. L. Foster, M. A. Tolbert, S. M. George, S. R. Carlo and V. H. Grassian, 2001, J. Phys. Chem. A, **105**, 694-702.

184. Huntzicker, J. J., R. A. Cary and C.-S. Ling, 1980, Environ. Sci. Technol., **14**, 819-824.
185. Huthwelker, T., T. Peter, B. P. Juo, S. L. Clegg, K. S. Carshlaw and P. Brimblecombe, 1995, J. Atmos. Chem., **21**, 81-95.
186. Hwang, H. and P. K. Dasgupta, 1985, Environ. Sci. Technol., **19**, 255-258.
187. Il'in, S. D., V. V. Selikhonovich, Y. M. Gershenson and V. B. Rozenshtein, 1991, Sov. J. Chem. Phys., **8**, 1858-1880.
188. Imamura, T. and H. Akiyoshi, 2000, Geophys. Res. Lett., **27**, 1419-1422.
189. Imamura, T., Y. Rudich, R. K. Talukdar, R. W. Fox and A. R. Ravishankara, 1997, J. Phys. Chem., **101**, 2316-2322.
190. Iraci, L. T., A. M. Essin and D. M. Golden, 2002, J. Phys. Chem. A, **106**, 4054-4060.
191. Iraci, L. T., A. M. Middlebrook, M. A. Wilson and M. A. Tolbert, 1994, Geophys. Res. Lett., **21**, 867-870.
192. Iraci, L. T. and M. A. Tolbert, 1997, J. Geophys. Res., **102**, 16,099-16,107.
193. Ivanov, A. V., Y. M. Gersherzon, F. Gratpanche, P. Devolder and J.-P. Saverysyn, 1996, Am. Geophys., **14**, 659-664.
194. Jaegle, L., C. R. Webster, R. D. May, D. C. Scott, R. M. Stimpfle, D. W. Kohn, P. O. Wennberg, T. F. Hansico, R. C. Cohen, M. H. Proffitt, K. K. Kelly, J. Elkins, D. Baumgardner, J. E. Dye, J. C. Wilson, R. F. Pueschel, K. R. Chan, R. J. Salawitch, A. F. Tuck, S. J. Hovde and Y. L. Yung, 1997, J. Geophys. Res., **102**, 13,235-13,253.
195. Jans, U. and J. Hoigne, 2000, Atmos. Environ., **34**, 1069-1085.
196. Jayne, J. T., P. Davidovits, D. R. Worsnop, M. S. Zahniser and C. E. Kolb, 1990, J. Phys. Chem., **94**, 6041-6048.
197. Jayne, J. T., S. X. Duan, P. Davidovits, D. R. Worsnop, M. S. Zahniser and C. E. Kolb, 1991, J. Phys. Chem., **95**, 6329-6336.
198. Jayne, J. T., S. X. Duan, P. Davidovits, D. R. Worsnop, M. S. Zahniser and C. E. Kolb, 1992, J. Phys. Chem., **96**, 5452-5460.
199. Jayne, J. T., U. Poschl, Y. Chen, D. Dai, L. T. Molina, D. R. Worsnop, C. E. Kolb and M. J. Molina, 1997, J. Phys. Chem. A, **101**, 10,000-10,011.
200. Jayne, J. T., D. R. Worsnop, C. E. Kolb, E. Swartz and P. Davidovits, 1996, J. Phys. Chem., **100**, 8015-8022.
201. Jefferson, A., F. L. Eisele, P. J. Zieman, R. J. Weber, J. J. Marti and P. H. McMurry, 1997, J. Geophys. Res., **102**, 19,021-19,028.
202. Jenkins, J. and M. B. King, 1965, Chem. Engin. Sci., **20**, 921-922.
203. Johnson, B. J., E. A. Betterton and D. Craig, 1996, J. Atmos. Chem., **24**, 113-119.
204. Kalberer, M., M. Ammann, F. Arens, H. W. Gaggeler and U. Baltensperger, 1999, J. Geophys. Res., **104**, 13825-13832.
205. Kalberer, M., M. Ammann, H. W. Gaggeler and U. Baltensperger, 1999, Atmos. Environ., **33**, 2815-2822.
206. Kalberer, M., K. Tabor, M. Ammann, Y. Parrat, E. Weingartner, D. Piguet, E. Rossler, D. T. Jost, A. Turler, H. W. Gaggeler and U. Baltensperger, 1996, J. Phys. Chem., **100**, 15487-15493.
207. Kames, J. and U. Schurath, 1992, J. Atmos. Chem., **15**, 79-95.
208. Kames, J. and U. Schurath, 1995, J. Atmos. Chem., **21**, 151-164.
209. Kames, J., S. Schweighoefer and U. Schurath, 1991, J. Atmos. Chem., **12**, 169-180.
210. Kamm, S., O. Mohler, K.-H. Naumann, H. Saathoff and U. Schurath, 1999, Atmos. Environ., **33**, 4651-4661.
211. Kane, S. M. and M.-T. Leu, 2001, J. Phys. Chem. A, **105**, 1411-1415.
212. Kane, S. M., R. S. Timonen and M.-T. Leu, 1999, J. Phys. Chem. A, **103**, 9259-9265.
213. Kelley, C. M. and H. V. Tartar, 1956, J. Amer. Chem. Soc., **78**, 5752-5756.
214. Kenner, R. D., I. C. Plumb and K. R. Ryan, 1993, Geophys. Res. Lett., **20**, 193-196.
215. Keyser, L. F. and M.-T. Leu, 1993, Micros. Res. Technol., **25**, 434-438.
216. Keyser, L. F. and M.-T. Leu, 1993, J. Colloid Interface Sci., **155**, 137-145.
217. Keyser, L. F., M.-T. Leu and S. B. Moore, 1993, J. Phys. Chem., **97**, 2800-2801.
218. Keyser, L. F., S. B. Moore and M. T. Leu, 1991, J. Phys. Chem., **95**, 5496-5502.
219. Khan, I., P. Brimblecombe and S. L. Clegg, 1995, J. Atmos. Chem., **22**, 285-302.
220. Kirchner, U., V. Scheer and R. Vogt, 2000, J. Phys. Chem. A, **104**, 8908-8915.
221. Klassen, J. K., J. Lynton, D. M. Golden and L. R. Williams, 1999, J. Geophys. Res., **104**, 26,355-26,361.
222. Kleffman, J., K. H. Becker, R. Broske, D. Rothe and P. Wiesen, 2000, J. Phys. Chem. A, **104**, 8489-8495.
223. Kleffman, J., K. H. Becker, M. Lackhoff and P. Wiesen, 1999, Phys. Chem. Chem. Phys., **1**, 5443-5450.
224. Kleffman, J., K. H. Becker and P. Wiesen, 1998, Atmos. Environ., **32**, 3129-3137.

225.   Koehler, B. G., L. S. McNeill, A. M. Middlebrook and M. A. Tolbert, 1993, J. Geophys. Res., **98**, 10563-10571.
226.   Koehler, B. G., V. T. Nicholson, H. G. Roe and E. S. Whitney, 1999, J. Geophys. Res., **104**, 5507-5514.
227.   Kolb, C. E., D. R. Worsnop, M. S. Zahniser, P. Davidovits, L. F. Keyser, M.-T. Leu, M. J. Molina, D. R. Hanson, A. R. Ravishankara, L. R. Williams and M. A. Tolbert. Progress and Problems in Atmospheric Chemistry. In *Adv. Phys. Chem. Series, 3*; Barker, J. R., Ed., 1994; pp 771-875.
228.   Kroes, G.-J. and D. C. Clary, 1992, J. Phys. Chem., **96**, 7079-7088.
229.   Langenberg, S., V. Proksch and U. Schurath, 1998, Atm. Environ., **32**, 3129-3137.
230.   Laux, J. M., J. C. Hemminger and B. J. Finlayson-Pitts, 1994, Geophys. Res. Lett., **21**, 1623-1626.
231.   Lemmon, E. W., M. O. McLinden and D. G. Friend. Thermophysical properties of fluid systems. In *NIST Chemistry WebBook*; Number 69 ed.; Mallard, W. G., linstrom, P. J., Eds.; National Institute of Standards and Technology: Gaithersburg, MD, 2000.
232.   Leu, M. T., 1988, Geophys. Res. Lett., **15**, 17-20.
233.   Leu, M.-T., 1988, Geophys. Res. Lett., **15**, 851-854.
234.   Leu, M. T., S. B. Moore and L. F. Keyser, 1991, J. Phys. Chem., **95**, 7763-7771.
235.   Leu, M.-T., R. S. Timonen, L. F. Keyser and Y. L. Yung, 1995, J. Phys. Chem., **99**, 13,203-13,212.
236.   Leu, M.-T. and R. Zhang, 1999, Geophys. Res. Lett., **26**, 1129-1132.
237.   Li, Z., R. R. Friedl, S. B. Moore and S. P. Sander, 1996, J. Geophys. Res., **101**, 6795-6802.
238.   Liberti, A., D. Brocco and M. Possanzini, 1978, Atmos. Environ., **12**, 255-261.
239.   Lind, J. A. and G. L. Kok, 1986, J. Goephys. Res., **91**, 7889-7895.
240.   Lind, J. A. and G. L. Kok, 1994, J. Geophys. Res., **99**, 21119.
241.   Livingston, F. E. and B. J. Finlayson-Pitts, 1991, Geophys. Res. Lett., **18**, 17-20.
242.   Longfellow, C. A., T. Imamura, A. R. Ravishankara and D. R. Hanson, 1998, J. Phys. Chem. A, **102**, 3323-3332.
243.   Longfellow, C. A., A. R. Ravishankara and D. R. Hanson, 1999, J. Geophys. Res., **104**, 13833.
244.   Longfellow, C. A., A. R. Ravishankara and D. R. Hanson, 2000, J. Geophys. Res., **105**, 24,345-24,350.
245.   Lovejoy, E. R., L. G. Huey and D. R. Hanson, 1995, J. Geophys. Res., **100**, 18,775-18,780.
246.   Luick, T. J., R. W. Heckbert, K. Schultz and R. S. Disselkamp, 1999, J. Atmos. Chem., **32**, 315-325.
247.   Luke, W. T., R. R. Dickerson and L. J. Nunnermacker, 1989, J. Geophys. Res., **94**, 14905-14921.
248.   Luo, B., K. S. Carslaw, T. Peter and S. L. Clegg, 1995, Geophys. Res. Lett., **22**, 247-250.
249.   Manion, J. A., C. M. Fittschen, D. M. Golden, L. R. Williams and M. A. Tolbert, 1994, Israel J. Chem., **34**, 355-363.
250.   Martin, L. R., H. S. Judeikis and M. Wun, 1980, J. Geophys. Res., **85**, 5511-5518.
251.   Massucci, M., S. L. Clegg and P. Brimblecombe, 1999, J. Phys. Chem. A, **103**, 4209-4226.
252.   Mawhinney, D. B. and J. J. T. Yates, 2001, Carbon, **39**, 1167-1173.
253.   McMurry, P. H., H. Takano and G. R. Anderson, 1983, Environ. Sci. Technol., **17**, 347-357.
254.   Mertes, S. and A. Wahner, 1995, J. Phys. Chem., **99**, 14,000-14,006.
255.   Michelangeli, D. V., M. Allen and Y. L. Yung, 1991, Geophys. Res. Lett., **18**, 673-676.
256.   Middlebrook, A. M., L. T. Iraci, L. S. McNeil, B. G. Koehler, M. A. Wilson, O. W. Saastad and M. A. Tolbert, 1993, J. Geophys. Res., **98**, 20473-20481.
257.   Middlebrook, A. M., B. G. Koehler, L. S. McNeill and M. A. Tolbert, 1992, Geophys. Res. Lett., **19**, 2417-2420.
258.   Mihelcic, D., D. Klemp, P. Msgen, H. W. Ptz and A. Volz-Thomas, 1993, J. Atmos. Chem., **16**, 313-335.
259.   Molina, M. J., R. F. Meads, D. D. Spencer and L. T. Molina, 1996, Geophys. Res. Lett., submitted.
260.   Molina, M. J., T. L. Tso, L. T. Molina and F. C. Wang, 1987, Science, **238**, 1253-1259.
261.   Molina, M. J., R. Zhang, P. J. Woolridge, J. R. McMahon, J. E. Kim, H. Y. Chang and K. D. Beyer, 1993, Science, **261**, 1418-1423.
262.   Moore, S. B., L. F. Keyser, M. T. Leu, R. P. Turco and R. H. Smith, 1990, Nature, **345**, 333-335.
263.   Mozurkewich, M. and J. Calvert, 1988, J. Geophys. Res., **93**, 15882-15896.
264.   Mozurkewich, M., P. H. McMurray, A. Gupta and J. G. Calvert, 1987, J. Geophys. Res., **92**, 4163-4170.
265.   Msibi, I. M., Y. Li, J. P. Shi and R. M. Harrison, 1994, J. Atmos. Chem., **18**, 291-300.
266.   Msibi, I. M., J. P. Shi and R. M. Harrison, 1993, J. Atmos. Chem., 17,339-17,351.
267.   Muenter, A. H. and B. G. Koehler, 2000, J. Phys. Chem. A, **104**, 8527-8534.
268.   Munder, B., H. Lidal and O. C. Sandall, 2000, J. Chem. Eng. Data, **45**, 1201-1204.
269.   Myhre, C. E. L., C. J. Nielsen and O. W. Saastad, 1998, J. Chem. Eng. Data, **43**, 617-622.
270.   Noyes, R. M., M. B. Rubin and P. G. Bowers, 1996, J. Phys. Chem., **100**, 4167-4172.
271.   Olszyna, K., R. D. Cadle and R. G. dePena, 1979, J. Geophys. Res., **84**, 1771-1775.
272.   Oppliger, R., A. Allanic and M. J. Rossi, 1997, J. Phys. Chem. A, **101**, 1903-1911.

273. O'Sullivan, D. W., M. Lee, B. C. Noone and B. G. Heikes, 1996, J. Phys. Chem., **100**, 3241-3247.
274. Percival, C. J., J. C. Mossinger and R. A. Cox, 1999, Phys. Chem. Chem. Phys., **1**, 4565-4570.
275. Peters, S. J. and G. E. Ewing, 1996, J. Phys. Chem., **100**, 14,093-14,102.
276. Ponche, J. L., C. George and P. Mirabel, 1993, J. Atmos. Chem., **16**, 1-21.
277. Poschl, U., M. Canagaratna, J. T. Jayne, L. T. Molina, D. R. Worsnop, C. E. Kolb and M. J. Molina, 1998, J. Phys. Chem. A, **102**, 10,082-10,089.
278. Pöschl, U., T. Letzel, C. Schauer and R. Niessner, 2001, J. Phys. Chem. A, **105**, 4029-4041.
279. Przyjazny, A., W. Janicki, W. Chrzanowski and R. Staszewski, 1984, J. Chromatogr., **280**, 249-260.
280. Pueschel, R. F., D. F. Blake, A. G. Suetsinger, A. D. A. Hansen, S. Verma and K. Kato, 1992, Geophys. Res. Lett., **19**, 1659-1662.
281. Quinlan, M. A., C. M. Reihs, D. M. Golden and M. A. Tolbert, 1990, J. Phys. Chem., **94**, 3255-3260.
282. Rattigan, O. V., J. Boniface, E. Swartz, P. Davidovits, J. T. Jayne, C. E. Kolb and D. R. Worsnop, 2000, J. Geophys. Res., **105**, 29,065-29,078.
283. Reihs, C. M., D. M. Golden and M. A. Tolbert, 1990, J. Geophys. Res., **95**, 16,545-16,550.
284. Rettich, T. R., R. Battino and E. Wilhelm, 1982, Ber. Bunsen. Phys. Chem., **86**, 1128-1132.
285. Rettich, T. R., R. Battino and E. Wilhelm, 2000, J. Chem. Themo., **32**, 1145-1156.
286. Rieley, H., H. D. Aslin and S. Haq, 1995, J. Chem. Soc. Faraday Trans., **91**, 2349-2351.
287. Rinker, E. B. and O. C. Sandall, 2000, Can. J. Chem. Eng., **78**, 232-236.
288. Rischbieter, E., H. Stein and A. Schumpe, 2000, J. Chem. Eng. Data, **45**, 338-340.
289. Robbins, R. C. and R. D. Cadle, 1958, J. Phys. Chem., **62**, 469-471.
290. Robinson, G. N., Q. Dai and A. Freedman, 1996, J. Phys. Chem., submitted.
291. Robinson, G. N., A. Freedman, C. E. Kolb and D. R. Worsnop, 1994, Geophys. Res. Lett., **21**, 377-380.
292. Robinson, G. N., A. Freedman, C. E. Kolb and D. R. Worsnop, 1996, Geophys. Res. Lett., **23**, 317.
293. Robinson, G. N., D. R. Worsnop, J. T. Jayne, C. E. Kolb and P. Davidovits, 1997, J. Geophys. Res., **102**, 3583-3601.
294. Robinson, G. N., D. R. Worsnop, J. T. Jayne, C. E. Kolb, E. Swartz and P. Davidovits, 1998, J. Geophys. Res., **103**, 25371-25381.
295. Rogaski, C. A., D. M. Golden and L. R. Williams, 1997, Geophys. Res. Lett., **24**, 381-384.
296. Rohrschneider, L., 1973, Anal. Chem., **45**, 1241-1247.
297. Rossi, M. J., F. F. Fenter, K. Tabor, F. Caloz and L. Gutzwiller. Heterogeneous Reactions of Nitrogen Oxides (NO_2, N_2O_5, HNO_3, $ClONO_2$) with Surfaces Representative of Atmospheric Aerosol. In *Heterogeneous and Liquid Phase Processes. Transport and Chemical Transformation of Pollutants in the Troposphere*; Warneck, P., Ed.; Springer-Verlag: Berlin, 1996; pp 213-220.
298. Rossi, M. J., R. Malhotra and D. M. Golden, 1987, Geophys. Res. Lett., **14**, 127-130.
299. Rubel, G. O. and J. W. Gentry, 1984, J. Aerosol Sci., **15**, 661-671.
300. Rudich, Y., R. K. Talukdar, R. W. Fox and A. R. Ravishankara, 1996, J. Geophys. Res., **101**, 21,023-21,031.
301. Rudich, Y., R. K. Talukdar, T. Imamura, R. W. Fox and A. R. Ravishankara, 1996, Chem. Phys. Lett., **261**, 467-473.
302. Rudolf, R. and P. E. Wagner, 1994, J. Aerosol Sci., **25**, 597-598.
303. Saastad, O. W., T. Ellerman and C. J. Nielson, 1993, Geophys. Res. Lett., **20**, 1191-1193.
304. Saathoff, H., K.-H. Naumann, N. Riemer, S. Kamm, O. Möhler, U. Schurath, H. Vogel and B. Vogel, 2001, Geophys. Res. Lett., **28**, 1957-1960.
305. Salgado-Muñoz, M. S. and M. J. Rossi, 2002, Phys. Chem. Chem. Phys., **4**, 5110-5118.
306. Sander, S. P., R. R. Friedl, W. B. DeMore, D. M. Golden, M. J. Kurylo, R. F. Hampson, R. E. Huie, G. K. Moortgat, A. R. Ravishankara, C. E. Kolb and M. J. Molina "Chemical Kinetics and Photochemical Data for Use in Stratospheric Modeling, Evaluation Number 13," JPL Publication 00-3, Jet Propulsion Laboratory, California Institute of Technology, Pasadena, CA, 2000.
307. Schwartz, S. E., 1984, J. Geophys. Res., **89**, 11589-11598.
308. Schwartz, S. E., 1988, Atmos. Environ., **22**, 2331.
309. Schwartz, S. E. and W. H. White. Kinetics of reactive dissolution of nitrogen oxides into aqueous solution. In *Trace Atmospheric Species. Properties, Transformations and Fates*; Schwartz, S. E., Ed.; John Wiley & Sons: New York, 1983; Vol. 12; pp 1-116.
310. Schweitzer, F., P. Mirabel and C. George, 1998, J. Phys. Chem. A, **102**, 3942-3952.
311. Seisel, S., B. Fluckiger and M. J. Rossi, 1998, Ber. Bunsenges. Phys. Chem., **102**, 811-820.
312. Shi, Q. and P. Davidovits, 1999, J. Phys. Chem. A, 8812-8823.
313. Shi, Q., P. Davidovits, J. T. Jayne, C. E. Kolb and D. R. Worsnop, 2001, J. Geophys. Res., **106**, 24259-24274.

314.   Shimono, A. and S. Koda, 1996, J. Phys. Chem., **100**, 10,269-10,276.
315.   Smith, D. M. and A. R. Chughtai, 1995, Colloids and Surfaces, **105**, 47-77.
316.   Smith, D. M. and A. R. Chughtai, 1996, J. Geophys. Res., **101**, 19607-19620.
317.   Smith, D. M. and A. R. Chughtai, 1997, J. Atmos. Chem., **26**, 77-91.
318.   Smith, D. M., W. F. Welch, S. M. Graham, A. R. Chughtai, B. G. Wicke and K. A. Grady, 1988, Appl. Spectrosc., **42**, 674-680.
319.   Smith, D. M., W. F. Welch, J. A. Jassim, A. R. Chughtai and D. H. Stedman, 1988, Appl. Spectros., **42**, 1473-1482.
320.   Snider, J. R. and G. A. Dawson, 1985, J. Geophys. Res., **90**, 3797-3805.
321.   Stadler, D. and M. J. Rossi, 2000, Phys. Chem. Chem. Phys., **2**, 5420-5429.
322.   Staffelbach, T. A. and G. L. Kok, 1993, J. Geophys. Res., **98**, 12713-12717.
323.   Stephens, S., M. J. Rossi and D. M. Golden, 1986, Int. J. Chem. Kinetics, **18**, 1133-1149.
324.   Tabazadeh, A., R. P. Turco and M. Z. Jacobson, 1994, J. Geophys. Res., **99**, 12,897-12,914.
325.   Tabor, K., L. Gutzwiller and M. J. Rossi, 1993, Geophys. Res. Lett., **20**, 1431-1434.
326.   Tabor, K., L. Gutzwiller and M. J. Rossi, 1994, J. Phys. Chem., **98**, 6172-7186.
327.   Tang, I. N. and J. H. Lee. In *The Chemistry of Acid Rain*; Gordon, G. E., Johnson, R. W., Eds.; Am. Chem. Soc. Symp. Series, 1987; pp 109-117.
328.   Tang, I. N. and H. R. Munkelwitz, 1989, J. Colloid Interface Sci., **128**, 289-295.
329.   Timonen, R. S., L. T. Chu, M.-T. Leu and L. F. Keyser, 1994, J. Phys. Chem., **98**, 9509-9517.
330.   Tolbert, M. A., J. Praff, I. Jayaweera and M. J. Prather, 1993, J. Geophys. Res., **98**, 2957-2962.
331.   Tolbert, M. A., M. J. Rossi and D. M. Golden, 1988, Science, **240**, 1018-1021.
332.   Tolbert, M. A., M. J. Rossi and D. M. Golden, 1988, Geophys. Res. Lett., **15**, 847-850.
333.   Tolbert, M. A., M. J. Rossi, R. Malhotra and D. M. Golden, 1987, Science, **238**, 1258-1260.
334.   Toon, O., E. Browell, B. Gray, L. Lait, J. Livingston, P. Newman, R. P. P. Russell, M. Schoeberl, G. Toon, W. Traub, F. P. J. Valero, H. Selkirk and J. Jordan, 1993, Science, **261**, 1136-1140.
335.   Utter, R. G., J. B. Burkholder, C. J. Howard and A. R. Ravishankara, 1992, J. Phys. Chem., **96**, 4973-4978.
336.   Van Dingenen, R. and F. Raes, 1991, Aerosol Sci. Technol., **15**, 93-106.
337.   Van Doren, J. M., L. R. Watson, P. Davidovits, D. R. Worsnop, M. S. Zahniser and C. E. Kolb, 1990, J. Phys. Chem., **94**, 3265-3269.
338.   Van Doren, J. M., L. R. Watson, P. Davidovits, D. R. Worsnop, M. S. Zahniser and C. E. Kolb, 1991, J. Phys. Chem., **95**, 1684-1689.
339.   Villalta, P. W., E. R. Lovejoy and D. R. Hanson, 1996, Geophys. Res. Lett., **23**, 1765-1768.
340.   Vitenberg, A. G., B. V. Ioffe, Z. S. Dimitrova and I. L. Butaeva, 1975, J. Chromatog., **112**, 319-327.
341.   Vogt, R., Elliott, C., Allen, H.C., Laux, J.M., J. C. Hemminger and B. J. Finlayson-Pitts, 1996, Atmos. Environ, **30**, 1729-1737.
342.   Vogt, R. and B. Finlayson-Pitts, 1994, J. Phys. Chem., **98**, 3747-3755.
343.   Vogt, R. and B. F. Finlayson-Pitts, 1994, Geophys. Res. Lett., **21**, 2291-2294.
344.   Vogt, R. and B. J. Finlayson-Pitts, 1995, J. Phys. Chem., **99**, 13,052.
345.   Wagman, D. D., W. H. Evans, V. B. Parker, R. H. Schumm, I. Halow, S. M. Bailey, K. L. Churney and R. L. Nutall, 1982, J. Phys. Chem. Ref. Data, **11**, 392 pp.
346.   Wang, L. and D. C. Clary, 1996, J. Chem. Phys., **104**, 5663-5673.
347.   Waschewsky, G. C. G. and J. P. D. Abbatt, 1999, J. Phys. Chem. A, **103**, 5312-5320.
348.   Watson, L. R., J. M. V. Doren, P. Davidovits, D. R. Worsnop, M. S. Zahniser and C. E. Kolb, 1990, J. Geophys. Res., **95**, 5631-5638.
349.   Watts, S. F. and P. Brimblecombe, 1987, Environ. Technol. Lett., **8**, 483-486.
350.   Weingartner, E., H. Burtscher and U. Baltensperger, 1997, Atmos. Environ., **31**, 2311-2327.
351.   Wilhelm, E., R. Battino and R. J. Wilcock, 1977, Chem. Rev., **77**, 219-262.
352.   Wilhelm, E., R. Battino and R. J. Wilcock, 1977, Chem. Rev., **77**, 219-262.
353.   Williams, L. R. and D. M. Golden, 1993, Geophys. Res. Lett., **20**, 2227-2230.
354.   Williams, L. R., D. M. Golden and D. L. Huestis, 1995, J. Geophys. Res., **100**, 7329-7335.
355.   Williams, L. R. and F. S. Long, 1995, J. Phys. Chem., **99**, 3748-3751.
356.   Wolff, E. W. and R. Mulvaney, 1991, Geophys. Res. Lett., **18**, 1007-1010.
357.   Wong, P. K. and Y. H. Wang, 1997, Chemosphere, **35**, 535-544.
358.   Worsnop, D. R., L. E. Fox, M. S. Zahniser and S. C. Wofsy, 1993, Science, **259**, 71-74.
359.   Worsnop, D. R., M. S. Zahniser, C. E. Kolb, J. A. Gardner, L. R. Watson, J. M. V. Doren, J. T. Jayne and P. Davidovits, 1989, J. Phys. Chem., **93**, 1159-1172.
360.   Yaws, C. L., J. R. Hopper, X. Wang and A. K. Rathinsamy, 1999, Chem. Eng., 102-105.

361. Yoshizumi, K., K. Aoki, I. Nouchi, T. Okita, T. Kobayashi, S. Kamakura and M. Tajima, 1984, Atmos. Environ., **18**, 395-401.
362. Zetzsch, C. and W. Behnke, 1992, Ber. Bunsenges. Phys. Chem., **96**, 488-493.
363. Zhang, R., J. T. Jayne and M. J. Molina, 1994, J. Phys. Chem., **98**, 867-874.
364. Zhang, R. and M.-T. Leu, 1997, J. Geophys. Res., **102**, 8837-8843.
365. Zhang, R., M.-T. Leu and L. F. Keyser, 1994, J. Phys. Chem., **98**, 13,563-13,574.
366. Zhang, R., M.-T. Leu and L. F. Keyser, 1995, Geophys. Res. Lett., **22**, 1493-1496.
367. Zhang, R., M.-T. Leu and L. F. Keyser, 1995, J. Geophys. Res., **100**, 18,845-18,854.
368. Zhang, R., M.-T. Leu and L. F. Keyser, 1996, J. Phys. Chem., **100**, 339-345.
369. Zhang, R., M.-T. Leu and L. F. Keyser, 1997, J. Phys. Chem. A, **101**, 3324-3330.
370. Zhang, R., P. J. Wooldridge and M. J. Molina, 1993, J. Phys. Chem., **97**, 8541-8548.
371. Zhou, X. and Y. N. Lee, 1992, J. Phys. Chem., **96**, 265-272.
372. Zhou, X. and K. Mopper, 1990, Environ. Sci. Technol., **24**, 1864-1869.
373. Zolensky, M. E., D. S. McKay and L. A. Kaczor, 1989, J. Geophys. Res., **94**, 1047-1056.
374. Zondlo, M. A., S. B. Barone and M. A. Tolbert, 1998, J. Phys. Chem. A, **102**, 5735-5748.